Title
COMPOSITIONAL, STRUCTURAL, AND PHYSICAL STUDIES OF SOME GRAPHITE HEXAFLUOROARSENATES AND THEIR RELATIVES

Author
Okino, F.

Publication Date
1984-09-01

Lawrence Berkeley Laboratory

UNIVERSITY OF CALIFORNIA

Materials & Molecular Research Division

COMPOSITIONAL, STRUCTURAL, AND PHYSICAL STUDIES OF SOME GRAPHITE HEXAFLUOROARSENATES AND THEIR RELATIVES

F. Okino
(Ph.D. Thesis)

September 1984

Prepared for the U.S. Department of Energy under Contract DE-AC03-76SF00098

DISCLAIMER

LBL-18261

COMPOSITIONAL, STRUCTURAL, AND PHYSICAL STUDIES OF SOME GRAPHITE HEXAFLUOROARSENATES AND THEIR RELATIVES

Fujio Okino

Ph.D. Thesis

Lawrence Berkeley Laboratory
University of California
Berkeley, California 94720

September 1984

This work was supported by the U.S. Department of Energy under Contract No. DE-AC03-76SF00098.

To my mother who taught me the importance of discipline.

To my father who taught me the importance of "un-discipline".

To my sister who taught me "English".

To my brother who taught me science.

CONTENTS

COMPOSITIONAL, STRUCTURAL, AND PHYSICAL STUDIES OF SOME GRAPHITE HEXAFLUOROARSENATES AND THEIR RELATIVES

Fujio Okino

Materials and Molecular Research Division

Lawrence Berkeley Laboraory

and

Department of Chemistry

University of California

Berkeley, California 94720

ABSTRACT

The molar ratio F/As of the vacuum stable graphite intercalation compounds made by the interaction of graphite powder (1) with a large amount of AsF_5, (2) with large amounts of AsF_5 and F_2, and (3) with O_2AsF_6, followed by evacuation, has been established to be 6 by chemical analyses for C, H, N, As, F and O. X-ray absorption spectra in the arsenic pre-K-absorption-edge region, on vacuum stable compounds of the type (1) indicate that the AsF_6^- anion is the sole guest species. While the vacuum stable compounds made by route (1) are invariably mixtures of first- and second-stage phases, those from route (2) are pure first-stage compounds. Pure first-stage compounds can be made by method (3). Although repeated treatment of graphite with AsF_5 leads to salts with higher arsenic content than a single treatment does, the failure of AsF_5 alone, to produce pure first-stage $C_x^+AsF_6^-$ salts, is attributed to the lower oxidizing potential of AsF_5 relative to AsF_5/F_2 or O_2AsF_6. While

the I_c-spacings of the compounds of the type (1) and (2) before evacuation are ca. (8.00-8.20) + 3.35 (n - 1) Å (where n is the stage), those of the vacuum stable compounds are ca. 7.60 + 3.35 (n - 1) Å. The vacuum stable compounds with $I_c \simeq 7.6$ Å are represented by the formula $C_{14n}AsF_6$. The observed I_c-spacing (~7.6 Å) indicated that the AsF_6^- anions have three-fold sets of F ligands nestled in contiguous three-fold sets of hexagons of the graphite, the D_{3d} symmetry of the AsF_6^- thus requiring a staggering of the enclosing carbon layers, as in graphite. The X-ray diffraction patterns of the vacuum stable compounds with $I_c \simeq$ 7.6 Å have been accounted for by the nestled model. In this model carbon layers, staggered relative to a nearest neighbor as in graphite, contain nestled AsF_6^- in an ordered, closest-packed assembly consistent with the composition $C_{14}AsF_6$. The layers, with the restriction imposed by AsF_6^- nestling, are otherwise randomly stacked. The arrangement of AsF_6^- anions within each graphite gallery has a domain size of ca. 20×20 Å^2. The diffraction patterns of the compounds with $I_c \simeq 8.0$ Å have also been simulated successfully. In this model the AsF_x species are un-nestled. The guest species are randomly distributed between the carbon atom sheets, with, in this case, all of the carbon atoms of one sheet eclipsing those of adjacent sheets. Addition of AsF_5 to a vacuum stable $I_c \simeq 7.6$ Å material generates an structurally different $I_c \simeq 8.0$ Å material. Removal of volatiles reverses the change. Conductivity measurements suggest that the specific conductivity of $C_{14n}AsF_6$ is comparable to that of $C_{8n}AsF_5$ (n = 1-2). Addition of fluorine to these compounds leads to a formation of $C_xAsF_6 \cdot (1\text{-}2)F$ materials, accompanied by a drastic decrease in conductivity to that comparable to graphite.

Chapter 1

INTRODUCTION

Graphite/AsF_5 intercalation compounds[1] have aroused much interest because of their high electrical conductivity.[2,3] A central issue, on which there has been much controversy, and which is crucial to any accounting of conductivity and other physical properties, has concerned the nature of the guest species in the graphite. Although there has been much effort to elucidate the nature of the guest species based on physical measurements,[3-24] insufficient attention has been given to the chemical aspects of the preparations.

X-ray arsenic pre-absorption edge studies by Bartlett et al.[25,26] had previously established that the intercalation of graphite by AsF_5 was accompanied by electron oxidation of the graphite according to the equation:

$$3\ AsF_5 + 2\ e^- \rightarrow 2\ AsF_6^- + AsF_3. \qquad (1.1)$$

The impact of this on the preparation of graphite/AsF_5 intercalation compounds, and thus on their physical properties, has not been fully appreciated. Little attention has been given to appreciable loss of AsF_3, as well as that of AsF_5, upon evacuation, or upon removal of the gases remaining over the AsF_5/C reactants. Because of this it is probable that most materials described in the literature as "C_xAsF_5" must be richer in fluorine than this formula allows for, i.e., the molar ratio of F/As probably exceeds 5 in most cases.

Falardeau and his coworkers[27] characterized graphite/AsF_5 intercalation compounds by the formula $C_{8n}AsF_5$ with the I_c-spacings (_c_-axis repeat distance) $I_c = 8.10 + 3.35\ (n - 1)$ Å, where n is the stage, by using X-ray diffraction, gravimetry, and the _c_-axis thickness

measurements on HOPG intercalated samples. This characterization, which reasonably fits most of the observed data, has been generally accepted. But it should be noticed that subsequent compositional characterization has usually been made in the same way employed by Falardeau et al., i.e., by measuring the weight of a sample, assuming its weight change is solely attributable to the uptake or loss of AsF_5. Consequently the compounds are almost invariably described as "C_xAsF_5", and the further discussions of the properties, e.g., nuclear magnetic resonance,[4-7] electron spin resonance,[7-9] conductivity,[3,10-15] magnetic susceptibility,[6,9,16] X-ray photoelectron spectra,[17,18] optical reflectance,[18,21,22] quantum oscillations,[19,20] structure,[28] etc., of the compounds are made based on this formulation. Even when the allowance of conversion of AsF_5 into AsF_6^- and AsF_3 is made, the overall composition of the compound has usually been fixed to "C_xAsF_5", (i.e., AsF_3 gas was assumed not to leave the product). A point has now been reached at which the controversy, concerning the magnitude of the positive charge borne by the carbon,[17,18,29] and interpretation of physical measurements, makes it imperative that the chemical composition of the "C_xAsF_5" products be precisely specified.

In some cases, it has been observed that the I_c-spacing of freshly made "C_xAsF_5" samples decreases as much as 0.5 Å when evacuated.[14,16] The decrease was accompanied by the changes in the physical properties of the sample. Such residual compounds have been described as "C_yAsF_5" where y is larger than x. Although such changes in I_c-spacing and the physical behavior could have been a consequence of different arrangements of the same intercalant species, it seemed more likely that the changes might be associated with differences in the chemistry. We have addressed

this problem.

In a study by Pentenrieder and Boehm[30], chemical anlyses on F and As on "C_xAsF_5" samples have been made. They found that the F/As molar ratio was invariably slightly higher than 5. Although they recognized the possiblity of the loss of AsF_3, they argued that it was very small because of the closeness of their F/As ratio to 5. Consequently they did allow for the existence of some AsF_6^- within the graphite galleries. Nevertheless they represented that those samples were essentially "C_xAsF_5", and even allowed that the F/As molar ratio being slightly higher than 5, could be explained by fluorination of carbon atoms on the periphery of carbon layers.

Chapter 2 addresses the chemical compositions of the vacuum stable products derived from the interactions of graphite with AsF_5, with AsF_5/F_2, and with O_2AsF_6. The findings show that AsF_6^- salts are generated by each of the above routes and that the solids so prepared are indistinguishable from one another. The AsF_5/F_2 and O_2AsF_6 oxidants, however, yield, in the oxidation limit, salts containing more AsF_6^- than those derivable from AsF_5 alone. Also described in Chapter 2 are the results of X-ray pre-absorption-edge studies on the vacuum stable compounds derived from the interaction of graphite with AsF_5. These studies support the identification of the guest species as AsF_6^-.

In Chapter 3 novel structures for first-stage $C_{14}AsF_6$ and C_xAsF_y ($8 < x < 14$, $5 < y < 6$) are proposed. The vacuum stable first-stage salt of composition $C_{14}AsF_6$, and its higher stage relatives $C_{14n}AsF_6$, are properly identified for the first time. A novel structure accounts for the small value of the I_c-spacings (~7.6 Å). The graphite stages richer in arsenic fluoride guests have large I_c-spacings (ca. 8.0-8.20 Å) and a

structure which involves greater disorder in the placement of the AsF_x species. The $I_c \simeq 8.0$ Å materials also differ from the $I_c \simeq 7.6$ Å salts in having a different relative arrangement of the carbon atom sheets.

In Chapter 4 the structural model for $C_{14}AsF_6$ is mathematically elaborated. Domains of AsF_6^- arrangement within the graphite gallery is included in the model, and the domain size is estimated.

In Chapter 5 some reactions of $C_{14n}AsF_6$ and the conductivity measurements on the related materials are described. Addition of neutral species to $I_c \simeq 7.6$ Å materials reversibly produces structurally different $I_c \simeq 8.0$ Å materials. Fluorine uptake by $C_{8n}AsF_5$ and $C_{14n}AsF_6$ is associated with a drastic decrease in their conductivities. The compositions associated with such low conductivities are of the form $C_xAsF_6 \cdot (1\text{-}2)F$.

Chapter 2

COMPOSITIONS OF GRAPHITE + AsF_5, + AsF_5/F_2, AND + O_2AsF_6 REACTION PRODUCTS AND THEIR RELATIONSHIP TO THE I_c-SPACING

2.1 Experimental

2.1.1 Apparatus

Most preparations were carried out in a stainless steel cell made by drilling a 5/16" diameter chamber in a 3" length of 3/8" diameter rod. This was attached via Swagelock fittings to a stainless steel Whitey IKS4 valve. A small TFE Filter Membrane (Chemplast, Inc.) was placed between the valve and the cell to avoid the loss of graphite powder when it was evacuated. Some reactions were carried out in quartz or FEP (Chemplast, Inc.) tubes. All of the solid materials were handled in the dry atmosphere of a Vacuum Atmospheres Corporation Drilab. Volatiles were manipulated with a Monel metal and stainless steel vacuum line provided with Autoclave Engineering 30VM-6071 valves.

2.1.2 Reagents

Two kinds of graphite were used: Union Carbide SP-1 graphite powder and Union Carbide highly oriented pyrolytic graphite (HOPG). The latter was used for arsenic X-ray pre-absorption-edge studies, and the former for all other reactions. The graphite was pre-treated by heating it to 1500° in a dynamic vacuum and was then exposed to fluorine gas (~500 torr) at ~20°. Fluorine was used as obtained from Matheson Gas Co. Inc.. Arsenic pentafluoride was either supplied by Ozark-Mahoning or prepared by the interaction of elemental arsenic (Allied Chemical Corporation) with excess F_2 at ~200°. It was purified by vacuum distillation from a trap at -78° to one at -196°, followed by evacuation at -126°, and was checked for purity by infrared spectroscopy.

Dioxygenyl hexafluoroarsenate was prepared by a standard procedure.[31]

2.1.3 Instrumentation

Infrared spectra were recorded with a Perkin-Elmer Model 597 spectrometer over the range 200-4000 cm^{-1}. The cell was of Monel metal and had a 10 cm path length. It was silver plated to prevent interaction with the silver chloride windows, which were sealed to the body by Teflon gaskets. The silver chloride windows were cut from 1 mm thick sheet (Harshaw Chemical Company). A side arm to the cell provided for the condensation of volatiles. X-ray powder diffraction patterns were obtained using a General Electric Co. Precision Camera (circumference 45 cm), using Ni filtered Cu-K_α radiation. Powdered samples were loaded into 0.3, 0.5, or 0.7 mm diameter thin-walled (1/100 mm) quartz capillaries (Charles Supper Company, Inc.) in the Drilab. Two microdensitometers of Dobson type[32] were used to determine line intensities. X-ray diffraction patterns of intercalated HOPG samples were recorded with a Phillips diffractometer equipped with a graphite monochromator (Cu-K_{α_1} radiation). The leak-tight sample holder[33] protected exposure of the water-sensitive materials to atmospheric moisture. X-ray arsenic pre-absorption-edge spectra were obtained utilizing the high intensity X-ray source at the Stanford Linear Accelerator Synchrotron Facility. Samples were housed in air-tight Teflon-gasketed containers provided with thin-Teflon-sheet windows.

2.1.4 Chemical Analyses

Routine CHN analyses were performed on all samples by the Microanalytic Laboratory in the College of Chemistry, University of California, Berkeley. Some samples were fully analyzed by Galbraith Laboratories, Inc. (P.O. BOX 4187-Knoxville, Tennessee, 37921); C, H, N,

As, F, and O analyses being carried out.

2.1.5 General Procedures

For each reaction ~100 mg (~8 mmol) of graphite, characterized by X-ray diffraction, was used. In terms of gravimetry, a larger amount of graphite was preferred, but it was found, in the course of the study, that, if the sample size much exceeded 100 mg, it was difficult to maintain the efficient mixing of the solid and gaseous reactants, necessary for product homogeneity. A major practical difficulty was caused by the gross expansion of the graphite (along the c-axis). Gas-tight plugs of the solid thus formed in the reactor. The space provision and mechanical agitation had to be arranged to prevent the formation of such plugs. To ensure homogeneity, a cell containing a sample was shaken mechanically during reaction and evacuation whenever possible. Inhomogeneity of the products was detected by the differences in I_c-spacing ($\Delta I_c \simeq 0.2$-0.3 Å in some cases) and the differences in carbon content ($\Delta C\% \simeq 5\ \%$) from different parts of the same sample. Another indication of such inhomogeneity was the sporadic appearence of AsF_5 gas in the volatiles when the product was evacuated (see Section 2.2.1). In such cases, solid plugs of product were invariably found in the reactor, the solid below the plug giving a different X-ray powder photograph from that above it.

In all cases the products of reaction were subjected to a dynamic vacuum for 0-500 hours at room temperature. Volatiles were trapped at -196° and were examined by infrared spectroscopy. During the evacuation the reactor was constantly agitated whenever possible to ensure the homogeneity of the sample.

2.2 Interaction of Graphite with Gaseous AsF_5

2.2.1 Single treatment with AsF_5

Graphite was transferred into the cell (pre-weighed after evacuation) in the Drilab. Weighing the cell after evacuation of nitrogen (dry atmosphere) determined the amount of graphite. AsF_5 was condensed on to the graphite at -196° through the vacuum line. The cell was weighed again to determine the amount of transferred AsF_5. By applying the ideal gas law, tensimetry (from the measured pressure and the known system volume) provided a rough estimate of the amount of AsF_5. Whenever AsF_5 was transferred from the cylinder to the vacuum line, an appreciable pressure drop (e.g., from 700 torr to 650 torr) was observed over a period of a few seconds, after which the pressure became constant. Such a pressure decrease was not observed with SO_2ClF, PF_5 etc.. This ready absorption of AsF_5 by the inner walls of the vacuum line is probably associated with the combination of strong oxidizer and acid properties leading to metal hexafluoroarsenate (e.g. $Ni(AsF_6)_2$). The mixture in the small volume cell was warmed to room temperature and was shaken mechanically overnight. Volatiles were removed from the sample in a dynamic vacuum at ~25° and were monitored repeatedly by IR.

Initial volatiles consisted of mainly AsF_5, and a little AsF_3. After several minutes of evacuation, AsF_3 became the only observable volatile by IR (see Figure 2.1). A typical weight loss curve represented by carbon content increase is given in Figure 2.2. Small concentrations of AsF_5, which must occur in the volatiles from $C_xAsF_{5+\delta}$ that has already been subjected to a dynamic vacuum for several minutes, were probably absorbed by the vacuum line. The evolution of volatiles, and the associated I_c-spacing decrease, was very slow (see Figure 2.3).

2.2.2 Repeated Treatment with AsF_5

In some experiments graphite was repeatedly treated with AsF_5. In the initial cycle an excess of AsF_5 (molar ratio $C/AsF_5 < 8$) was used and the reaction was run in the same way as described above. After overnight reaction, the remaining gases were removed and the sample was exposed to a dynamic vacuum overnight. In the second and the later cycles, a relatively large amount of AsF_5 was used (molar ratio $C/AsF_5 \simeq 8$). Each overnight reaction with AsF_5 was followed by an overnight evacuation in a dynamic vacuum, and the cycle was repeated 4-8 times.

The volatiles from the sample in the first cycle were, of course, the same as those discussed above. In the second and later cycles, after the removal of the non-intercalated gases (which contained some AsF_3 and large amount of AsF_5), only AsF_3 was observed in the volatiles. After the 3rd - 4th cycles, the amount of AsF_3 became very small, and the gravimetry also indicated that the sample was not taking up appreciable amounts of AsF_5 at the end of each cycle (i.e. after evacuation). With larger graphite samples (~200 mg), AsF_5 was sometimes observed even after the removal of the initial volatiles. This is probably due to the inhomogeneity of the samples. Further evacuation after the last cycle saw a slow evolution of AsF_3 and the usual associated decrease in I_c-spacing (see Figure 2.3).

2.3 Interaction of Graphite with Gaseous AsF_5 and F_2

The interaction of graphite with AsF_5 and F_2 was carried out in a similar manner to preparations with AsF_5 alone. Large amounts of AsF_5 and F_2 (molar ratios $AsF_5 : F_2 : C = (>1) : (>1) : 8$) were condensed consecutively on to the graphite at -196° and the cell was warmed up to room temperature. In this way interaction of AsF_5 alone with graphite

was avoided. The difference in results between of this type and of the interaction of graphite with AsF_5 followed by the addition of F_2 is speculative. The molar ratio F/As of the latter type itself is currently of interest and may or may not depend on the stage (see Chapter 5).[11,12,18,30,34-36] In this chapter the molar ratio As:F of graphite/AsF_5/F_2 interaction is strictly limited to that of the vacuum stable sample obtained by the simultaneous reaction of graphite with excess amounts of AsF_5 and F_2, followed by evacuation.

After the initial removal of remaining gases, which contained AsF_5 and F_2, no IR active gas was found in the volatiles in the later evacuation, except occasional traces of CF_4 and SiF_4. When they were observed at all, it seemed that CF_4 was observed at the earlier stage of evacuation. This can be due to the difference in size of the molecules. The I_c-spacing of the samples usually decreased ca. 0.2-0.4 Å from initial value of ~8.0 Å during the few days of the evacuation process (see Figure 2.3). The carbon content of the samples increased from ~40 % to ~45 %. This increase was attributable to the loss of AsF_5, CF_4, SiF_4, and possibly even F_2. When small in amount, AsF_5 would not be observed, since it would have been absorbed by the inner wall-surfaces of the vacuum line.

2.4 Interaction of Graphite with Solid O_2AsF_6[37]

After the initial removal of remaining gases over the sample of this type, the behavior of the sample during evacuation with respect to the volatiles, weight loss, and the I_c-spacing decrease was similar to that observed for graphite/AsF_5/F_2 system. Except, when the amount of O_2AsF_6 was small ($C/O_2AsF_6 > \sim 14$), the I_c-spacing of the samples was smaller (ca. $7.6 + 3.35(n - 1)$ Å) even before the evacuation, than in the AsF_5 or

AsF_5/F_2 preparations (see Figure 2.4). Further pumping did not cause the I_c-spacing to decrease. A small weight loss, however, was usually observed. (See 5.2.5 for the reaction of graphite with O_2AsF_6 in SO_2ClF.)

2.4.1 Direct mixing at room temperature with molar ratio $C/O_2AsF_6 > 14$

Both graphite and O_2AsF_6 were transferred to the cell in the Drilab. After removing nitrogen from the system by evacuation, the cell, which contained graphite and O_2AsF_6, as the mixed solids, was subjected to violent mechanical vibration at room temperature. An FEP tube was preferred, because of its elasticity, which made the mixing more efficient, and because of its transparency, which provided for a monitoring of the extent of reaction. The reactions were run 1-16 days depending on the relative amounts of graphite and O_2AsF_6, and on the efficiency of their mixing. After the reaction the evolved gas was removed. No infrared active gases were present in it, and a clear mercury surface was not clouded by it, i.e., neither F_2 nor O_3 was present. The amount of evolved gas corresponded well to that of oxygen produced according to the reaction

$$x\,C + O_2AsF_6 \rightarrow C_xAsF_6 + O_2 \qquad (2.1)$$

The gases over the sample after the reaction apparently contained O_2 and small traces of CF_4 and SiF_4, but no AsF_5 was observed.

2.4.2 Direct mixing at room temperature with molar ratio $C/O_2AsF_6 < 14$

When O_2AsF_6 in excess of a molar ratio ($C/O_2AsF_6 < \sim 14$) was used, some O_2AsF_6 remained unreacted. To remove it, the mixture was subjected to a dynamic vacuum at ~60° for 1-4 days. Evacuation at room temperature

was not effective in removing remaining O_2AsF_6.

The gases over the product before the evacuation of O_2AsF_6 at 60° were essentially the same as the previous case, i.e., no AsF_5 was observed. The reaction was apparently initiated by the direct solid-solid contact between carbon and O_2AsF_6. The independent decomposition of O_2AsF_6 evidently was not a part of the mechanism of the reaction.

2.4.3 At an elevated temperature

Some of the graphite/O_2AsF_6 reactions were run by keeping the solid mixture at ~120° for 1-6 days. Under those circumstances residual O_2AsF_6 was not observed, even when an excess amount of O_2AsF_6 was used, i.e., O_2AsF_6 decomposes to O_2, F_2, and AsF_5 at ~120°.

When the amount of O_2AsF_6 used was in excess of the ratio $C/O_2AsF_6 < 14$, AsF_5 was observed in the remaining gases.

Some oxygen from O_2AsF_6 may have entered the graphite gallery, probably as oxide. Although the chemical analyses on these samples indicated the presence of oxygen, this might have been caused by the hydrolysis of the compound by the moisture in the air. Such hydrolysis was definitely observed from time to time for some of the graphite/AsF_5 and graphite/AsF_5/F_2 products. When oxygen was detected in a significant amount, the sum of C, H, N, As, F, and O weight-percentages usually deviated from 100 % grossly.

2.4.4 By thermal decomposition of O_2AsF_6

In some of the reactions, graphite and O_2AsF_6 were placed separately in an inverted-Y-shaped cell. One end containing O_2AsF_6 was kept at ~130° and another containing graphite at room temperature for 1-14 days. This type of reaction, after all, may be the same as the reaction

$$x\,C + AsF_5 + 1/2\,F_2 \rightarrow C_xAsF_6 \qquad (2.2)$$

with the presence of oxygen. An "advantage" to $C/AsF_5/F_2$ interaction is that the molar ratio F/As in the reaction system was exactly 6.

As was the case with the previous reaction in Section 2.4.3, AsF_5 was observed in the remaining gases when excess O_2AsF_6 was employed.

2.5 Samples for Synchrotron Radiation Studies

Three samples were prepared for X-ray arsenic pre-absorption-edge studies using HOPG chips of ~0.1 mm thickness. Two of them were treated with AsF_5 once (one with molar ratio C : AsF_5 of 1 : 4 and the other of 1:8) and the third was treated with AsF_5 five times, each treatment being followed by evacuation in a dynamic vacuum. The procedures were the same as those described in Section 2.2.2. All of the solids were exposed to a dynamic vacuum for ~20 hours. In the case of the third sample this followed the fifth treatment with AsF_5.

2.6 Results and Discussion

The infrared spectra of the volatiles from the product made by the interaction of graphite with AsF_5, together with those of pure AsF_5 and AsF_3 gases are shown in Figure 2.1. Figure 2.2 illustrates a typical weight loss curve for a sample intercalated by AsF_5 losing volatiles in a dynamic vacuum. Loss in weight represents carbon content increase. This was followed by gravimetry. Infrared spectra of the volatiles seldom revealed carbon fluorides. The assumption was therefore made that, during evacuation, no carbon containing gases were lost. This was supported by the combination of gravimetry and chemical analyses.

The possibility, that AsF_3 was observed as a product of reduction of AsF_5 by the vacuum line or the IR cell after it had left the product, was ruled out by blank experiments. Spectroscopically pure AsF_5 was transferrable from an empty reaction cell to the IR cell and AsF_3 was not

detected. The gas appeared to be pure AsF_5. The transfer of AsF_5, however, was not quantitative. When the amount of AsF_5 was very small, no infrared spectrum was observed after the supposed transfer. This is presumed to arise by absorption of the acid fluoride by the metal fluorides of the vacuum line system (see Section 2.2.1).

The composition after the initial removal of the gases over the product was usually $C_{8-10}AsF_{5+\delta}$ which corresponds to a carbon content of ~40 %. Compounds made in this way have been usually reported as $C_{10}AsF_5$.[1,4,9,34,35,38] But the F/As ratio must be larger than 5, since loss of AsF_3 has occurred. Even if a sample has never left an AsF_5 atmosphere after the reaction, its composition must be expressed by $C_xAsF_{5+\delta}$, since some AsF_3, produced according to equation (1.1), can enter the gas (or condensed) AsF_5 phase. Such loss, however, is usually small, as the analytical data by Pentenrieder and Boehm indicate.[30]

In this work, the point at which AsF_5 disappeared from the volatiles seemed to depend upon the amount of the sample and the effectiveness of the stirring of the contents of the cell during evacuation. The gross swelling of the graphite which occurs as a consequence of intercalation causes impenetratable plugs to form in "long" samples. It took much experimentation to find a design which afforded homogeneous materials. With such preparations, usually, after several minutes of evacuation, AsF_5 was not observed in the infrared spectrum. After 200 hours of evacuation the carbon content of the particular sample, illustrated in Figure 2.2, became 55 %, which, assuming the remaining guest species is AsF_6^-, corresponds to $C_{\sim 19}AsF_6$. The carbon content after 200 hours of pumping was confirmed by CHN analyses (55.2 %). The amount of AsF_3, attributable to the weight lost after AsF_5 had become unobservable by

infrared spectrum, sometimes exceeded that allowed according to Equation (1.1). As was pointed out in Section 2.2.1, absorption of AsF_5 by the inner walls of the vacuum line was likely to be the cause of this. Nevertheless, it was evident that AsF_5 was the major volatile only in the earlier stage of evacuation.

The ready loss of AsF_5 stands in marked contrast to the very slow removal of AsF_3, and calls for comment. Imagine AsF_5 and AsF_3 each surrounded by AsF_6^-. The AsF_5 can form $As_2F_{11}^-$ with AsF_6^- ,[39] and AsF_5 can thereby be generated in a new location without much translational motion of As. On the other hand AsF_3 is unlikely to have such a mechanism. A burrowing of the AsF_3 molecule through the AsF_6^- medium is more likely to be necessary in this instance.

Since neither the ratio of AsF_5:AsF_3 nor their quantities lost during the evacuation process can be accurately determined by gravimetry alone, chemical analyses (C, H, N, As, F, and O) were carried out on the vacuum stable products. As was mentioned in Chapter 1, although chemical analyses on a freshly made sample would be useful, the instability of such samples, with respect to the loss of gases, made such analytical work difficult and of dubious value. For definitive analyses, vacuum stable samples were necessary. The results are shown in Table 2.1. It shows that interaction of graphite with AsF_5 alone, indeed, is an effective route to the production of C_xAsF_6 salts, so long as care is taken to remove the volatiles completely. Although repeated treatment of graphite with AsF_5 leads to compounds richer in AsF_6^-, the products of graphite/AsF_5 interaction were always mixtures of first- and second-stage phases, i.e., the oxidation potential of AsF_5 according to Equation (1.1) is not high enough to produce a first-stage salt (see below). After

several cycles the first-stage phase was in much greater concentration than the second, whereas the reverse was true for one cycle.

X-ray pre-absorption-edge spectra on HOPG samples also supported the formation of C_xAsF_6 salts by graphite/AsF_5 interaction. In the earlier studies it was found that, when the samples were not evacuated after the reaction of graphite with AsF_5, two absorption peaks which corresponded well to AsF_6^- and AsF_3 were observed.[25,26] The same observation was made in the recent work, when graphite was sealed into capillaries with AsF_5. In the present work all three samples were evacuated for ~20 hours after the reaction. They showed essentially the same results (see Figure 2.5), and had one peak which corresponds to that of AsF_6^- as in $KAsF_6$. This is not totally in accordance with the results mentioned above on the volatiles, i.e., even after 20 hours of evacuation some AsF_3 was observed in the volatiles from the samples made from graphite powder. The thinness of the samples used for the synchrotron studies could result in much more rapid loss of volatiles than in the case of the SP-1 samples.

It has been reported that, when "C_xAsF_5" was evacuated, the I_c-spacing decreased drastically (as much as ~0.5 Å),[17] although the process was relatively slow. The nature of this decrease in I_c-spacing has neither been adequately accounted for nor fully investigated.[14] As is shown in Figure 2.3, the present study shows that the I_c-spacings of second-stage phases more readily decreased than those of first-stage phases. The reason can be that the access which the guest species have to host edges is greater for the second-stage than for the first-stage, and that loss of AsF_3 is thus more efficient in the second-stage. Another observation on the behavior of the decrease in I_c-spacing

suggests that, though tenuous, the I_c-spacing of samples treated repeatedly by AsF_5 decreases faster than for those treated once. This is probably because most of AsF_3 has been washed out in the process of cycling. As has already been remarked, AsF_5 leaves graphite much more effectively than AsF_3.

One of the major difficulties in characterizing the graphite intercalation compounds of this system, especially in utilizing X-ray diffraction analyses, was that pure one-phase (stage) compounds were hard to obtain.

In order to find a more effective way to obtain C_xAsF_6 salts, and possibly pure first-stage compounds, reaction of graphite with AsF_5/F_2 was carried out. In this study excess of AsF_5 and F_2 were always used. The results in Table 2.1 show that a pure first-stage C_xAsF_6 salt was produced by this route. For the lower stage compounds, the ratio F/As may exceed 6, although discussion of this should await the definitive chemical analyses on vacuum-stable compounds.

Figure 2.3 clearly indicates that the I_c-spacing decrease in these samples is very rapid compared with that in those made from graphite and AsF_5 alone. No AsF_3 was observed in the volatiles during the evacuation process, and this absence of AsF_3 in the galleries is probably the reason for the rapid decrease of I_c-spacing. This is, of course, because the formation of C_xAsF_6 salt has occured according to Equation (2.2). Gradual loss of CF_4, SiF_4 (seldom seen in the intercalation by AsF_5 alone), AsF_5, etc. seems to be the cause of the decrease in both I_c-spacing and weight. It is not clear whether the quick decrease is a consequence of the readiness of CF_4, SiF_4, and AsF_5 departure, or small quantities of CF_4, SiF_4, and AsF_5 involved. Perhaps both factors apply.

Although O_2AsF_6 was reported to react with graphite in SO_2ClF as a solvent to produce a first-stage salt characterized as C_8AsF_6,[25,26,35,37] it was found in this study that such compounds contain a large amount of SO_2ClF (ca. $C_{12}AsF_6 \cdot \frac{1}{2}SO_2ClF$, see Chapter 5).

In order to circumvent the complexity caused by the involvement of SO_2ClF in characterizing those compounds, attempts to make C_xAsF_6 salts by direct reactions of graphite with O_2AsF_6 were made. It was found that the reactions were slow even when the two solids were mixed well by mechanical agitation, but that it was possible to make pure first-stage compounds. Separation of the product from O_2AsF_6 at the end of the reaction necessitated several kinds of experiment. The results of chemical analyses on these compounds are summarized in Table 2.1. They show that C_xAsF_6 salts were formed. The amounts of oxygen found in these compounds, compared with those found in graphite/AsF_5 and graphite/AsF_5/F_2 systems, suggest that there has been essentially no envolvement of oxygen from O_2AsF_6.

When the amount of O_2AsF_6 used for the reaction was small, the I_c-spacing of the product was already minimal and the further evacuation did not bring about further I_c-spacing decrease. When the amount of O_2AsF_6 was large, small decrease in I_c-spacing of the sample was observed. This is probably caused by the loss of AsF_5, CF_4, SiF_4, O_2 etc.. Instead of plotting I_c-spacing against pumping time, it was plotted against the composition, i.e., against x in C_xAsF_6. In most of the cases x was calculated based on carbon analyses assuming the rest of the sample consisted of AsF_6^-. Such plots are shown in Figure 2.4. Three samples fully analyzed by Galbraith Lab. Inc. are indicated by filled circles. Arrows in the figure indicate materials which were mixtures of first- and

second-stage phases. For such materials the pure first- and second-stage phases, respectively, in each sample must have smaller and larger values. Nevertheless, even with those uncertainties, the Figure 2.4 indicates very clear trends: (1) second-stage phases always have a very small I_c-spacing (~10.9 Å), (2) first-stage phases have a small I_c-spacing value (~7.6 Å), when x is larger than ~14, (3) first-stage phases with x smaller than ~14 have larger I_c-spacing (ca. 7.6-8.0 Å), (4) the limit of x in C_xAsF_6 could be ~10, (5) although not fully revealed in the figure, the composition of pure second-stage compounds is ca. $C_{28}AsF_6$.

These observations suggest that the vacuum stable C_xAsF_6 salts have a composition $C_{14n}AsF_6$ with I_c-spacing of $I_c \simeq 7.6 + 3.35\ (n - 1)$ Å. Some discrepancies in Figure 2.4 can be explained by inhomogeneity in the samples, e.g., even though the composition of the first-stage phase is $C_{<14}AsF_6$, there may be a small domain of second-stage, and the sample may be meta-stable with repect to the conversion toward a mixture of two phases with smaller I_c-spacings, when the overall composition of the sample allows it, i.e., $C_{>14}AsF_6$ (overall).

Attainability of pure first-stage salts by AsF_5/F_2 or by O_2AsF_6 in contrast to the mixtures of first- and second-stage phases obtained by AsF_5 alone raises the matter of the oxidizing power of the intercalants. Dividing Equation (1.1) by 2 we have

$$3/2\ AsF_5(g) + e^-(g) \rightarrow AsF_6^-(g) + \tfrac{1}{2}\,AsF_3(g) \qquad (2.3)$$

The free energy change of Equation (2.3) is estimated to be -124 (kcal/mole-e^-),[41]. The lattice energy of O_2AsF_6 can be estimated to be 135 (kcal/mole) and the free energy changes of Equations (2.4) and (2.5), respectively, to be -170 and -155 (kcal/mole).[41,42]

$$AsF_5(g) + \tfrac{1}{2}\,F_2(g) + e^-(g) \rightarrow AsF_6^-(g) \qquad (2.4)$$

$$O_2AsF_6(c) + e^-(g) \rightarrow AsF_6^-(g) + O_2(g). \qquad (2.5)$$

Table 2.1. Analytical data* and I_c-spacings (Å) for the vacuum-stable solid products obtained from (a) graphite +AsF_5; (b) graphite + O_2AsF_6; and (c) graphite + AsF_5 + F_2.

Reactants	Initial reaction stoichiometry and conditions	I_c (Å)	Weight percentages C	H	N	As	F	O	C+As+F	Composition
(a) C+AsF_5:	C:AsF_5≃4.6:1	7.64	56.12	0.70	<0.001	17.26	26.30	<0.5	99.68	$C_{20.28}AsF_{6.01}$
	Six cycles of treatment of graphite with large excess of AsF_5	7.84	50.15	0.05	0.003	19.63	29.79	—-	99.57	$C_{15.94}AsF_{5.98}$
(b) C+AsF_5+F_2:	C:AsF_5:F_2≃4:1:1	7.71	45.09	0.09	0.01	21.56	32.85	<0.5	99.50	$C_{13.05}AsF_{6.01}$
(c) C+O_2AsF_6:	C:O_2AsF_6≃11.6:1	7.57	46.96	0.21	0.023	20.91	31.85	<0.3	99.72	$C_{14.01}AsF_{6.01}$
	C:O_2AsF_6≃5.5:1 followed by evacuation at ~60°	7.56	51.79	<0.01	0.001	19.05	28.98	<0.3	99.82	$C_{16.96}AsF_{6.00}$
	C:O_2AsF_6≃6.8:1 O_2AsF_6 decomposed at ~140°	7.75	43.42	0.11	0.001	22.23	33.78	<0.5	99.43	$C_{12.81}AsF_{5.99}$

* Analytical data (from samples sealed in dry Pyrex capsules) were determined by Galbraith Laboratories, Inc.

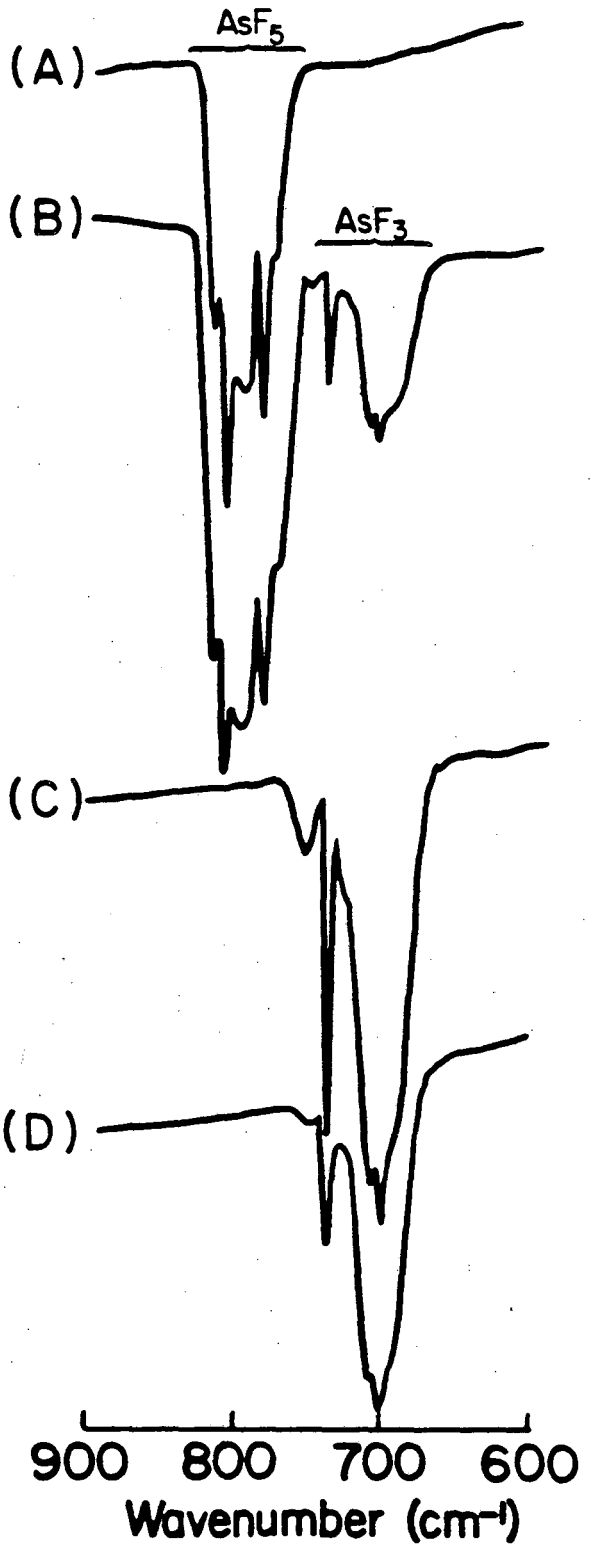

XBL 849-3736

Figure 2.1. Infrared spectra of $AsF_5(g)$, $AsF_3(g)$ and volatiles from C_xAsF_5: (A) pure $AsF_5(g)$ used for reaction; (B) first volatiles from solid ca. C_8AsF_5; (C) volatiles after several minutes of of evacuation; (D) pure $AsF_3(g)$.

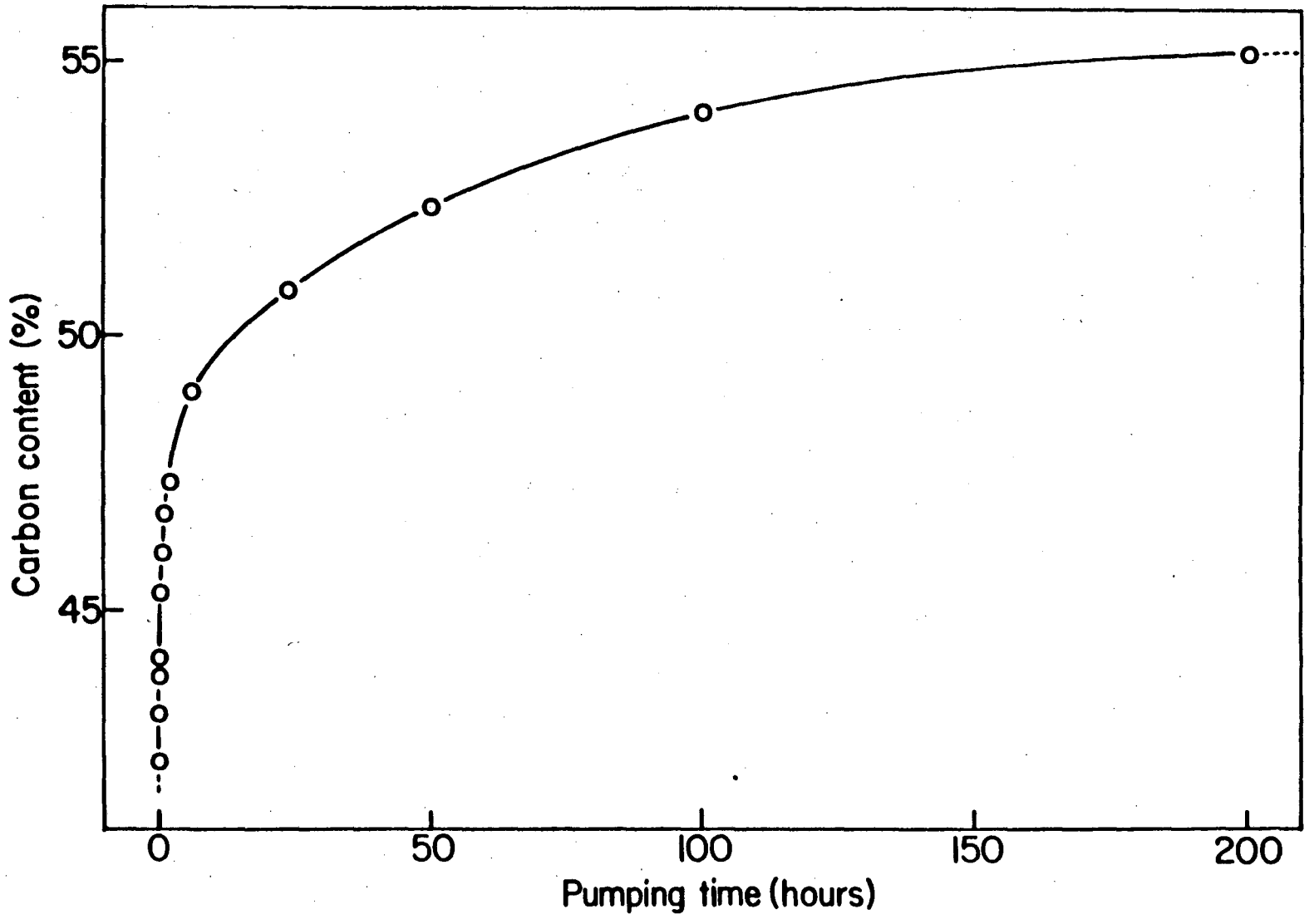

Figure 2.2. Loss of AsF_3 and AsF_5, represented by carbon content increase as a function of pumping time, from the first-stage material of initial composition ca. C_8AsF_5. XBL 849-3737

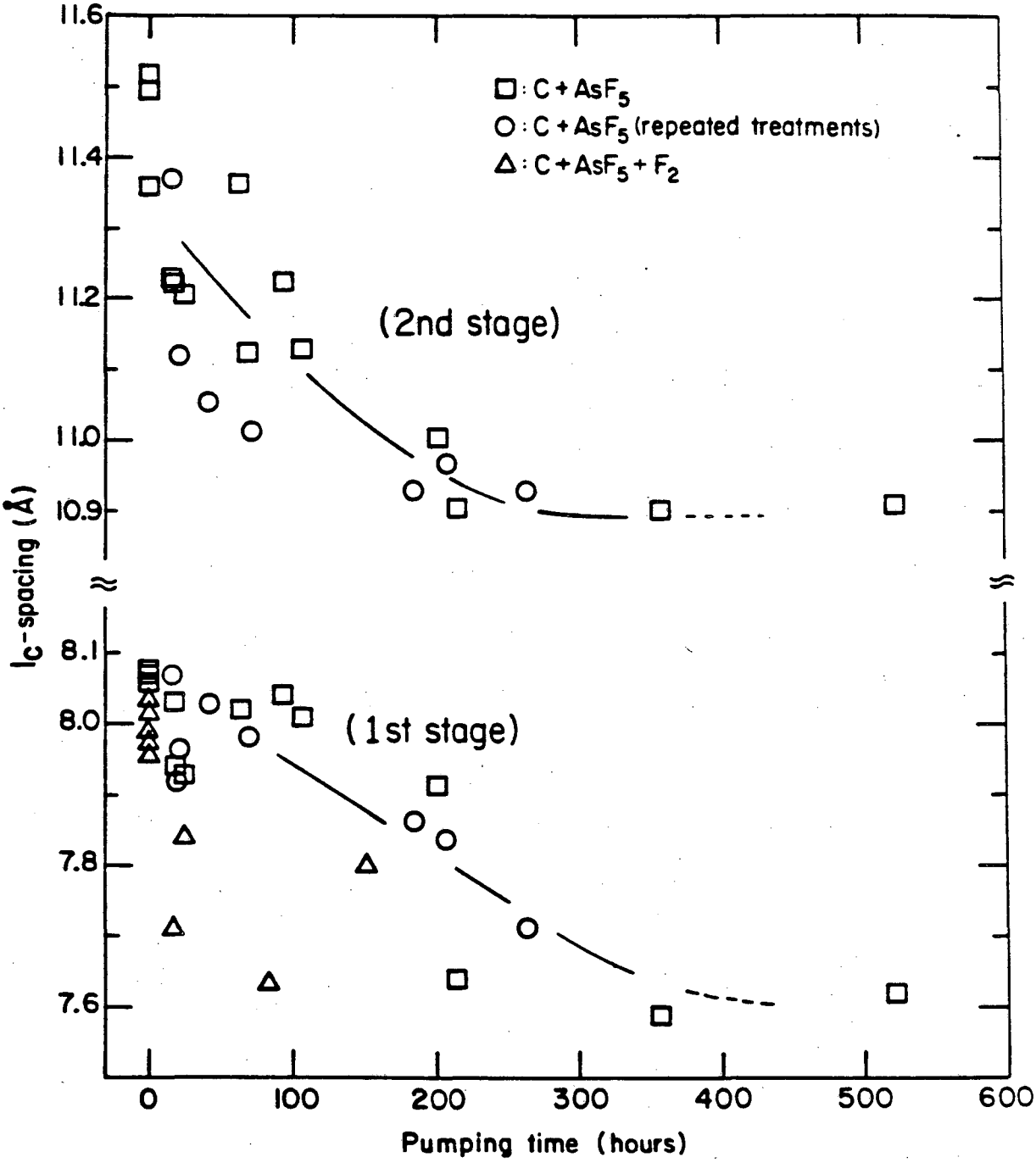

XBL 849-3738

Figure 2.3. The relationship between the I_c-spacing and the pumping time for graphite intercalated by AsF_5 (after the last cycle for the samples treated with AsF_5 repeatedly).

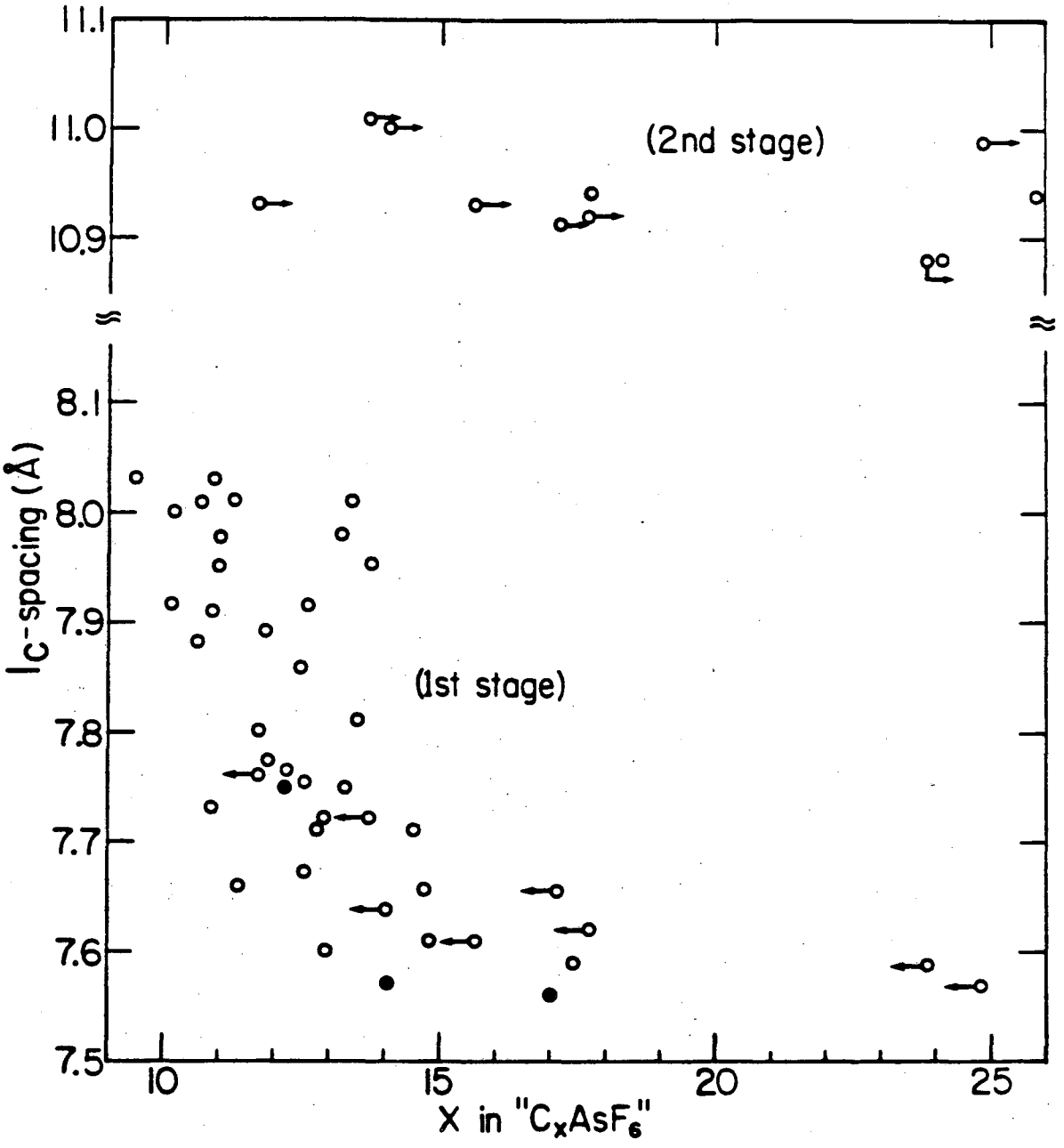

XBL 849-3739

Figure 2.4. The relationship between the I_c-spacing and the carbon content of the samples made by the reaction of graphite and O_2AsF_6(c). (The values of x were calculated based on carbon analyses assuming the formula C_xAsF_6. The samples with filled circles were confirmed to be $C_xAsF_{5.99-6.01}$ by C, H, N, As, F and O analyses. Arrows in the figure indicate materials which were mixtures of first- and second-stage phases. For such materials the pure first- and second-stage phases, respectively, in each sample must have smaller and larger values of x.)

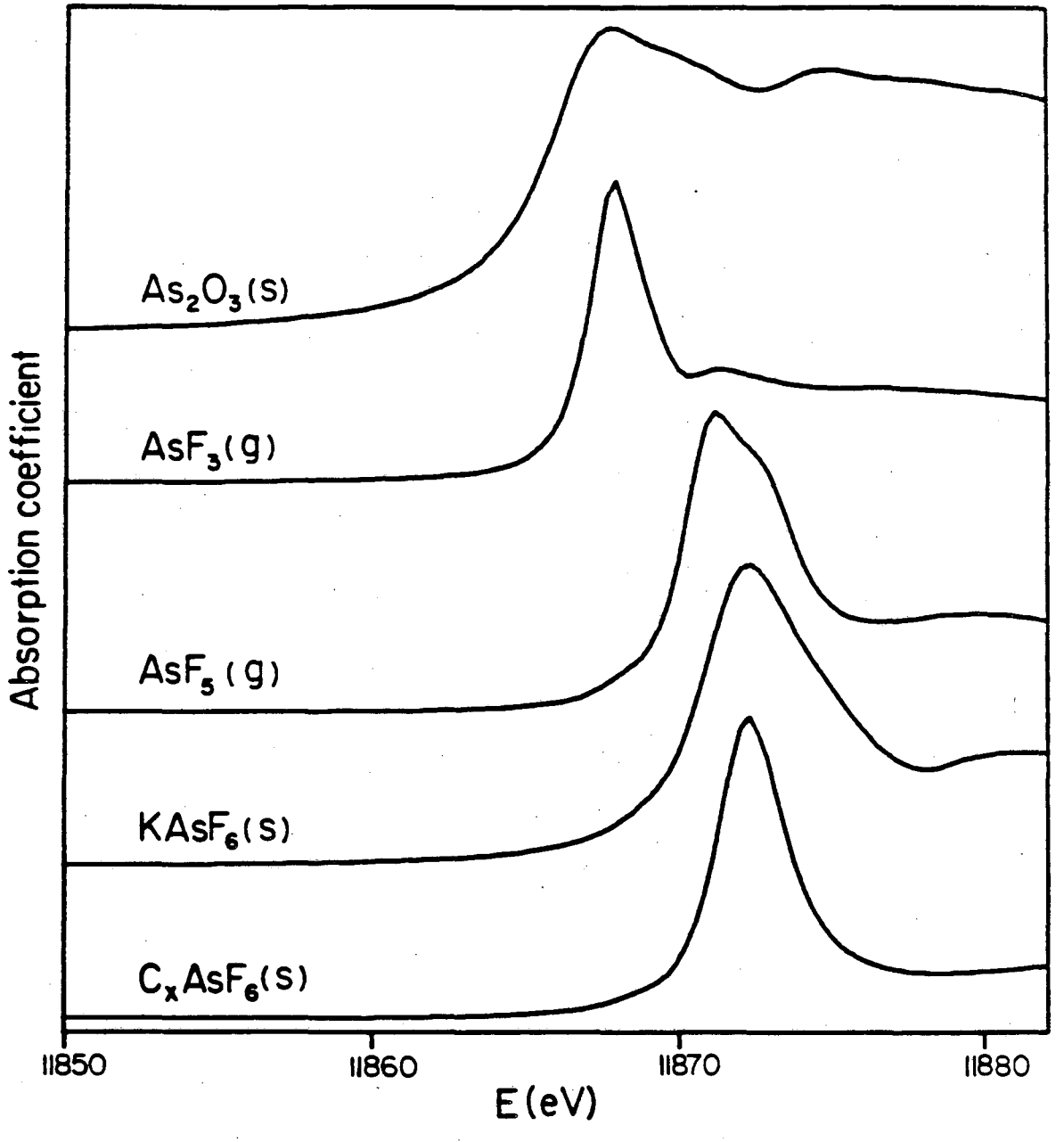

XBL 849-3740

Figure 2.5. Chemical shifts in the arsenic K-shell pre-absorption edge feature (As 1s → 4p transition) for "C_xAsF_6".

Chapter 3

STRUCTURAL MODELS FOR $C_{14}AsF_6$ AND C_xAsF_y ($8 < x < 14$, $5 < y < 6$)

3.1 Description of the Observed X-Ray Diffraction Patterns

The X-ray powder patterns of the first-stage samples with I_c-spacing of ~8.0 Å and those of ~7.6 Å differ not only in the shift of corresponding lines associated with the difference in I_c-spacings, but also in peculiar line broadening and the total absence of (10ℓ) lines in the powder pattern of the samples with small I_c-spacing. Representative powder patterns, read by a microdensitometer, for the two kinds of samples are shown in Figures 3.1 and 3.2. The $1/d^2$ values and possible indexing for these two diffraction patterns are shown in Tables 3.1 and 3.2.

The following discussion of the X-ray powder patterns and the structural models will be limited to first-stage phases.

Although all the lines in the I_c = 8.00 Å sample are satisfactorily indexed by the smallest unit cell with $a_0 = a_g$, and c_0 = 8.00 Å, where a_g is the lattice constant a_0 (= 2.46 Å) of graphite, two broad lines of the I_c = 7.63 Å sample designated (C) and (D) in Figure 3.1 cannot be indexed in a similar way, and it is impossible to explain the big halos designated (A) and (B), by a unit cell with $a_0 = a_g$ and c_0 = 7.63 Å. Line (C), which could be roughly indexed as (100), has a slightly larger value of $1/d^2$ (0.2233 for line (C) in this sample) compared with that (0.2203) of the I_c = 8.00 Å sample. Furthermore, hexagonal symmetry requires that the $1/d^2$ value of (100) be 1/3 of that of (110). Although this requirement was always met in the case of the $I_c \simeq$ 8.0 Å samples, that was not the case with the $I_c \simeq$ 7.6 Å samples. The $1/d^2$ values for (110) line for the two kinds of samples were usually very similar. The

slightly larger value of $1/d^2$ for line (C) than 1/3 of that of (110) line in the $I_c \simeq 7.6$ Å samples was consistently observed, and they looked a little broader than line (100) in larger I_c-spacing samples. Line (D) can be roughly indexed as (101), by the unwary, but the discrepancy between calculated and observed $1/d^2$ values was consistent. The broadness of lines (C) and (D), and the weakness of the latter, as well as the peculiarity of the small I_c-spacing suggested that something else lay at the basis of the X-ray data of the small I_c-spacing samples. Another difference between the patterns of the small and large I_c-spacing data is that, although (10ℓ) lines are observed in the latter, those lines are missing in the former. This suggested that, although the materials were each given to considerable disorder, there were nevertheless very real structural differences. Effort was therefore directed to discovering what these structural differences were.

3.2 Structural Models for the First-Stage $C_{14}AsF_6$ Salt with $I_c \simeq 7.60$ Å

The structure of graphite is shown in Figure 3.3. The lattice constants are $a_0 = 2.46$ Å ($\equiv a_g$) and $c_0 = 6.7$ Å. The inter-layer distance, which is equal to the thickness of each layer, is 3.35 Å, and the distance between the centers of neighboring hexagons is, by definition, equal to the lattice constant a_g. Based on chemical analyses and the vacuum stablity of the samples, the guest species of the samples with $I_c \simeq 7.6$ Å are understood as AsF_6^-. In order to explain the very small value of I_c-spacing of 7.6 Å, physical and geometrical restrictions were imposed. Because of the size of an AsF_6^- anion, shown in Figures 3.4 and 3.5, one of the three-fold axes of the anion must be parallel to the c-axis of graphite host lattice (see Figures 3.6 and 3.7). Although the As-F distance of AsF_6^- anion in various ionic solids varies, it can be

roughly set equal to $\sqrt{3}$ (≃ 1.73) Å. The O_h symmetry of the anion, then, requires the F-F distance to be $\sqrt{6}$ (≃ 2.45) Å. This value is very close to the lattice constant a_0 of graphite. If one of the three-fold axes of AsF_6^- is coincident with one of the three-fold axes of graphite layer at two eclipsed carbon atoms, the geometrical relationship between the graphite host lattice and AsF_6^- anions allows the nestling of three-fold sets of F ligands in contiguous three-fold sets of hexagons of the graphite. The D_{3d} symmetry of the AsF_6^- anion thus requires a staggering of the enclosing carbon layers as in graphite (see Figure 3.8). If the F ligands are nestled into the ring of π electon density by approximately 0.2 Å, then the requirement of a small I_c-spacing of 7.6 Å can be met (see Figure 3.6). When the steric requirement in the ab-plane is considered, the composition $C_{14}AsF_6$ is also explained. Figure 3.9 shows the possible closest arrangement of AsF_6^- anions, with the requirements: (1) all F ligands must be nestled, (2) two F ligands belonging to two different AsF_6^- anions cannot nestle in neighboring hexagons of graphite. The second requirement comes from the van der Waals radius of F ligands. If the neighboring hexagons are occupied by two F ligands of different AsF_6^- anions, they can no longer nestle comfortably. In such a situation the I_c-spacing should increase. This explains the drastic increase in the I_c-spacing for the materials with the composition $C_{<14}AsF_6$ as shown in Figure 2.4.

Although the nestling of AsF_6^- anions requires the staggering of carbon layers, the stacking sequence of carbon layers is not obvious. It can be AB/AB/AB.... as in usual hexagonal graphite, ABC/ABC/ABC.... as in rhombohedral graphite, totally random, or some other sequence with the repeat unit of several carbon layers. To make the consideration easier

at the beginning, the contribution of AsF_6^- to the diffraction intensity is ignored as a first approximation. Although the AB stacking sequence will produce a strong line $\langle 103 \rangle^{43}$ in terms of the unit cell with the lattice constants $a_0 = a_g$ and $c_0 = 15.2$ Å, near line (D) in Figure 3.1, this sequence cannot explain the absence of (10ℓ) lines. The ABC sequence will explain the absence of (10ℓ) lines, but line (D) cannot be explained by this sequence. The ABC sequence does result in $\{100\}^{43}$ (= (100)) being absent. Thus the absence of a definitive (100) line in the observed powder pattern is partly accounted for. The observed broad line (C), however, is not explained. Whichever of these stacking sequence is selected, they are so ordered that the models require many strong lines to be present which are not observed, i.e., $\langle 100 \rangle$, $\langle 101 \rangle$, $\langle 105 \rangle$, etc. for the AB/AB sequence, and $\{101\}$, $\{102\}$, $\{104\}$, etc. for the ABC/ABC sequence.

Although the intervention of nestled AsF_6^- anions physically requires the staggering of the two enclosing carbon layers, there is no strong physical requirement that the guests of one gallery have any registration with respect to the guests of another gallery. This last assumption naturally leads to a random sequence of carbon layers. Each of the layers, however, is staggered with respect to its neighbors on each side. Based on these considerations intensity calculations were made on two models for $I_c \simeq 7.6$ Å samples.

3.2.1 Nestled-small-cell model

Although the requirements of the composition $C_{14}AsF_6$ and the nestling of F ligands do not allow any randomness within one gallery, in the absence of definitive extra lines that would suggest an existence of a super lattice, except the broad large halos (A) and (B), and partly to

minimize the calculation time, the model with the unit cell with $a_0 = a_g$ and $c_0 = 7.6 \times$ (number of carbon layers) Å was assumed. A part of the unit cell used for the calculation is shown in Figure 3.10. An assumption made was that, although the AsF_6^- anions are nestled, they are otherwise randomly distributed. Thus As atoms are placed between two eclipsed carbon atoms (notice that half of the carbon atoms are eclipsed even though carbon layers are staggered), and F atoms are placed in the middle (in terms of (x,y) coordinates) of the hexagons of the closer carbon layers and are, at the same time, eclipsed with the carbon atoms of the farther carbon layers. This model no longer takes care of the O_h or D_{3d} symmetry of AsF_6^-, and does allow F ligands of two different AsF_6^- anions (this description, however, is no longer valid in this model) to nestle in neighboring hexagons. The numbers of atoms are weighted to make a composition of $C_{14}AsF_6$, i.e., C, As, and F atoms are weighted by 7, 1, and 3, since the ratios of the actual numbers of the atoms are C : As : F = 2 : 1 : 2 in this model illustrated in Figure 3.10. 600 carbon layers were randomly stacked according to this principle. The numbers of A, B and C carbon layers were made equal, i.e., each 200 layers. The lattice constants are $a_0 = 2.456$ Å and $c_0 = 4560$ Å. x, y, and z coordinates of atoms used for the calculation should be clear from Figures 3.6 and 3.10. The Lorentz-polarization factor used was

$$Lp = (1 + \cos^2 2\theta)/(\sin\theta^2 \cos\theta),$$

which is appropriate for the Debye-Scherrer powder method. The effects of preferred orientation, which definitely exists for samples placed on a flat surface of a sample holder for a diffractometer, were not obvious in this case. This was probably due to the granular nature of the SP-1 graphite particles and the absence of heavy compacting pressures in the

capillary loading. Absorption corrections were not made partly because the effect is monotonic with respect to 2θ. After all, those corrections were not easy to carry out because of the peculiar flat shape arising from the layered structure. Even though the sample is powder, it cannot be assumed as a totally randomly oriented aggregate of powdered particles. Scattering factors were taken from the International Tables for X-ray Crystallography, Vol. IV. Dispersion corrections were estimated to change the calculated intensities ~10 % at most. They were not made. The poor quality of the X-ray powder data did not warrant corrections of this magnitude. Anisotropic thermal factors were, however, required to account for some of the line intensities. The calculated (111) line intensity, for example, was very weak without anisotropic thermal parameters for As and F atoms. The values for the anisotropic thermal parameters are given in Table 3.3. The anisotropic thermal factors are in harmony with the anisotropic nature of graphite itself. Intensities of all the possible reflections with the $1/d^2$ values of less than 0.82 were calculated and accumulated into the corresponding 2θ degree with a width of 1/10 degree.

The results are shown in Figure 3.11. The blank diffraction pattern of a quartz capillary is shown in Figure 3.12. Figure 3.13 was obtained by giving a Gaussian function with a standard deviation of 0.3 degree in 2θ to each accumulated intensity, and by adding the blank diffraction pattern by a quartz capillary. The relative ratio of the background to the calculated peaks were adjusted to match the observed pattern. Considerations of structure factors are very revealing. The (x,y) coordinates of all the atoms are either (0,0), (1/3,2/3), or (2/3,1/3), and all layer-units are equivalent in terms of the z-coordinates of the

atoms. Therefore $[00\ell]^{43}$ and $[11\ell]$ reflections with $\ell \neq 600n$, and [1,0,600n] reflections, which correspond to (10ℓ) reflections in the smallest unit cell, are all extinct, i.e., all the extra lines brought about by enlarging the cell along the c-axis are $[10\ell]$ with $\ell \neq 600n$, and appreciable intensities are accumulated at lines (C) and (D) in Figure 3.1. Specifically, line (C) consists of the reflections from [101] to [1,0,~360], and line (D) from [1,0,601] to [1,0,~1000]. The other $[10\ell]$ lines are weak and spread out on 2θ scale. The excellent agreement with the observed data is not fortuitous simply for the 600 layer calculation. Preliminary calculations done with 60, 150, and 300 layers all showed similar results but with less smoothed peaks for (C) and (D), and the less smoothed "background" arising from $[10\ell]$ reflections. This model accounted for most features of the powder pattern of the samples with small I_c-spacing reasonbly well, except the big halos (A) and (B).

A major "defect" of this nestled-small-cell model is that small change in weighting the numbers of atoms did not cause large deviations from the observed pattern, i.e., although the chemical analyses set y in C_xAsF_y to be 6, the intensity data do not require x to be 14. A value for x as low as 12 would be acceptable in this context alone. The value smaller than 14 does seem unlikely, however, because collision of nestled ligands of different guest molecules would occur for close packed arrangements. Larger values of x than 14 are also unlikely, because such samples would contain some second-stage phase (see Figure 2.4).

3.2.2 Nestled-large-cell model

A further consideration suggested that halo (B) is situated very close to the $[100]^{43}$ reflection of the "real" unit cell for $C_{14}AsF_6$ shown in Figure 3.9. The lattice constant is $a_0 = \sqrt{7}a_g$. If the same kind of

phenomenon is occurring for this larger cell, a broad line should be formed near [100] by accumulation of [10ℓ] intensities, if many layers were randomly stacked. Based on this observation, 84 layers of carbon with nestled AsF_6^- anions with the composition $C_{14}AsF_6$, such as shown in Figure 3.9 were randomly stacked. The calculation time was increased not only because of the cell size but also because of the lowered symmetry. The "space group " is P1, and the above and the following indices [hkℓ] were based on the pseudo-hexagonal lattice. The computer program for this nestled-large-cell model is given in the Appendix.

The results are shown in Figures 3.14 and 3.15. The same procedures, as in the case of the nestled-small-cell model, were made to obtain Figure 3.15 from Figure 3.14. As was expected, the broad halo (B) was reasonably explained, as well as the apparent disappearence of the quartz background peak in the observed diffraction pattern. It is almost totally covered by the big halo (B). Although some extra lines might be smoothed out if more layers are stacked randomly, it is likely that this model is too "ordered" to represent the graphite powder intercalation compounds. This was suggested by the very small difference between the calculated intensities with 21 layers (not shown) and those with 84 layers. Figure 3.16 shows the summary of the observed and calculated diffraction patterns for the $I_c \approx 7.6$ Å samples.

This large-cell model fails to explain halo (A) at ~8° in the observed diffraction pattern (see Figure 3.1), since [0,0,84] (= (001)) is the possible lowest angle reflection. This lower angle halo (A) will be satisfactorily explained by assuming domains of AsF_6^--superlattice arrangement within a graphite gallery (see Chapter 4).

3.3 A Structural Model for the First-Stage C_xAsF_y ($8 < x < 14$, $5 < y < 6$) with $I_c \simeq 8.00$ Å

Since all the reflections are explained by the smallest unit cell ($a_0 = a_g$ and $c_0 = 8.00$ Å) (see Table 3.2), it is probably possible to make a model within the size of this unit cell. This assumption already rules out the staggering of carbon layers, since it requires the lattice constant c_0 to be multiples of 8.00 Å. Further argument against the staggering of carbon layers, however, can be given. First of all, if they are staggered at all, they are likely to be randomly stacked. If that is the case, the powder pattern should show the same kind of peculiar features as those of the smaller I_c-spacing samples described above. If the stacking sequence were AB, $\langle 1,0,2n+1\rangle$ reflections, which have no counterparts in the smallest unit cell, should show up. If it were ABC, $\{1,0,3n\}$ (= (10ℓ)) reflections must be absent. Evidently the carbon layers are eclipsed. A reasoning for eclipsing of carbon layers can be provided. With the larger I_c-spacing of ~8.0 Å, the guest species have more vibrational freedom. Because of its size, the AsF_6^- anion is unlikey to be freely rotating, except, possibly around the three-fold axis in the z direction. Trigonal bipyramidal AsF_5 can undergo pseudo rotation (Berry mechanism), and AsF_3 may under go inversion or may actually freely rotate. CF_4 and SiF_4 may be tumbling if they are present. Because of these movements, each species can be considered as a big sphere, and may be "nestling" between the two facing carbon hexagons of eclipsed graphite layers. This contribution of the "nestling" to the eclipsing of carbon layers may be true, but its requirement is unlikely to be as rigorous as in the previous model (see below). Since all AsF_x species cannot be fit into the size of this unit cell, some randomness

must be involved for the guest species in order to be consistent with the cell size. When As and F atoms are registered to either middle of hexagons, to carbon atoms, and/or somewhere else (in terms of (x,y) coordinates), and weighted appropriately, a good fit was not obtained. On the assumption that the guest species are totally randomly distributed (without any registration) or are moving parallel to the ab-plane within each gallery, satisfactory agreement was obtained (see below). Because of the inter-layer spacing, the z-coordinates were relatively fixed for both As and F atoms, the former being always near the midpoint of the two facing carbon layers, and the latter being ~1 Å off from the midpoint in the z-direction. In the case of AsF_3, the lone electron pair will force As atom to be near the midpont of the carbon layers. This model was realized by giving the anisotropic thermal factors given in Table 3.2. A schematic drawing of the model is shown in Figure 3.17. This model is in accordance with the room temperature F^{19} NMR data,[4,6,7,9] which indicate a motionally narrowed line, and the electron density distribution along z-axis,[20,28] on "C_xAsF_5" materials. A composition, $C_{10}AsF_5$, was used, although the changes in composition ($8 < x < 14$, $5 < y < 6$ in C_xAsF_y) did not cause drastic change in calculated intensities. x, y, and z coordinates for C, As, and F atoms are shown in Table 3.4. The value of 2 for the thermal parameters correspond to the vibration amplitude of 1.414 Å. This is to be compared with the C-C distance of 1.42 Å in graphite. With the values given in Table 3.3 for thermal parameters, flat ellipsoids of As and F are forming flat continuous layers of As and F atoms, and the change in the (x,y) coordinates of the As and F atoms does not cause any change in the calculated intensities, as the model was aimed at. The results are shown in Figures 3.18 and 3.19. The same

procedures, as in the case of the nestled models, were made to obtain Figure 3.19 from Figure 3.18. The shoulder and the halo near (002) in the observed diffraction pattern are accounted for as a mixture of (002) line with the diffraction by a quartz capillary. Figure 3.20 shows the summary of the observed and calculated diffraction patterns for the $I_c \simeq 8.0$ Å samples.

3.4 Discussion

The same kind of peculiar diffuse scattering characteristic for the I_c=7.6 Å materials were oberved in the X-ray diffraction patterns of graphite/fluorosulfate (C_xSO_3F) and graphite/acid fluorosulfate ($C_x \cdot y\ HSO_3F \cdot z\ SO_3F^-$) compounds.[33] The former had smaller I_c-spacing of ~7.7 Å and showed the same kind of peculiar features in the observed X-ray powder pattern. The latter, on the other hand, had an I_c-spacing of ~8.0 Å and resembled the $I_c \simeq 8.0$ Å sample in this study. The difference in I_c-spacing has been attributed[33] to the difference in size of SO_3F^- and HSO_3F, to the coulombic attraction between SO_3F^- and the carbon layers, which is smaller for the latter compound. Possible hydrogen bonding was also attributed to the larger I_c-spacing materials. There must be, however, some associated difference in the structure of the intercalation compounds as a whole, which is responsible for the differnce in the observed X-ray powder patterns.

With the structural models proposed in this chapter, the following model nicely explains the earlier findings. The SO_3F^- anion is a pseudo T_d ion. If we orient the ion so that the one of the three-fold axes is parallel to the c-axis of graphite, three of the four ligands can, as in the case of AsF_6^-, nestle into the three contiguous hexagons of one carbon layer, while the fourth ligand is nestling into a hexagon of the facing

carbon layer, thus requiring staggering of the two facing carbon layers. In order for a tetrahedral AX_4 species to nestle comfortably, the A-X bond distance must be ~1.5 Å. Since the average bond distance S-X in SO_3F^- is estimated to be 1.46 Å,[33] the nestling model is equally applicable. On the other hand, the geometry of HSO_3F will not allow comfortable nestling. Not only the geometry of the guest species, but also the coulombic attraction is probably necessary for the nestling, i.e., CF_4, SiF_4 or SiF_6, for example may not nestle without some attraction force between it and the carbon layers.

A more general description for the nestling is possible. Assume the two layers of AB-stacked ligands to be close-packed spheres. Suppose that the size of the spheres are such that all spheres of one layer can placed (nestled) into the close packed hexagons of a carbon layer. If the other layer of ligand spheres does the same, the "stacking" sequence of two carbon layers will be AB. The central atoms, e.g., As in AsF_6^-, and S in SO_3F^-, can either occupy O_h or T_d hole sites between the two layers of ligand spheres, depending on the symmetry of the guest species. This provides a model for randomly distributed guest species. This corresponds to the nestled-small-cell model of this study. Note, however, that the size of the ligands forbids the filling of all hexgons.

All atoms in the nestled model are probably more restrained than in the un-nestled model. For the un-nestled model, it is therefore likely that the carbon layers have larger space to move not only in the c-axis-direction but also within the ab-plane. The movement in the c-axis-direction, however, is probably larger than that in the pure graphite. The reported thermal parameters of the pure graphite for the best fit are $U_{11} = 0.33$ and $U_{33} = 1.4$.[44] The thermal parameters (× 100) of the

graphite were all set equal to 0 for the nestled model and 2, 2, 2, 1. 0, and 0, respectively, for U_{11}, U_{22}, U_{33}, U_{12}, U_{13}, and U_{23}, for the unnestled model. The above values resulted in relaively good reproduction of the observed diffraction patterns, but rigorous refinements have not been made.

In a single crystal structure study of a second-stage "$C_{16}AsF_5$" material, Kasper and his coworkers[28] concluded that the carbon stacking sequence was AB with twinning. Their lattice constants are given as a_0 = 2.46 Å and c_0 = 11.50 Å. The present study suggest that, because the sample was not evacuated and the I_c-spacing was large (the I_c-spacing of 11.50 Å corresponds to the I_c-spacing of ~8.15 Å of the first-stage phase), the guest species were unlikely to be nestled. It is therefore probable that the carbon layers, which enclose the guest species, were eclipsed. Adjacent carbon layers without guest species between them are likely to be AB-stacked as in pure graphite. Because of the intervention of guest species, there will be no correlation between two sets of directly facing carbon layers. Therefore the stacking sequence will be random (similar to the case of the first-stage nestled model), e.g., AGA/BGB/CGC/BGB.... where G indicates a guest species layer. Simple structure factor considerations immediately reveal that the same kind of diffraction as that provided by the first-stage sample with the small I_c-spacing should occur. Without the detailed data obtained by the workers on the single crystal at hand, it is not possible to assert that this solution is superior to theirs.

Assuming the existence of a nestled-second-stage material, the stacking sequence of carbon layers would be, for example, AGBCGBCGB...., with again, a random stacking sequence of carbon layers. Our data from

powdered materials indicate that samples with the small I_c-spacing of ~10.9 Å show similar diffraction patterns to the first-stage samples with I_c-spacing of ~7.6 Å. For the samples with larger I_c-spacing the indication is ambiguous.

Milliken and Fischer, in recent study,[18] contend that the ionization limit of a graphite host layer is C_{20}^+, and further oxidation by the fluoride results in the formation of covalently bonded fluorine. The materials of composition $C_{\sim 14}AsF_6$, prepared in this work, would have to be thus represented as: $10 \times C_{14}AsF_6 = 7 \times C_{20}AsF_6 + 3\ AsF_5 + 3\ F_{cov.}$. The AsF_5 would have to be associated with AsF_6^- as $As_2F_{11}^-$, since it is not removed in a vacuum. But the capture of F^- from AsF_6^- by carbon would result in the release of AsF_5. It is conceivable that such AsF_5 would form $As_2F_{11}^-$. This would have to be vacuum stable. If so, the addition of AsF_5 to C_xAsF_6 ought to result in all AsF_6^- being similarly complexed to yield $As_2F_{11}^-$ salts. Since the addition of AsF_5 to C_xAsF_6 does not result in a vacuum stable complex (see Chapter 5), it is extremely unlikely that $As_2F_{11}^-$ or related complex species exists in $C_{14}AsF_6$.

The analytical data, the sychrotron data, the agreement of the nestled-model X-ray diffraction data with that observed: all indicate that the C_xAsF_6 materials are salts with AsF_6^- as the sole As-containing species. Therefore the carbon sheet charge in first-stage $C_{14}AsF_6$ must be C_{14}^+.

Table 3.1. Observed and calculated $1/d^2$ values and possible indexing (hkℓ) for one of the representative samples with I_c-spacing of ca. 7.6 Å. Indices [h,k,ℓ] and [h,k,ℓ], respectively, by the nestled-small-cell and the nestled-large-cell models are also shown.

a_0 = 2.45 Å, I_c = 7.63 Å ca. $C_{14}AsF_6$				
(hkl)	$1/d^2$(obs.)	$1/d^2$(calc.)[a]	[h,k,ℓ]	[h,k,ℓ]
001	.0169	.0171	0,0,600	0,0,84
B[b]	.0312	---	----	1,0,1 to 1,0,~100
002	.0683	.0687	0,0,1200	0,0,168
003	.1541	.1547	0,0,1800	0,0,252
C[b]	.2233	---	1,0,1 to 1,0,~360	2,1,00 to 2,1,~50
D[b]	.2597	---	1,0,601 to 1,0,~1000	2,1,85 to 2,1,~140
004	.2753	.2750	0,0,2400	0,0,336
005	.4287	.4297	0,0,3000	0,0,420
006	.6194	.6188	0,0,3600	0,0,504
110	.6635	.6642	1,1,0	4,1,0
111	.6813	.6814	1,1,600	4,1,84
112	.7324	.7330	1,1,1200	4,1,168
113	.8205	.8189	1,1,1800	4,1,252

a) Least-squares fitted.

b) See Figure 3.1. for the line designations (B, C, and D).

Table 3.2. Observed and calculated values of $1/d^2$ and possible indexing for one of the representative samples with I_c-spacing of ca. 8.0 Å.

a_0 = 2.46 Å, I_c = 8.00 Å		ca. $C_{10}AsF_6$
hkℓ	$1/d^2$(obs.)	$1/d^2$(calc.)[1)]
001	.0154	.0156
002	.0624	.0625
003	.1404	.1407
100	.2206	.2204
101	.2367	.2361
004	.2498	.2502
102	.2832	.2830
103	.3606	.3612
005	.3911	.3910
104	.4712	.4707
006	.5635	.5630
110	.6618	.6614
111	.6782	.6771
112	.7235	.7240
113	.8012	.8022

1) Least-squares fitted

Table 3.3 Anisotropic thermal parameters* (× 100) used for the calculations

		U_{11}	U_{22}	U_{33}	U_{12}	U_{13}	U_{23}
Nestled model	C	0	0	0	0	0	0
$C_{14}AsF_6$, I_c = 7.60 Å	As	10	10	5	5	0	0
	F	20	20	10	10	0	0
Un-nestled model	C	2	2	2	1	0	0
$C_{10}AsF_5$, I_c = 8.00 Å	AS	200	200	6	100	0	0
	F	200	200	16	100	0	0

* The anisotropic thermal factor expression used is

$$\exp[-2\pi^2(U_{11}h^2a^{*2} + U_{22}k^2b^{*2} + U_{33}\ell^2c^{*2} + 2U_{12}hka^*b^* + 2U_{13}h\ell a^*c^* + 2U_{23}k\ell b^*c^*)].$$

U_{ij}: Thermal parameters expressed in terms of mean-square amplitude of vibration in angstroms.

Table 3.4. x, y, and z coordinates of atoms used for the un-nestled model with I_c = 8.00 Å.

	x	y	z
C(1)	1/3	2/3	0
C(2)	2/3	1/3	0
As	1/3*	2/3*	1/2
F(1)	2/3*	1/3*	3/8
F(2)	1/3*	2/3*	5/8

* With the large anisotropic thermal parameters for As and F given in Table 3, their x and y can be thought of as dummy coordinates, i.e., any values will give the same result.

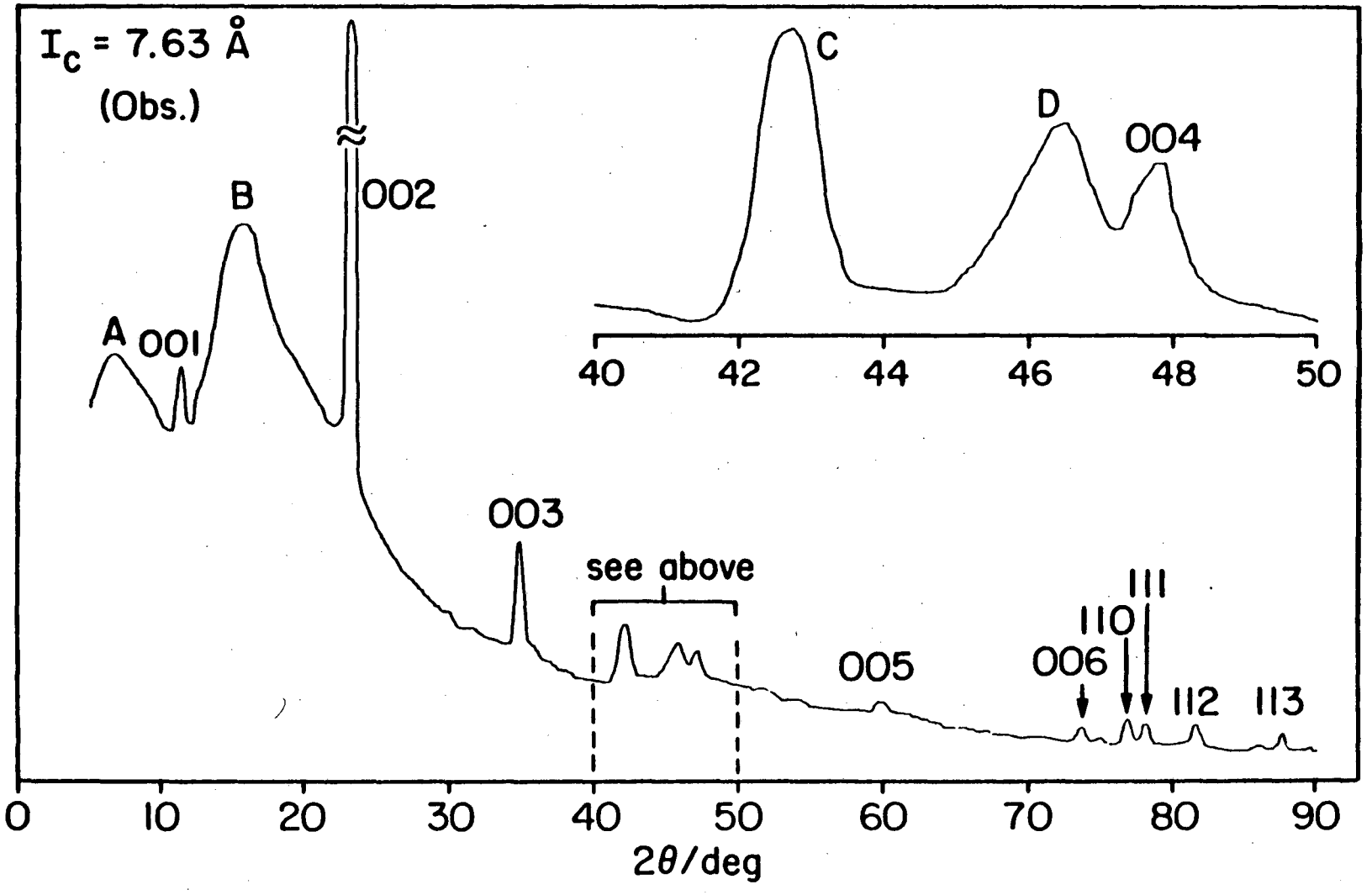

Figure 3.1. Observed X-ray diffraction pattern for a sample of the composition ca. $C_{14}AsF_6$ with I_c = 7.63 Å.

XBL 849-3741

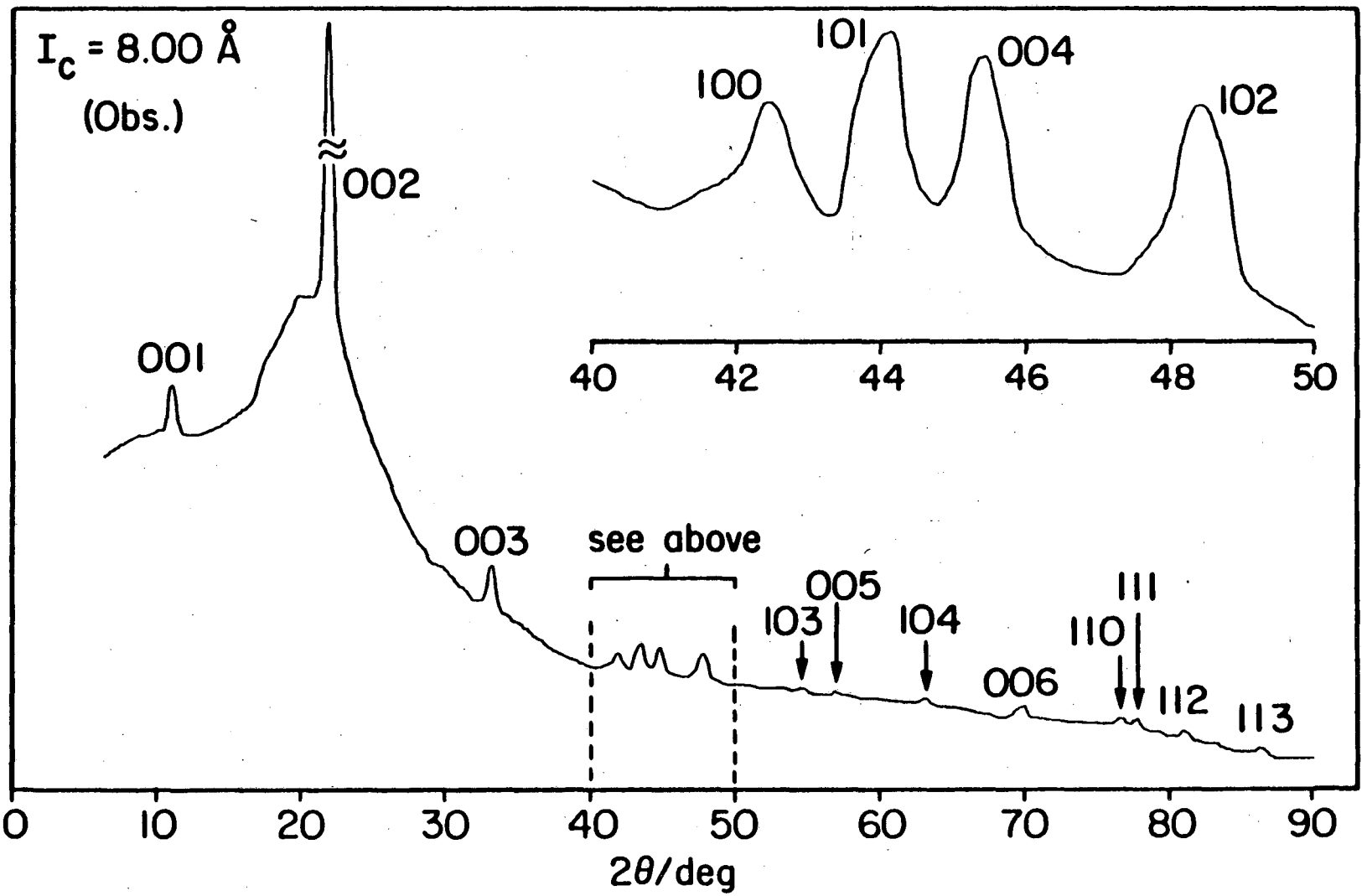

Figure 3.2. Observed X-ray diffraction pattern for a sample of the composition ca. $C_{10}AsF_6$ with I_c = 8.00 Å.

XBL 849-3742

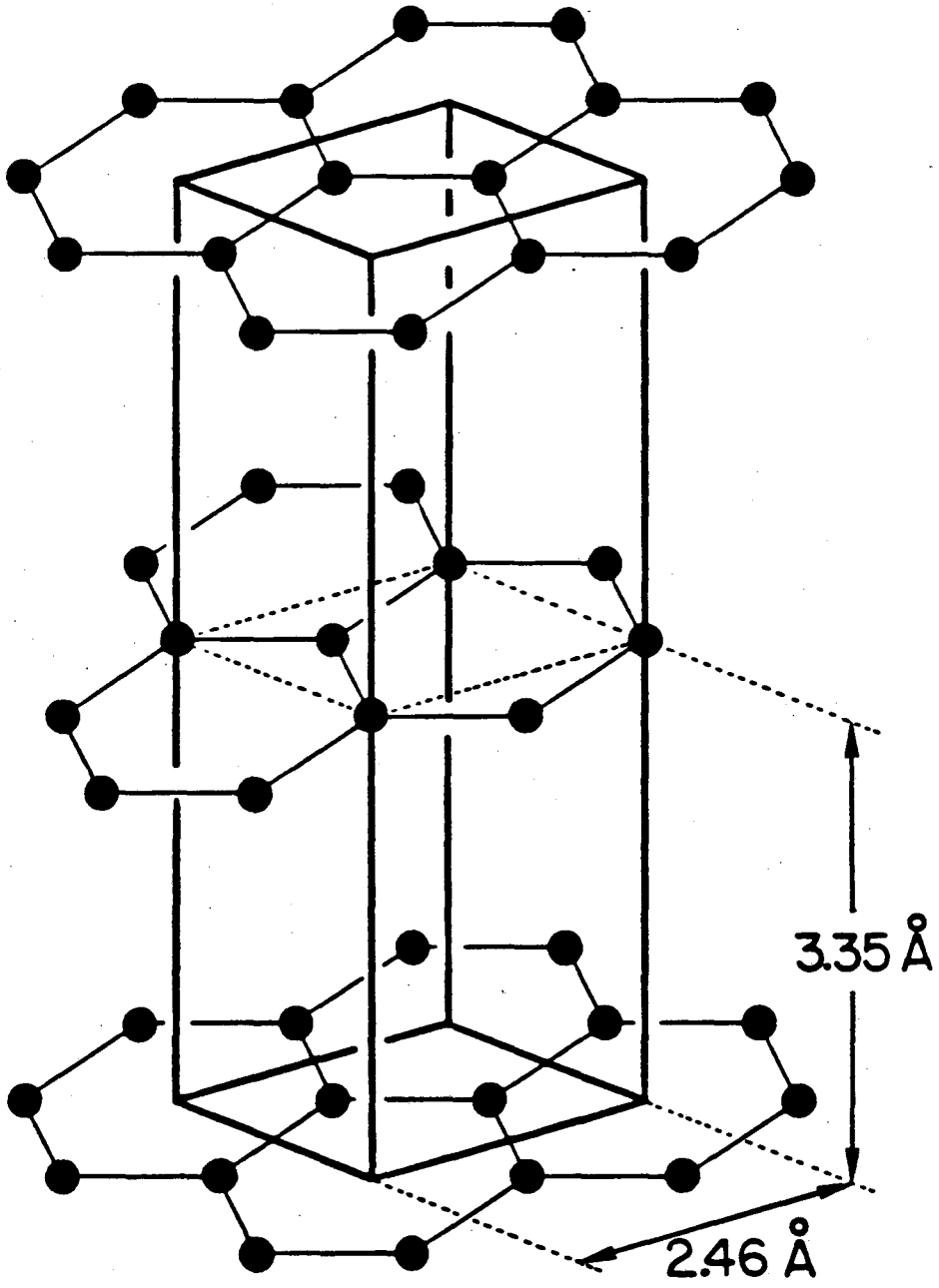

XBL 849-3743

Figure 3.3. Structure of graphite: a_0 = 2.46 Å and c_0 = 6.70 Å.

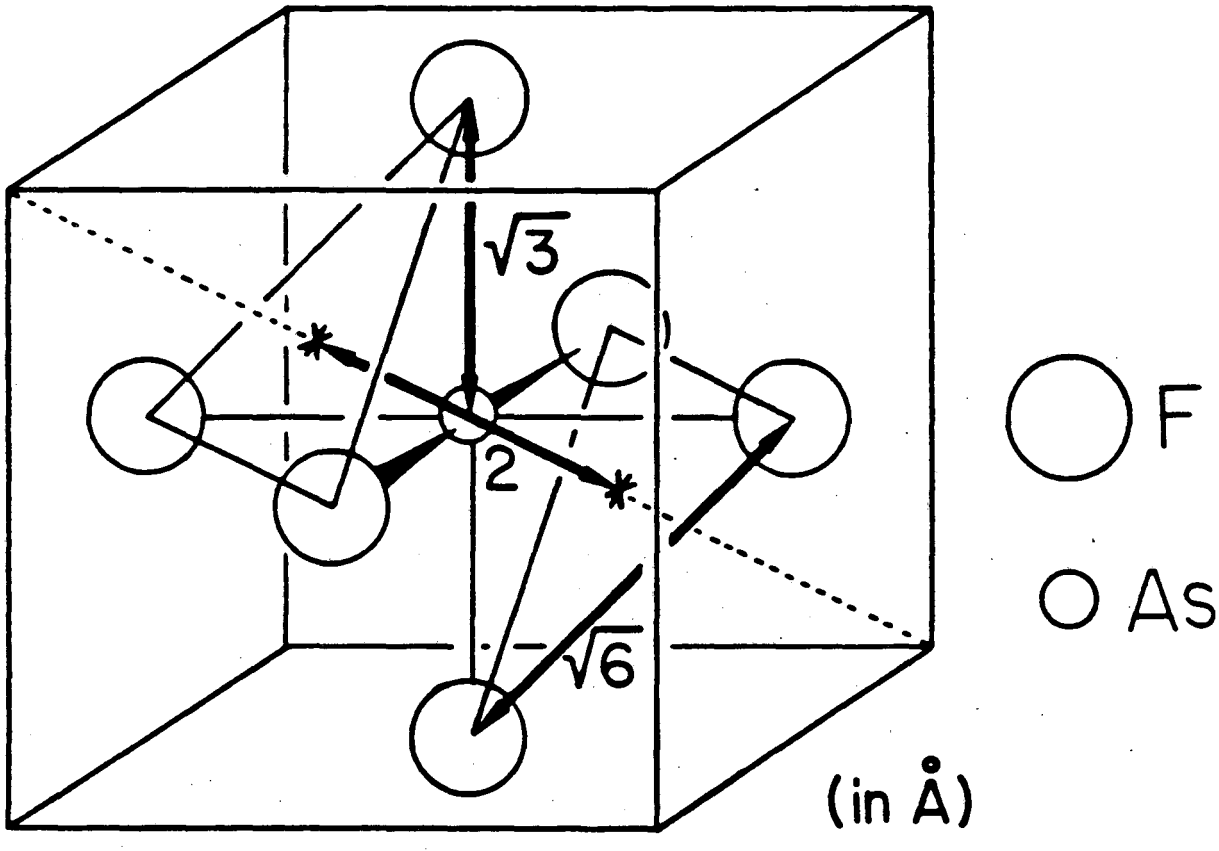

XBL 849-3744

Figure 3.4. Geometry of the AsF_6^- anion. The relationships of As-F, F-F and inter-plane (defined by two sets of three fluorine atoms) distances in O_h symmetry. The As-F distance is set equal to $\sqrt{3}$ Å. ($\sqrt{3} \approx 1.73$, $\sqrt{6} \approx 2.45$)

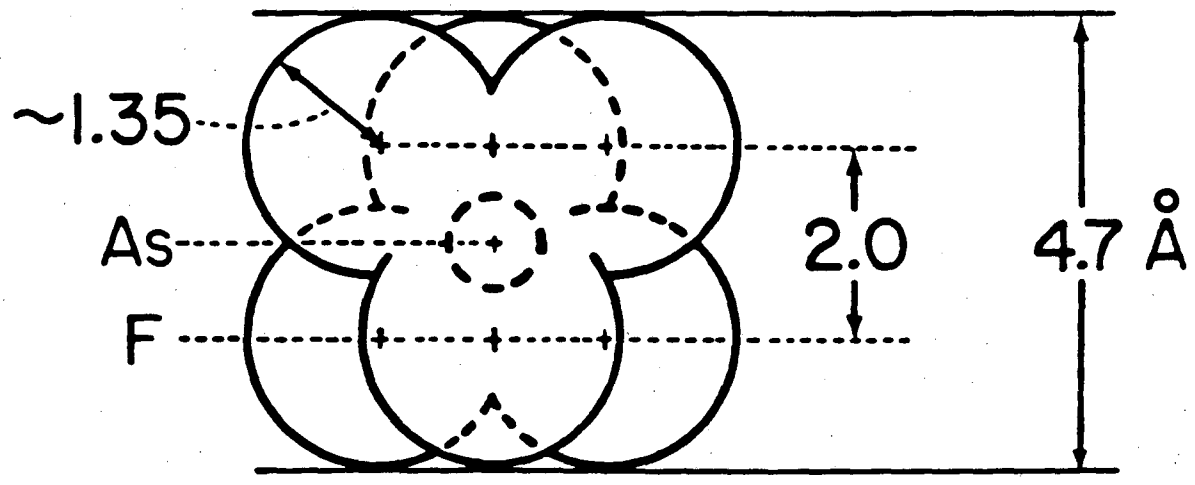

Figure 3.5. Geometry of the AsF_6^- anion. The "height" of the AsF_6^- anion.

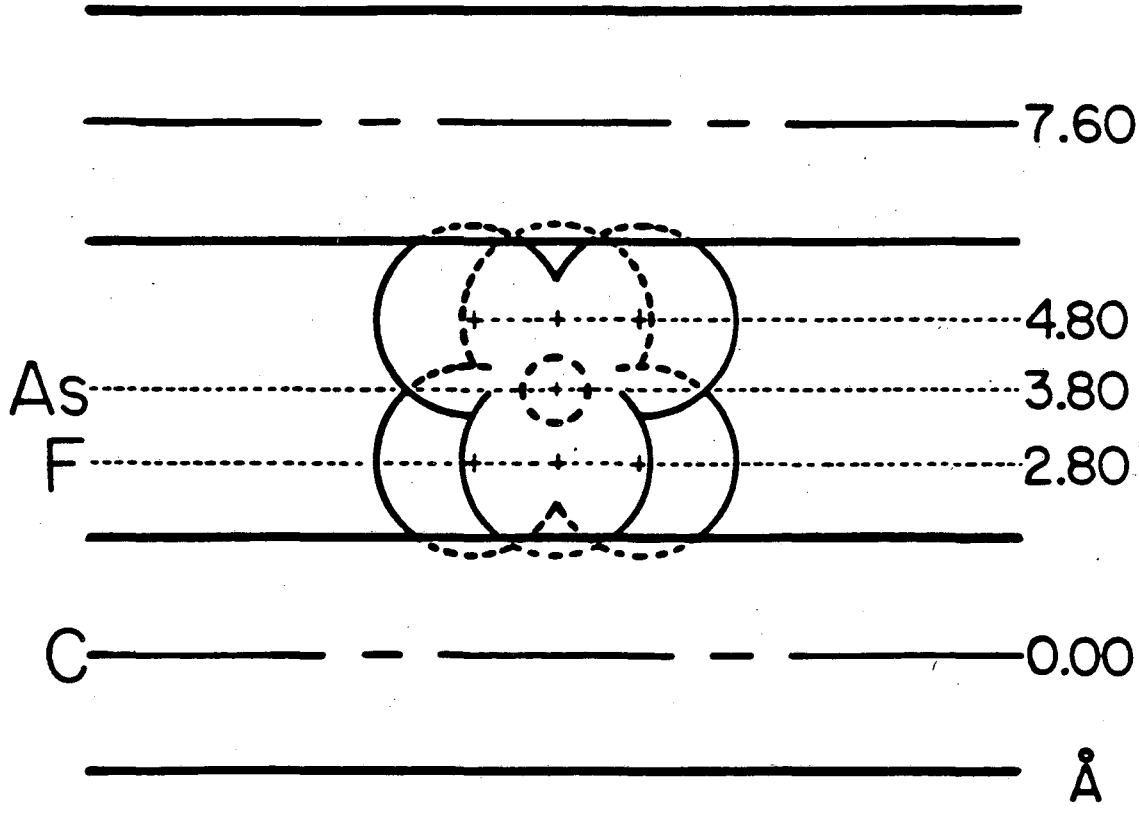

XBL 849-3746

Figure 3.6. A view along an axis parallel to the carbon ab-plane for the nestled AsF_6^- anion between carbon layers with I_c = 7.60 Å. (z values given were used for the calculation.)

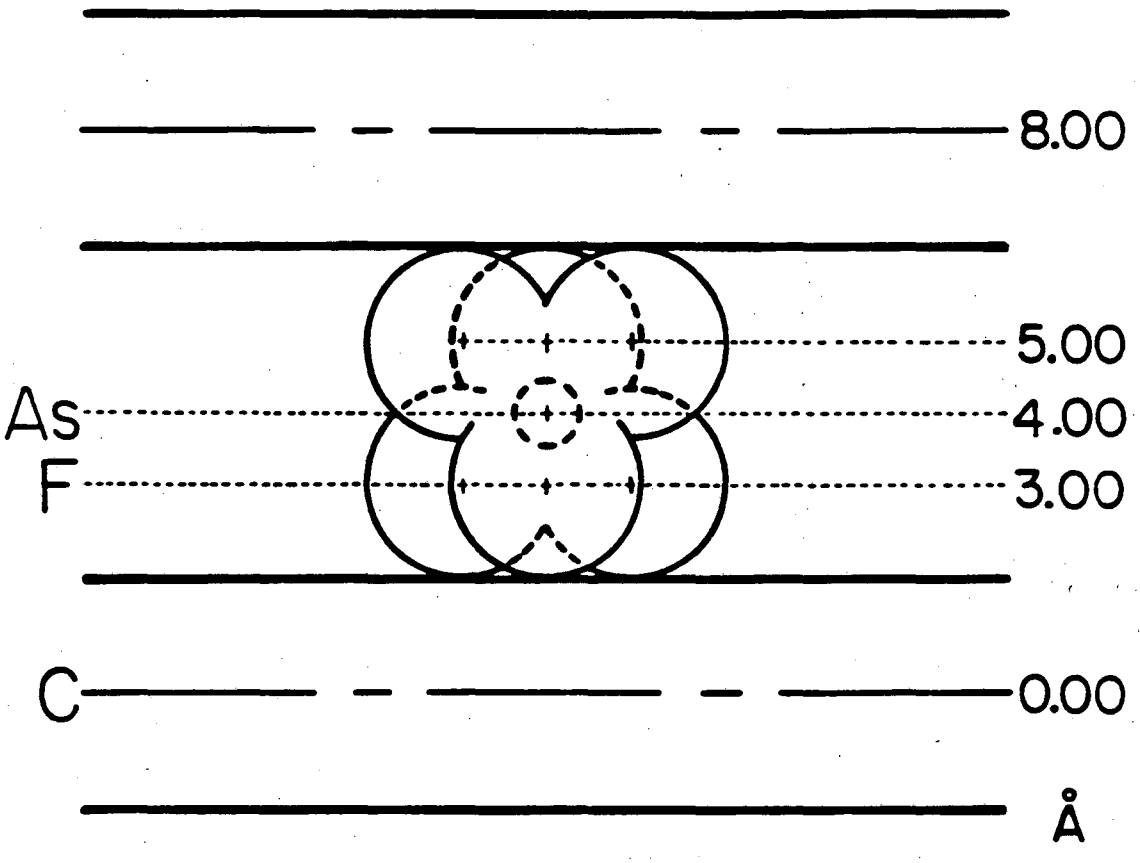

Figure 3.7. A view along an axis parallel to the carbon ab-plane for the un-nestled AsF_6^- anion between carbon layers with I_c = 8.00 Å. (z values given were used for the calculation.)

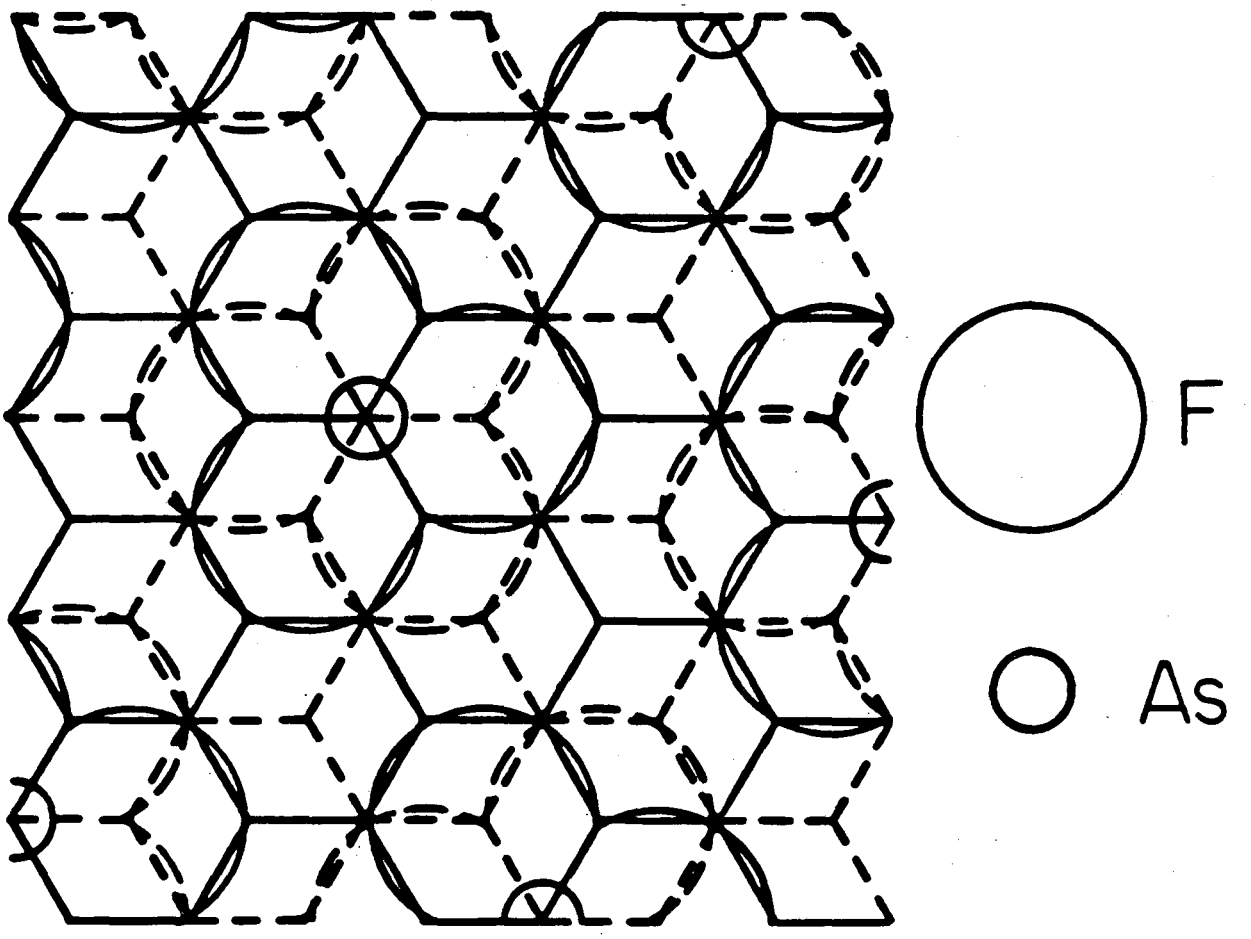

XBL 849-3748

Figure 3.8. Requirement of staggering of carbon layers (as in graphite) imposed by the nestling of AsF_6^- anions. (Solid-, and dashed-lined fluorine atoms, respectively, are nestled on solid-, and dashed-lined carbon hexagonal nets.)

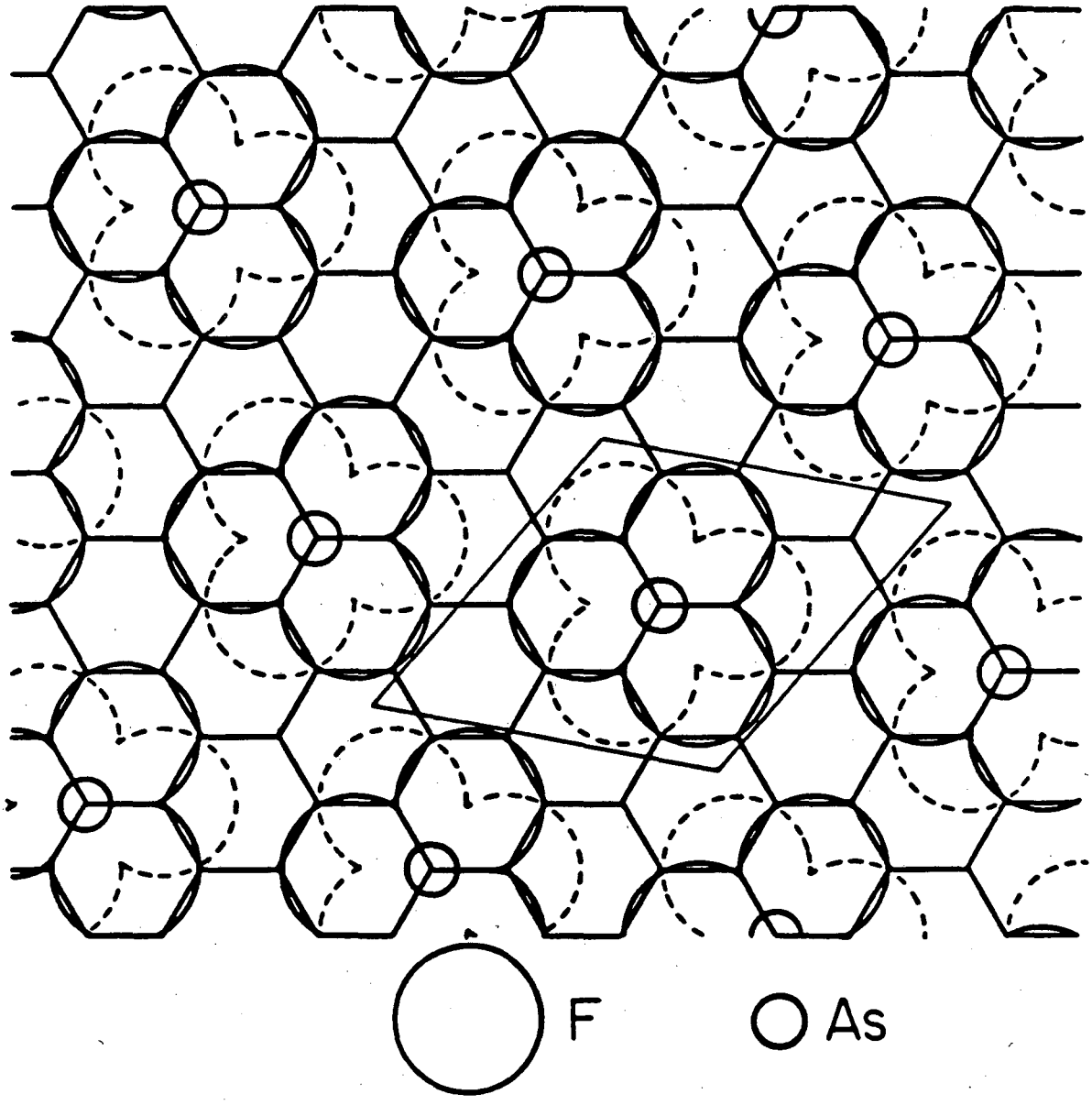

XBL 849-3749

Figure 3.9. Structure of nestled model with the composition $C_{14}AsF_6$. A unit layer of idealized nestled structure for $C_{14}AsF_6$. A possible pseudo-hexagonal unit cell with $a_0 = \sqrt{7}a_g$ (in the ab-plane projection) is shown.

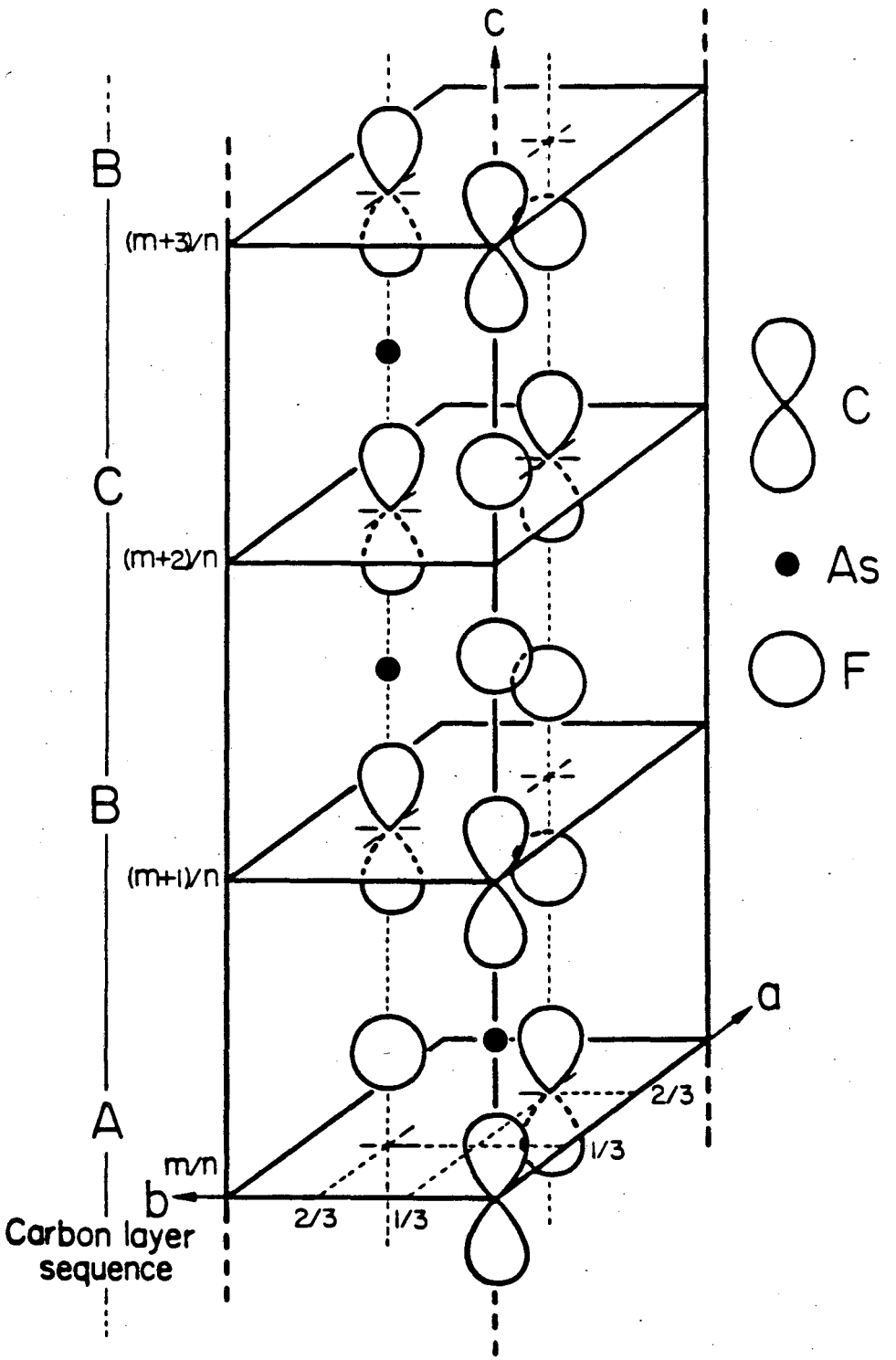

Figure 3.10. A part of the unit cell used for the intensity calculation of the nestled-small-cell model.

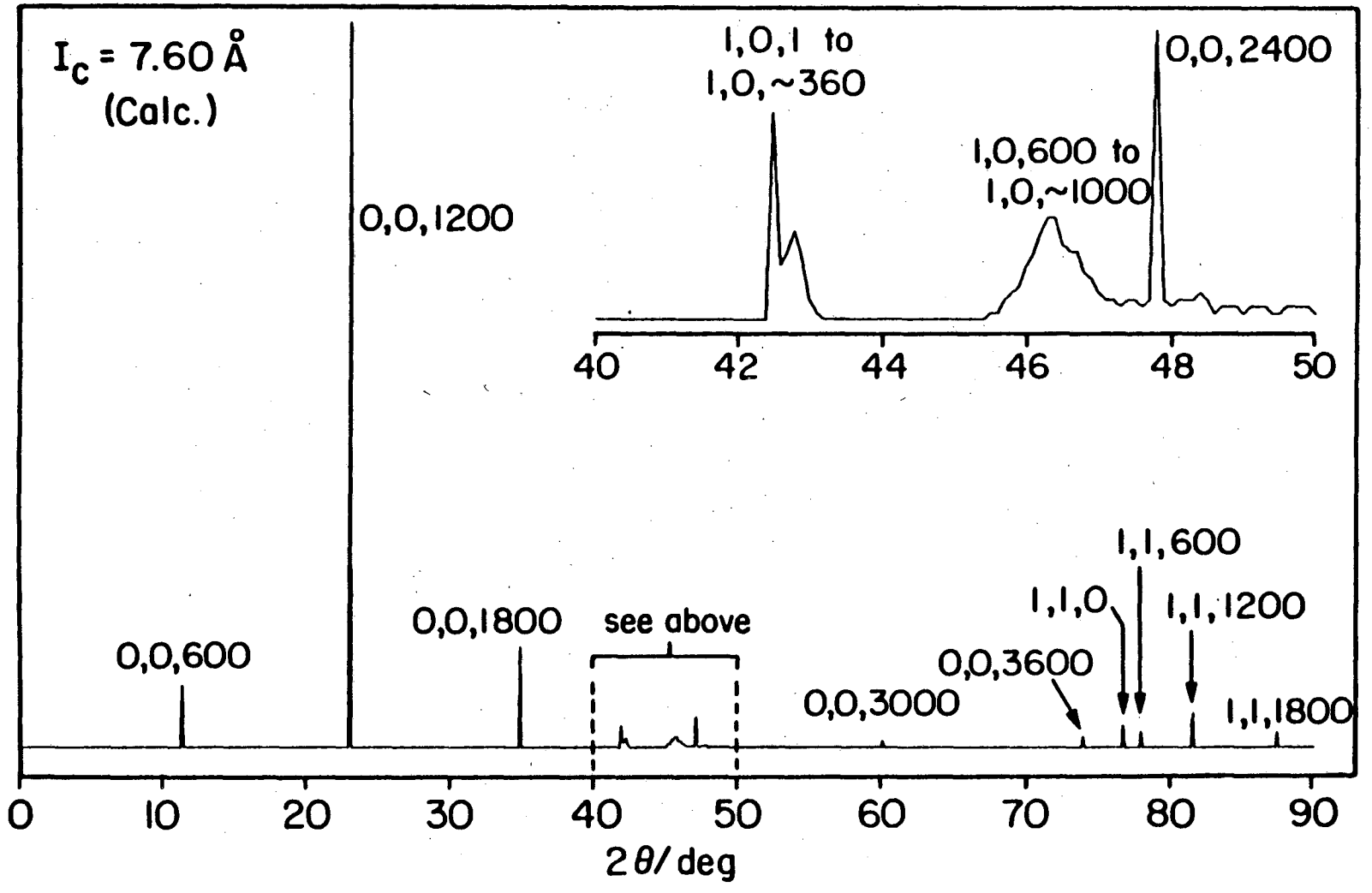

Figure 3.11. Calculated intensities by the nestled-small-cell model. XBL 849-3751

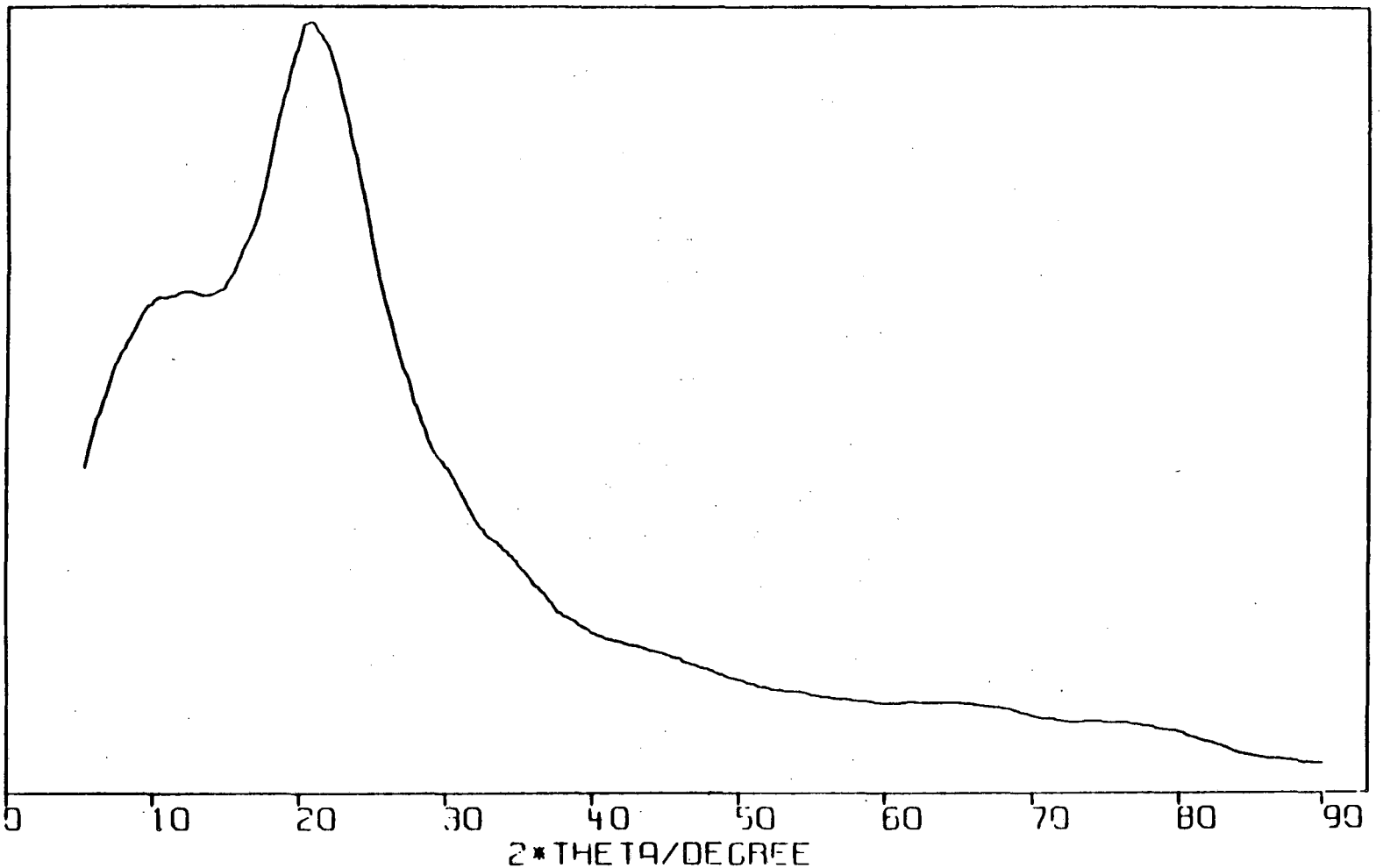

Figure 3.12. The blank X-ray diffraction pattern of quartz capillary of 0.7 mm diameter.

XBL 849-3752

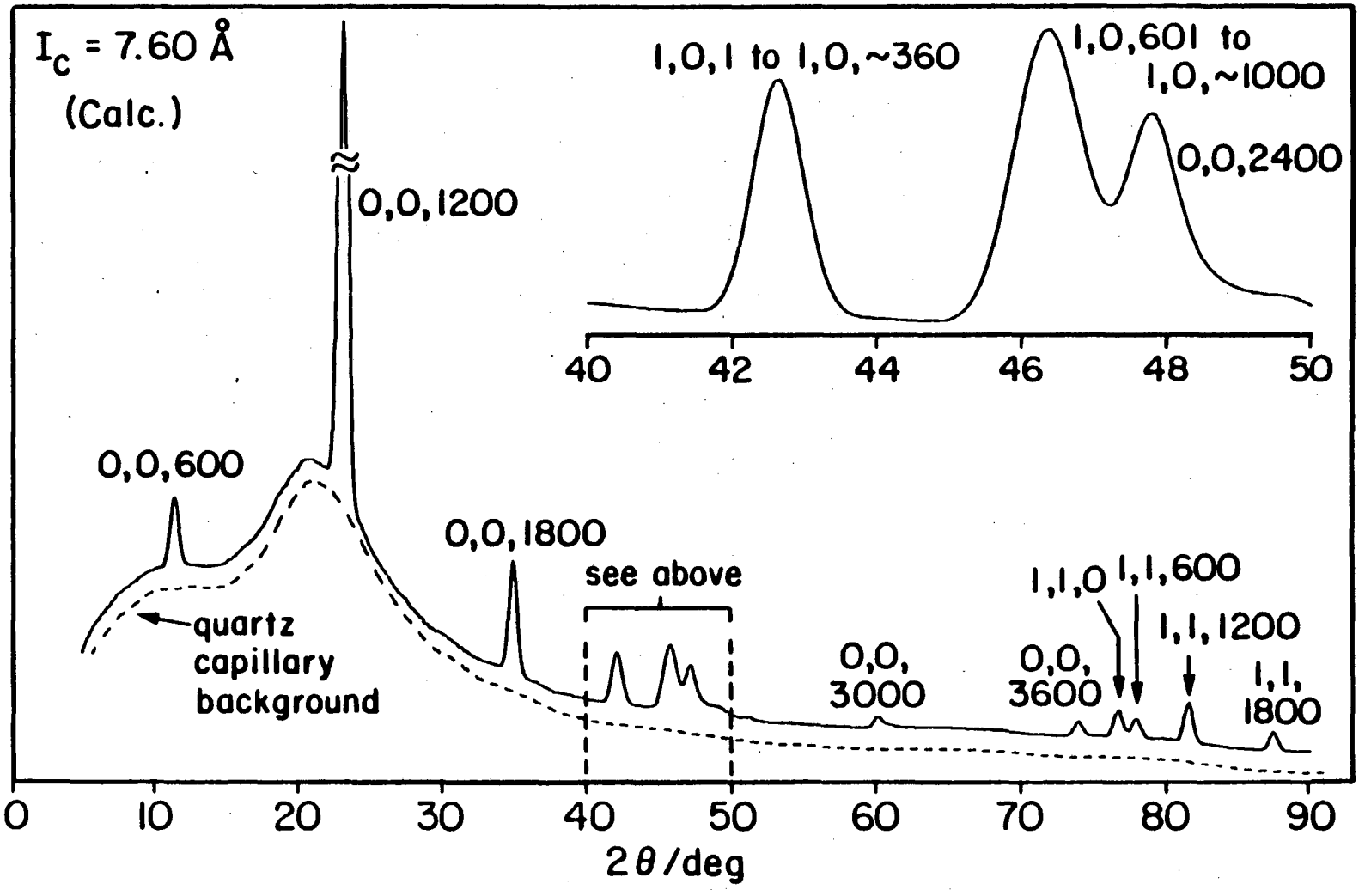

Figure 3.13. Simulated X-ray diffraction pattern by the nestled-small-cell model.

XBL 849-3753

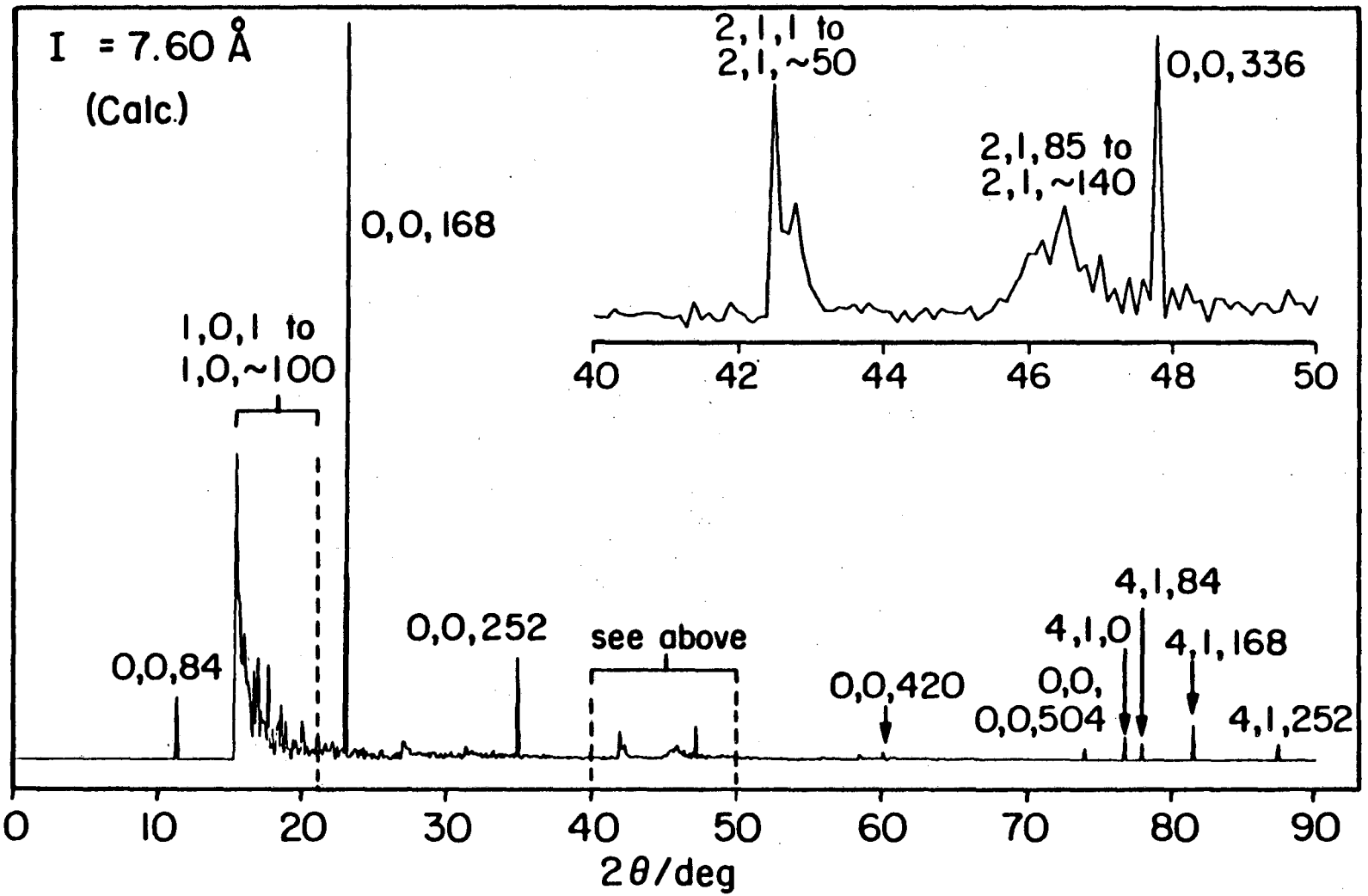

XBL 849-3754

Figure 3.14. Calculated pattern by the nestled-large-cell model. (Indices are given according to the pseudo-hexagonal unit cell with $a_0 = \sqrt{7}a_g$.)

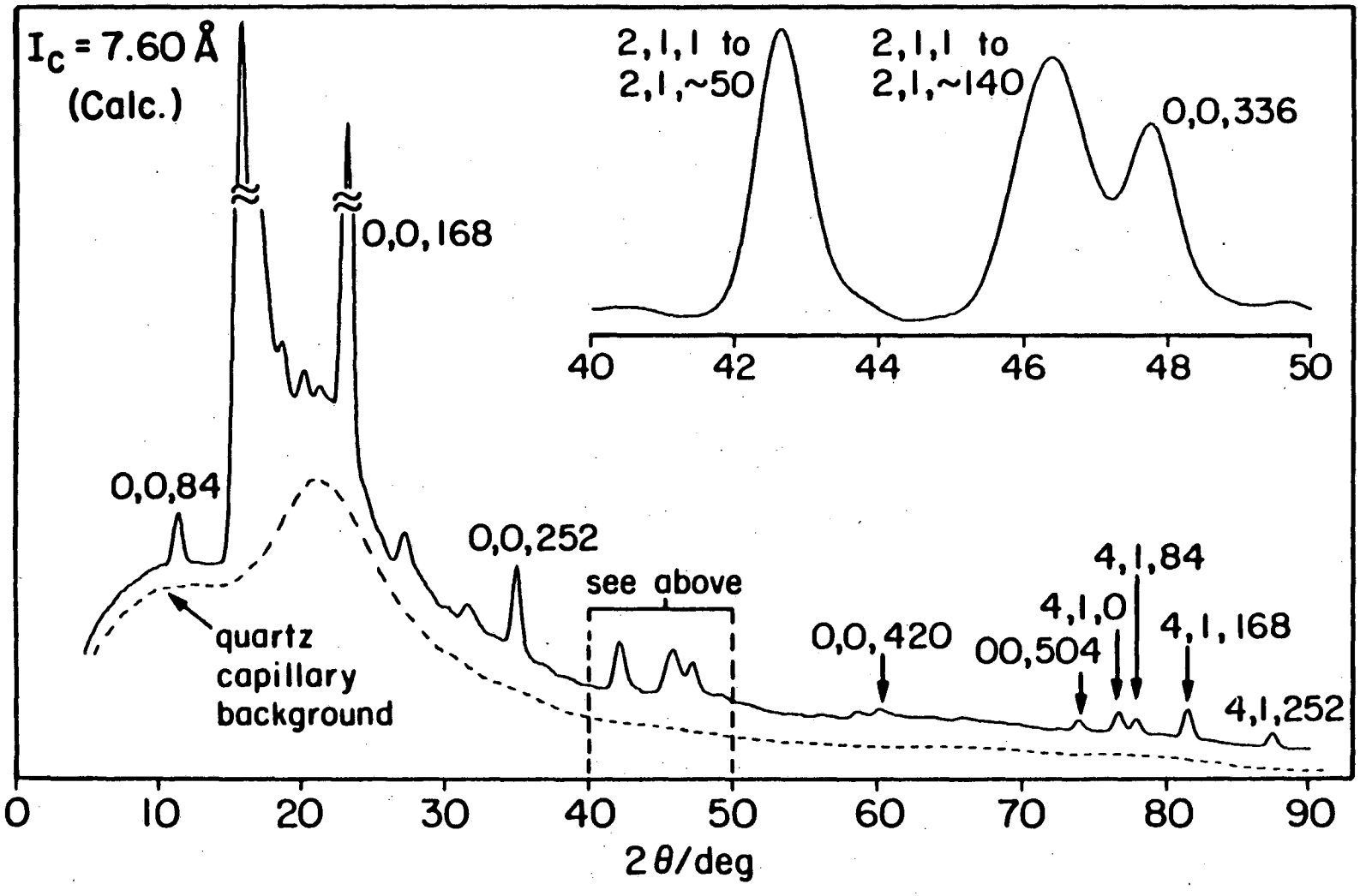

Figure 3.15. Simulated pattern by the nestled-large-cell model. XBL 849-3755

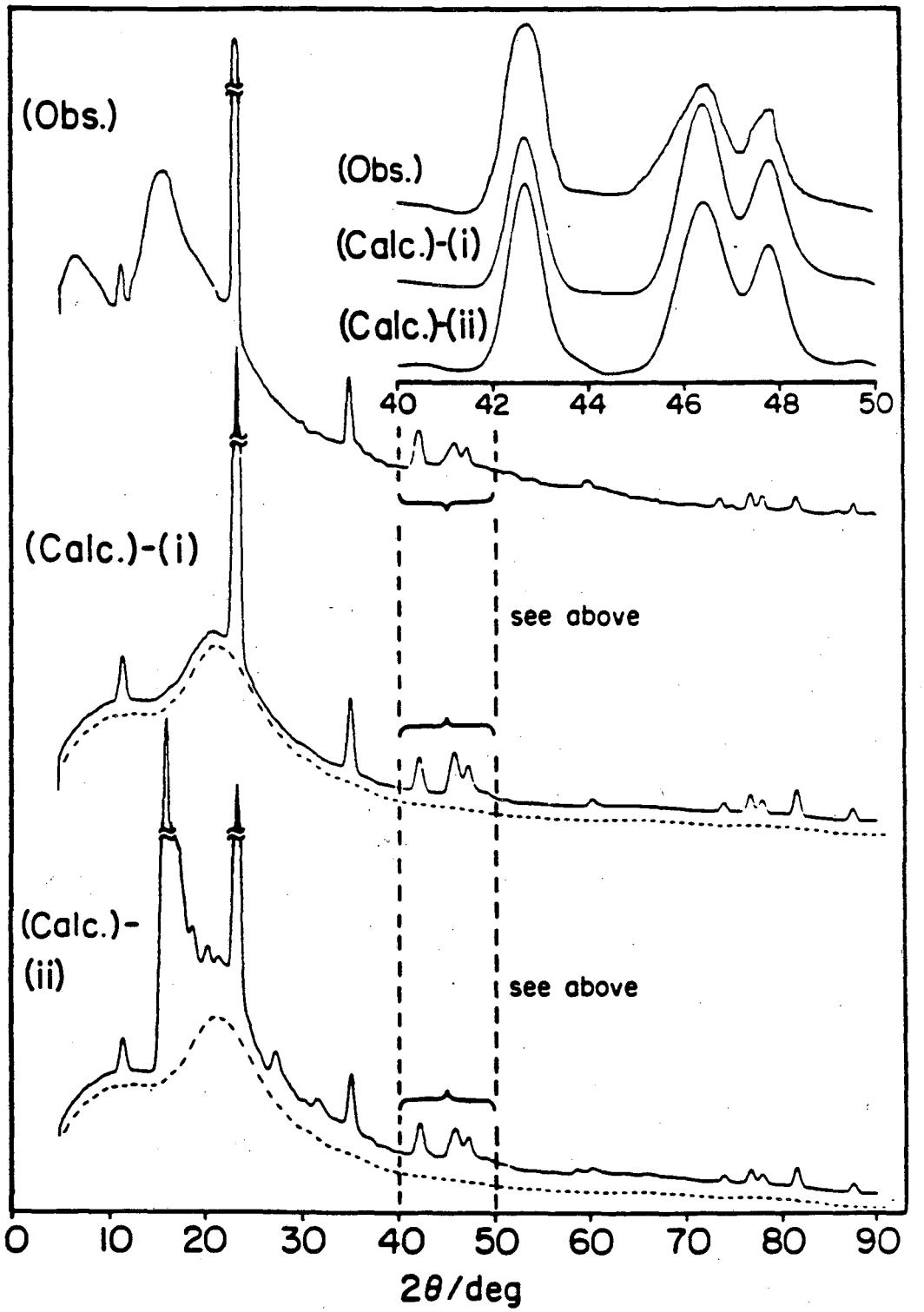

XBL 849-3756

Figure 3.16. Summary of the observed and calculated diffraction patterns for the small I_c-spacing (≈ 7.6 Å) material. Simulated patterns (i) and (ii), respectively, are calculated by the nestled-small-cell and the nestled-large-cell models.

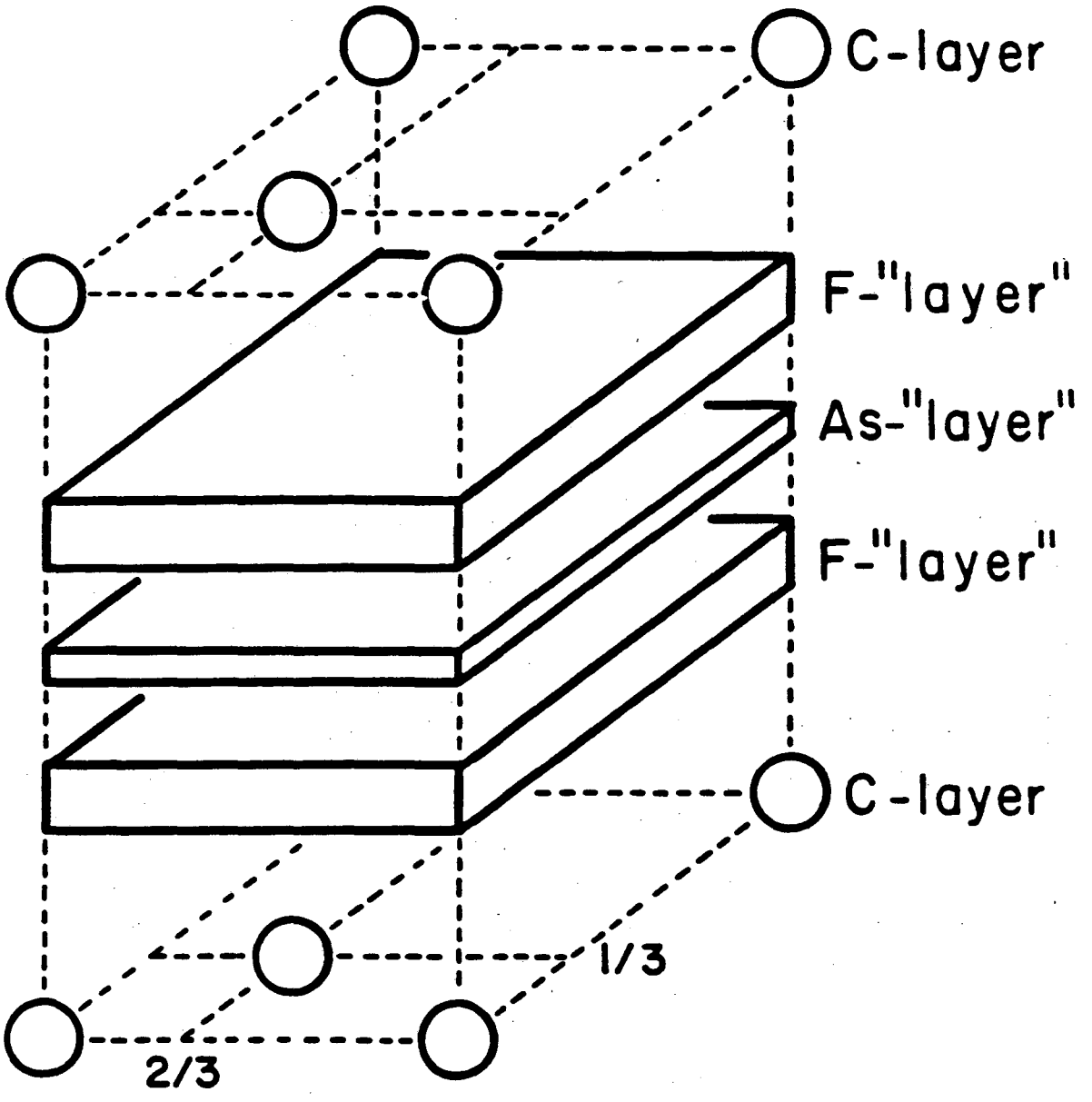

XBL 849-3757

Figure 3.17. A schematic drawing of the unit cell for the un-nestled model with $a_0 = a_g$ and $c_0 = 8.0$ Å.

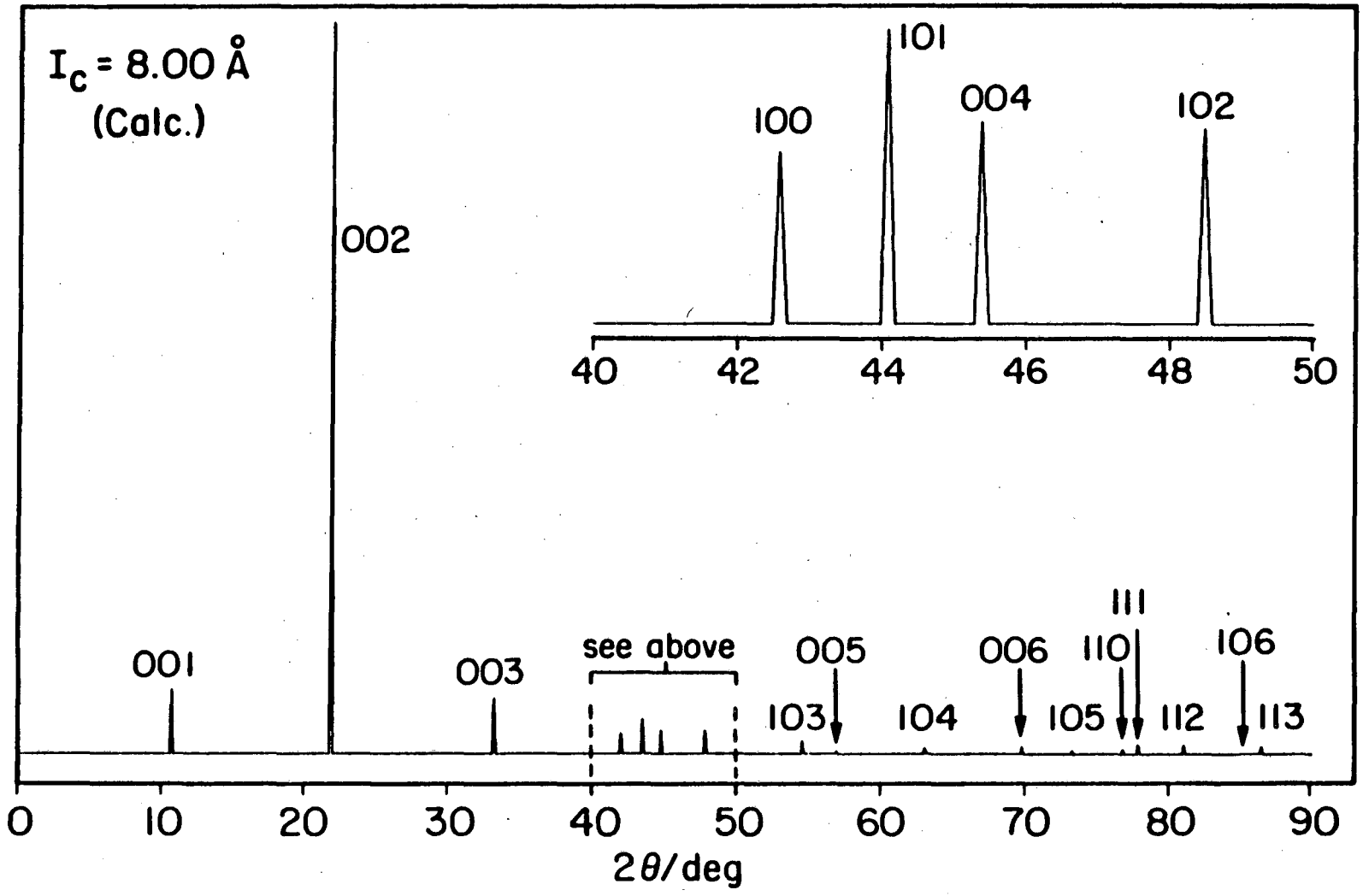

XBL 849-3758

Figure 3.18. Calculated intensities by the un-nestled model.

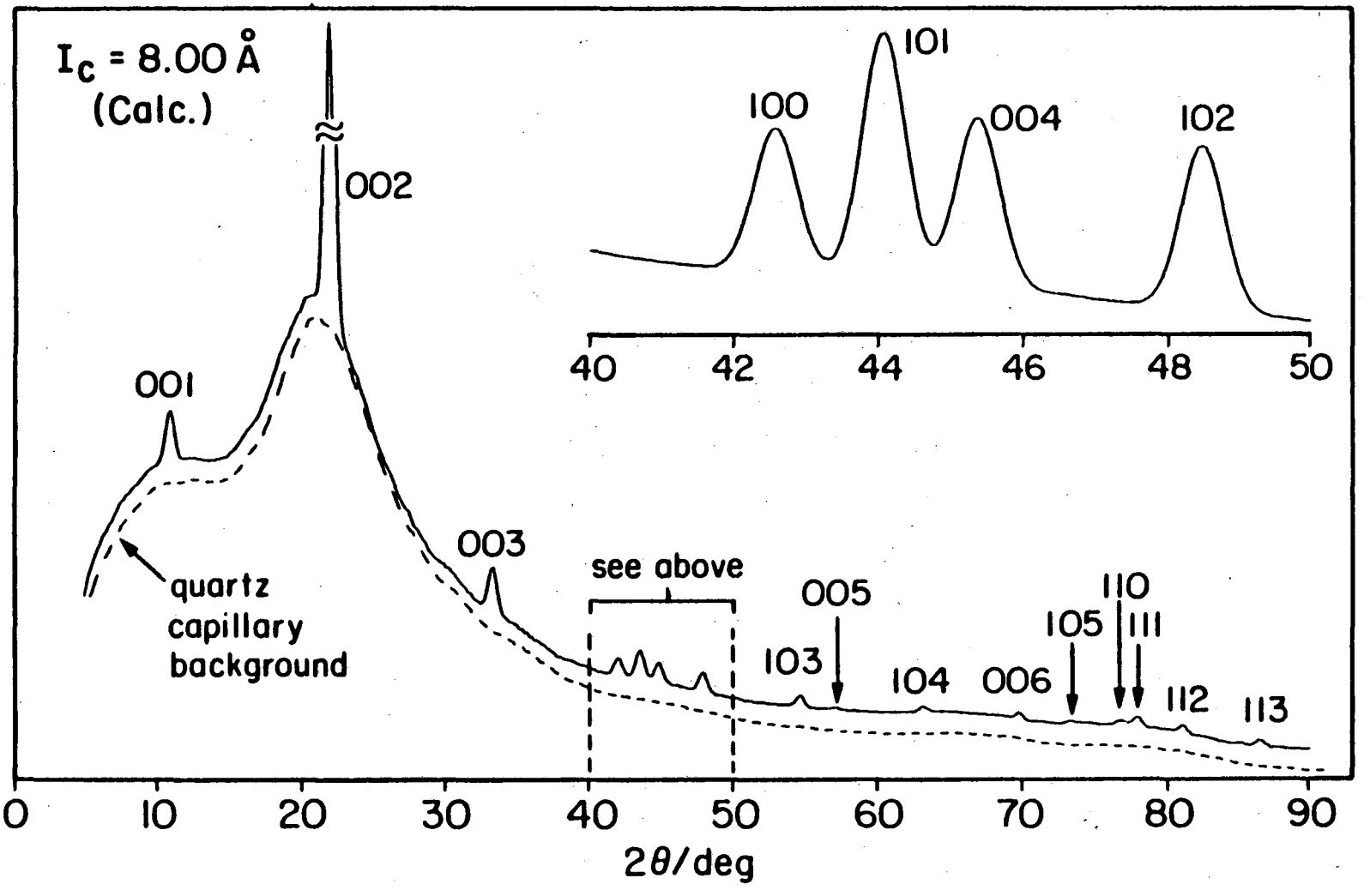

Figure 3.19. Simulated X-ray diffraction pattern by the un-nestled model.

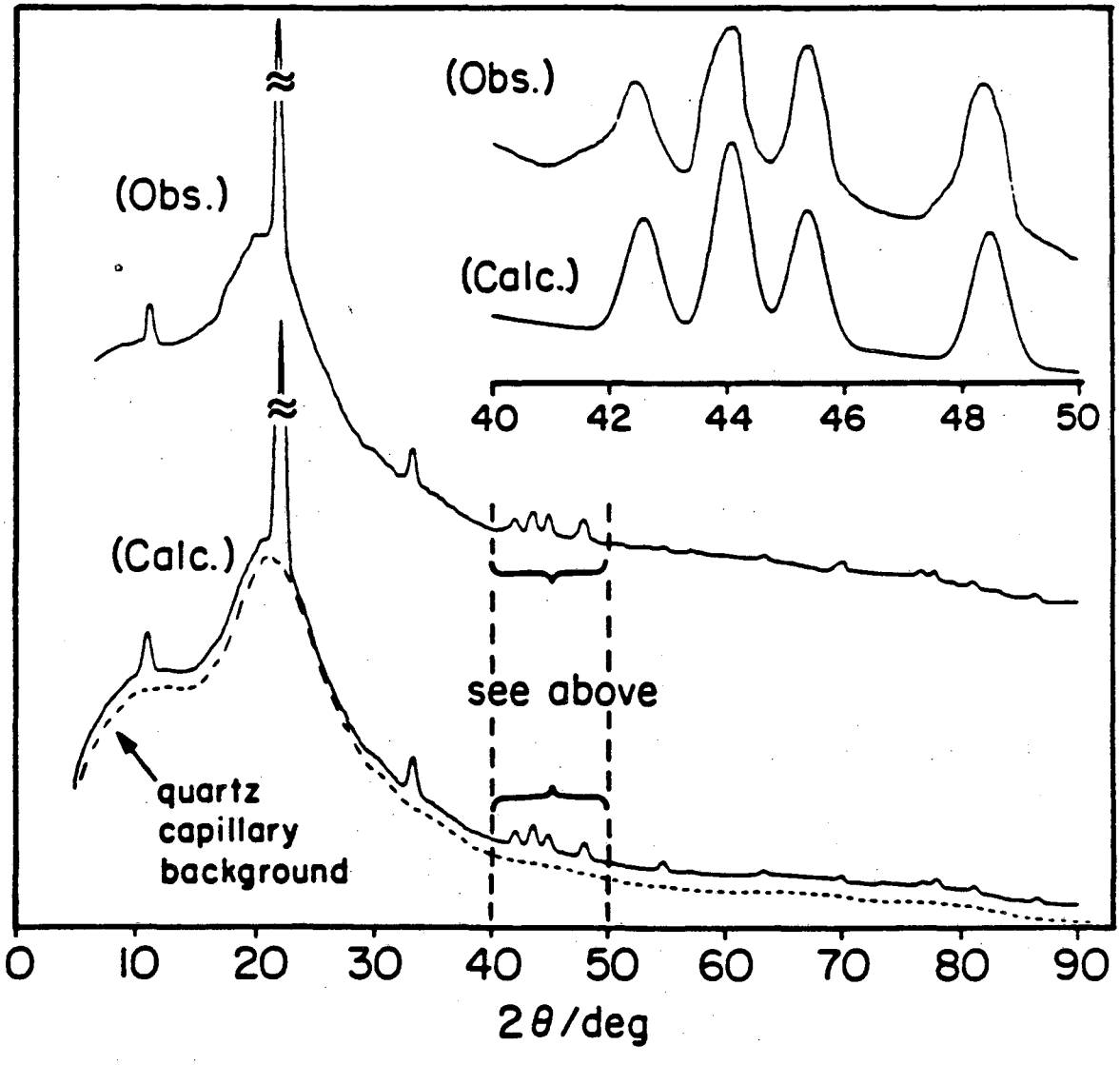

XBL 849-3760

Figure 3.20. Summary of the observed and calculated diffracion patterns for the large I_c-spacing (= 8.0 Å) material.

Chapter 4

MATHEMATICAL TREATMENT OF MODELS FOR $C_{14}AsF_6$: DISORDER BOTH ALONG THE C-AXIS AND WITHIN THE AB-PLANE

The nestled-small-cell model and the nestled-large-cell model proposed in the previous chapter were dealt with using probability functions which are to be described in this chapter. An extension of the large-cell model is also proposed. All of these models explicitly deal with the stacking disorder of carbon layers along the c-axis. The previously described small-cell model assumed perfectly random distribution of AsF_6^- consistent with the requirement of nestling, while the large-cell model and its extention assumed perfect ordering of AsF_6^- within each gallery. The lower angle X-ray diffraction halos (A) and (B) (see Figure 3.1), however, indicate only a short-range order in the AsF_6^- arrangement within each gallery. When the nestled AsF_6^- are ordered in small domains within each gallery, all observed X-ray diffraction data are satisfactorily accounted for.

4.1 Intensity Expression of Disordered Crystals[45-49]

The intensity of X-ray scattering by an object is given by

$$I = AA^*, \tag{4.1}$$

where A is the amplitude of the reflected beam by the whole object. If the object is a perfect crystal with many equivalent unit cells (strictly speaking the equivalency is attained only when the crystal is infinitely large.), A can be expressed by

$$A = \sum_j F \cdot \exp[(2\pi i/\lambda)(\mathbf{S}-\mathbf{S}_0)\cdot\mathbf{R}_j],$$

where $\mathbf{S}_0$ and $\mathbf{S}$ are unit vectors of the incident and scattered X-ray beams, $\mathbf{R}_j$ is a vector to define the position of the origin of the j-th unit cell, and F is the structure factor of the unit cell given by

$$F=\sum_n f_n \exp[(2\pi i/\lambda)(\mathbf{S}-\mathbf{S}_0)\cdot\mathbf{r}_n],$$

where f_n is the scattering factor of the n-th atom, and $\mathbf{r}_n$ is the position of the atom relative to the origin of the unit cell. Then the intensity is given by

$$I=\sum_{jj'} FF^* \exp[(2\pi i/\lambda)(\mathbf{S}-\mathbf{S}_0)\cdot(\mathbf{R}_j-\mathbf{R}_{j'})].$$

If the crystal is disordered, but the unit cells are still related by a translation vector $\boldsymbol{\delta}_j$ (displacement disorder), the amplitude will be

$$A=\sum_j F\cdot\exp[(2\pi i/\lambda)(\mathbf{S}-\mathbf{S}_0)\cdot(\mathbf{R}_j+\boldsymbol{\delta}_j)],$$

or

$$A=\sum_j F_j \exp[(2\pi i/\lambda)(\mathbf{S}-\mathbf{S}_0)\cdot\mathbf{R}_j],$$

where

$$F_j=F\cdot\exp[(2\pi i/\lambda)(\mathbf{S}-\mathbf{S}_0)\cdot\boldsymbol{\delta}_j]. \qquad (4.2)$$

If different atoms can occupy the same site of the unit cell one at a time (substitution disorder), the amplitude and the structure factors will be given by

$$A=\sum_j F_j \exp[(2\pi i/\lambda)(\mathbf{S}-\mathbf{S}_0)\cdot\mathbf{R}_j]$$

$$F_j=\sum_n f_{j,n}\exp[(2\pi i/\lambda)(\mathbf{S}-\mathbf{S}_0)\cdot\mathbf{r}_n].$$

If the disorder is such that the structure factors differ from one another, while the positions of the unit cells are like those in a perfect crystal, ("whole-unit-cell substitution"), A and F will be expressed by

$$A=\sum_j F_j \exp[(2\pi i/\lambda)(\mathbf{S}-\mathbf{S}_0)\cdot\mathbf{R}_j] \qquad (4.3)$$

$$F_j=\sum_{n=1}^{N_j} f_{j,n}\exp[(2\pi i/\lambda)(\mathbf{S}-\mathbf{S}_0)\cdot\mathbf{r}_n],$$

where N_j is the number atoms in the j-th unit cell. The above two equations can take care of both displacement and substitution disorders, and can be applied to any substance. This is because any substance can

be considered to be comprised of many parallelepipeds whose structure factors are different from one another. Since the models considered later cannot be expressed by displacement disorder alone, the following derivation is based on these two equations. This is because two AsF_6^- anions in different galleries are, in some cases, related by a mirror plane parallel to the ab-plane (plus by a displacement). The idea of displacement disorder, however, will be fully incorporated into structure factors by using equation (4.2), since the three types of carbon layers are related by a displacement. The stacking disorders of a simple cubic-face-centered structure, a hexagonal-close-packed structure, pristine graphite, etc. can be dealt with displacement disorder alone.[45,48]

From Equations (4.1) and (4.3), we have

$$I=\sum_{jj'}\sum FF^{*}\exp[(2\pi i/\lambda)(\mathbf{S}-\mathbf{S}_0)\cdot(\mathbf{R}_j-\mathbf{R}_{j'})] \tag{4.4}$$

Defining $(\mathbf{S}-\mathbf{S}_0)/\lambda$ and $\mathbf{R}_j$ by

$$(\mathbf{S}-\mathbf{S}_0)/\lambda \equiv h\mathbf{a}^{*}+k\mathbf{b}^{*}+\ell\mathbf{c}^{*}$$

$$\mathbf{R}_j \equiv j_1\mathbf{a}+j_2\mathbf{b}+j_3\mathbf{c},$$

and putting $j_n=j_n'+m_n$, Equation (4.4) is written as

$$I=\sum_{jm}\sum F_jF_{j+m}^{*}\exp 2\pi i(hm_1+km_2+\ell m_3), \tag{4.5}$$

where h, k and ℓ are continuous variables. For the rest of this chapter upper-case H, K, and L are used for integers and lower-case h, k, and ℓ for continuous variables.

4.2 Models (HKℓ)-(I), -(II), and -(III) (Disorder Along the c-Axis)

4.2.1 Description of the models

It is possible to express the intensities of disordered crystals by using probability functions. Three models have been considered which explicitly deal with the stacking disorder along the c-axis. The first

model corresponds to the nestled-small-cell model in Chapter 3, and will be called (HKℓ)-(I) model. The small-cell ((HKℓ)-(I)) model, "implicitly" assumes perfectly random distribution of AsF_6^- anions between two graphite layers (a gallery) with the requirement of nestling. Because of their "perfect" randomness the disordering in the occupied galleries relative to one another can be dealt with using the small lattice constant a_g appropriate for graphite. This implies a perfectly ordered structure for each small unit cell, but the occupancy in AsF_6^- is fractional (appropriate to the stoichiometry). The second model, (HKℓ)-(II), corresponds to the nestled-large-cell model in Chapter 3. The ordering of AsF_6^- anions is perfect, and the lattice consant a_0 is $\sqrt{7}a_g$. It should be noticed that there are two different arrangements of AsF_6^- nestled in a given pair of graphite carbon-atom layers. As shown in Figure 4.1, a given AsF_6^- (at the origin of the cell) can be surrounded by close AsF_6^- in two ways: designated R and S. The perfectly ordered arrangement in a given gallery will be represented either by a cell designated R or S. It is convenient to take hexagonal "unit" cell with $a_0 = 7a_g$, because such a unit has both patterns within its framework. This model will be called (HKℓ)-(III). The R-structure was arbitrarily chosen for model (II). It was assumed that AsF_6^- anions have a perfectly ordered arrangement within each gallery. This larger hexagonal "unit" cell was arrived at in the course of attempts to explain the very low angle halo (A) in Figure 3.1. However, the lower angle reflections below $\{210\}^{43}$, which corresponds to $[100]^{43}$ of model (II), should be extinct. To account for the low angle halo (A) it was necessary to make a more drastic change. This is described in Section 4.3.

The requirement in model (III) is more plausible than that in model

(II), in that it allows equal weight for the two orientations of the close-packed nestled AsF_6^- species labelled R and S. Model (I) implicitly assumes such a mixture of orientations; the close packing which gives rise to the R and S alternatives was not a part of the model. In models (II) and (III) it is assumed that the positions of AsF_6^- anions in one gallery have no influence on the relative positions of those in the neighboring galleries. In model (III) it is also assumed that there is no correlation between the R- and S-structures.

Models (I), (II), and (III), respectively, can be expressed by random stacking of 6, 42, and 84 different unit cells with lattice constants $a_0 = a_g$, $\sqrt{7}a_g$, and $7a_g$, and $c_0 = 7.60$ Å (see Table 4.1). The number of different unit cells will be designated by N. The subscript "p" in Table 4.1 deals with the fact that there are three kinds of carbon layers (A, B, and C). The subscript "q" was necessary because of the direction along the c-axis (two possible orientations of AsF_6^- anions related by a mirror plane parallel to the ab-plane). The subscript "r" was necessary because of the size of the superlattice $\sqrt{7}a_g$, i.e., there are 7 different sites whcih AsF_6^- can occupy. The subscript "s" was necessary to take care of the R and S types of the AsF_6^- arrangements. The assigned values for them are: $p = 0$, and ± 1; $q = \pm 1$; $r = 0, \pm 1, \pm 2$, and ± 3; and $s = \pm 1$. Model (I) deals with the ideas which the subscripts p and q represent, model (II) with p, q, and r, and model (III) with p, q, r, and s. The negative sign is replaced by a bar above the subscript. The definitions of the subscripts are such that the two R- and S-strucures given in Figure 4.1 are related via two operations, i.e $(HK\ell) \rightarrow (KH\ell) \rightarrow (KH\bar{\ell})$, according to Table 4.1, (III).

4.2.2 Structure Factors

The following discussion will be made mainly for model (I), unless special comments on the other models are necessary. The desired equations, however, will be given for all three models when a general equation is not applicable.

A side view of the six unit cells for model (I) is shown in Figure 4.2 (see also Figures 3.10, 3.9, and 4.1, respectively, for models (I), (II), and (III)).

Defining

(I) $\alpha \equiv 2\pi(H-K)/3$

(II) $\alpha \equiv 2\pi(H+5K)/21$

(III) $\alpha \equiv 2\pi(2H+K)/21$,

(I) β: not applicable

(II) $\beta \equiv 2\pi(3H+15K)/21$

(III) $\beta \equiv 2\pi(3H+3K)/21$,

and

$\eta \equiv \pi\ell$ and $\zeta \equiv 2\pi\ell z_f$,

where z_f is the z-coordinates of fluorine atoms (1.00/7.60), the structure factors F_{01}, F_{010}, and F_{0101} and their relations to those of the other unit cells can be given by

(I) $F_{01}(HK\ell) = 2f_c(\cos[\eta]+\cos[\alpha-\eta])+2f_f\cos[\alpha+\zeta]+f_{As}$

$F_{pq}(HK\ell) = F_{0q}(HK\ell)\exp\alpha ip$

$F_{p\bar{q}}(HK\ell) = F_{pq}(HK\bar{\ell})$,

$$(II)\quad F_{010}(HK\ell)=2f_c\sum_{n=0}^{6}\{\cos[\beta n-\eta]+\cos[\beta n+2\alpha-\eta]\}$$
$$+2f_F\{\cos[\alpha-\zeta]+\cos[4\beta-\zeta]+\cos[-5\beta-\zeta]\}+f_{As}$$
$$F_{pqr}(HK\ell)=F_{0qr}(HK\ell)\exp\alpha ip$$
$$F_{p\bar{q}r}(HK\ell)=F_{pqr}(HK\bar{\ell})$$
$$F_{pqr}(HK\ell)=F_{pq0}(HK\ell)\exp\beta ir,$$

and

$$(III)\quad F_{0101}(HK\ell)=2f_c\sum_{m=0}^{6}\sum_{n=0}^{6}\{\cos[6\pi(mH+nK)/21-\eta]$$
$$+\cos[6\pi(mH+nK)/21+\alpha-\eta]\}$$
$$+2f_F\sum_{m=0}^{6}\{\cos[\beta m-2\pi(2H+K)/21-\zeta]$$
$$+\cos[\beta m-2\pi(H-K)/21-\zeta]$$
$$+\cos[\beta m-2\pi(H+2K)/21-\zeta]\}+f_{As} \qquad (4.6)$$
$$F_{pqrs}(HK\ell)=F_{0qrs}(HK\ell)\exp\alpha ip$$
$$F_{p\bar{q}rs}(HK\ell)=F_{pqrs}(HK\bar{\ell})$$
$$F_{pqrs}(HK\ell)=F_{pq0s}(HK\ell)\exp\beta ir$$
$$F_{pqr\bar{s}}(HK\ell)=F_{pqrs}(KH\ell)\exp[2\pi ip(H-K)/21].$$

In models (I) and (II) the subscripts can be independently changed, whereas in model (III) the subscript s depends on p. In order to have the composition $C_{14}AsF_6$ the scattering factors for three kinds of atoms can be appropriately weighted. The factors $Wt_C:Wt_{As}:Wt_F$ are 7:2:6, 1:2:2, and 1:2:2, respectively, for models (I), (II), and (III).

The structure factors are defined between $-1/2 < z < 1/2$ with an arsenic atom at the origin. Since the structures at z and z+n, where n is an integer, are no longer equivalent, the requirement of $-1/2 < z < 1/2$ must be rigorous. This can be seen by noting that $\cos 2\pi\ell z$ is generally not equal to $\cos 2\pi\ell(z+1)$ when ℓ is a continuous variable. Such a requirement is not necessary for x and y. This is because the perfect ordering (or disordering in the case of model (I)) was assumed

within each graphite gallery, i.e., H and K are integers.

4.2.3 Expression of J_m (Probability functions)

If F_j in equation (4.5) depends only on m_3 and the crystal is large enough to validate an assumption that the summation variables j and m run from negative to positive infinites,[50] Equation (4.5) is transformed to

$$I=\sum_{m_1} \exp 2\pi i h m_1 \sum_{m_2} \exp 2\pi i k m_2 \sum_{m_3} J_{m_3} \exp 2\pi i \ell m_3, \qquad (4.7)$$

where $J_{m_3}=\langle F_j F^*_{j+m_3} \rangle$ is the mean value of $F_j F^*_{j+m_3}$ for all pairs of unit cells m_3-units apart along the c-axis. Equation (4.7) is non-zero only when h=H and k=K, where H and K are integers. Now we have

$$I(HK\ell) \propto \sum_m J_m \exp 2\pi i \ell m, \qquad (4.8)$$

where the subscript 3 in m_3 was omitted.

In order to calculate J_m it is necessary to know the probability of having one of the six unit cells m-layers away from a given cell. The m-th layer is stacked on the (m-1)-th layer, and the discussion is made for m>0. The same kind of discussion, however, can be made for m<0, and the final form of probabilities will be a function of the absolute value of m. Possible stacking sequences are shown in Figure 4.3 starting with the unit cell Φ_{01}. Defining $P_{pq,m}$ as the probability of finding one of the cells, Φ_{pq}, at the m-th layer, $P_{pq,m}$ can be expressed in terms of $P_{p'q',m-1}$ by

$$P_{\bar{1}1,m}=P_{0\bar{1},m}=(P_{\bar{1}\bar{1},m-1}+P_{11,m-1})/2$$

$$P_{11,m}=P_{\bar{1}\bar{1},m}=(P_{1\bar{1},m-1}+P_{\bar{1}1,m-1})/2$$

$$P_{01,m}=P_{1\bar{1},m}=(P_{11,m-1}+P_{0\bar{1},m-1})/2.$$

The cells with the same kind of carbon layers at the top and the bottom have the same probability of being at the m-th layer. By substituting $P_{p\bar{1},m}$ by equivalent $P_{p1,m}$, we have

$$2P_{\bar{1}1,m}=P_{01,m-1}+P_{11,m-1} \tag{4.9}$$

$$2P_{11,m}=P_{01,m-1}+P_{\bar{1}1,m-1}$$

$$2P_{01,m}=P_{11,m-1}+P_{\bar{1}1,m-1}.$$

If Φ_{01} is chosen as the zero-th layer, $P_{\bar{1}1,m}$ will be unique while $P_{11,m}$ and $P_{01,m}$ are left equivalent. Then we can put

$$P_{\bar{1}1,m}=(1/6)+u_t v^m$$

$$P_{11,m}=P_{01,m}=(1/6)+u_f v^m,$$

where the subscripts "t" and "f" stand for "two" and "four" (unit cells). By noting that the sum of the six probabilities is always one for any m (normalization), and that $P_{11,1}$ is zero in this case, we find $u_t = -2/3$, $u_f = 1/3$, and $v = -1/2$. Finally,

$$P_{\bar{1}1,m}=(1/6)-(2/3)(-1/2)^m \tag{4.9}$$

$$P_{11,m}=(1/6)+(1/3)(-1/2)^m. \quad (m>1) \tag{4.10}$$

Given a cell at the zero-th layer, the probability of having one of the two cells with the bottom carbon layer same as the top carbon layer of the zero-th layer cell is given by (4.9) and that of the other four cells including the same kind of unit cell at the origin is given by (4.10). In general

$$P_{t,m}=(1/N)-(4/N)(-1/2)^{|m|} \tag{4.11}$$

$$P_{f,m}=(1/N)+(2/N)(-1/2)^{|m|}. \quad (m\neq 0) \tag{4.12}$$

The equivalent probabilities for the sets of two and four for $m>1$ are different from those for $m<-1$: $P_{01,m}=P_{1\bar{1},m}$ for $m>1$, while $P_{01,m}=P_{\bar{1}\bar{1},m}$ for $m<-1$.

Now J_m is expressed by

$$NJ_m=J_t P_{t,m}+J_f P_{f,m} \quad (m\neq 0), \tag{4.13}$$

where J_t and J_f are

$$(I)\quad J_t \equiv \sum_{(pp')} [(F_{p1}+F_{p'\bar{1}})(F_{p\bar{1}}+F_{p'1})^*]$$

$$(II)\quad J_t \equiv \sum_{(pp')} [\sum_r (F_{p1r}+F_{p'\bar{1}r}) \sum_r (F_{p\bar{1}r}+F_{p'1r})^*]$$

$$(III)\quad J_t \equiv \sum_{(pp')} [\sum_{rs}\sum (F_{psrs}+F_{p'\bar{s}rs}) \sum_{rs}\sum (F_{ps\bar{r}s}+F_{p'srs})^*],$$

where $(pp')=(0\bar{1})$, $(\bar{1}1)$, and (10), and

$$(I)\quad J_f \equiv \sum_{(pp'p'')} [(F_{p1}+F_{p'\bar{1}})(F_{p1}+F_{p'1}+\sum_q F_{p''q})^*]$$

$$(II)\quad J_f \equiv \sum_{(pp'p'')r} [\sum (F_{p1r}+F_{p'\bar{1}r}) \sum_r (F_{p1r}+F_{p'1r}+\sum_q F_{p''r})^*]$$

$$(III)\quad J_f \equiv \sum_{(pp'p'')rs} [\sum\sum (F_{psrs}+F_{p''\bar{s}rs}) \sum_{rs}\sum (F_{ps\bar{r}s}+F_{p'srs}+\sum_q F_{p''srs})^*],$$

where $(PP'P'')=(0\bar{1}1)$, $(\bar{1}10)$, and $(10\bar{1})$.

The sum of J_t and J_f devided by N^2 is the square of the average of all the structure factors:

$$N^2\overline{F}^2 = J_t + J_f$$

and

$$(I)\quad N^2\overline{F}^2 = \left|\sum_{pq}\sum F_{pq}\right|^2$$

$$(II)\quad N^2\overline{F}^2 = \left|\sum_{pqr}\sum\sum F_{pqr}\right|^2$$

$$(III)\quad N^2\overline{F}^2 = \left|\sum_{pqrs}\sum\sum\sum F_{pqrs}\right|^2.$$

Defining

$$(I)\ (II)\ \text{and}\ (III)\quad P \equiv 1+2\cos[\alpha],$$

$$(I)\quad R \equiv 1$$

$$(II)\ \text{and}\ (III)\quad R \equiv 1+2(\cos[\beta]+\cos[2\beta]+\cos[3\beta]),$$

$$(I)\quad A \equiv F_{01}(HK\ell)$$

$$(II)\quad A \equiv F_{010}(HK\ell)$$

$$(III)\quad A \equiv F_{0101}(HK\ell)+F_{0101}(KH\bar{\ell}),$$

and

(I) $B \equiv F_{01}(HK\bar{\ell})$

(II) $B \equiv F_{010}(HK\bar{\ell})$

(III) $B \equiv F_{0101}(HK\bar{\ell}) + F_{0101}(KH\ell)$,

$N\bar{F}$ can be expressed by

$$N\bar{F} = PR(A+B).$$

From equations (4.13), (4.11) and (4.12) we have

$$\begin{aligned} N^2 J_m &= N(J_t P_{t,m} + J_f P_{f,m}) \\ &= (J_t + J_f) + 2(J_f - 2J_t)(-1/2)^{|m|} \\ &= N^2\bar{F}^2 + 2(J_f - 2J_t)(-1/2)^{|m|} \quad (m \neq 0), \end{aligned} \tag{4.14}$$

$(J_f - 2J_t)$ is calculated to be

$$J_f - 2J_t = 2R^2(1-\cos\alpha)\{(A^2+B^2-4AB)(2+\cos\alpha) - i3(A^2-B^2)\sin\alpha\}.$$

4.2.4 Intensity Expression

From Equation (4.8) we have

$$\begin{aligned} I &= N^2 \sum_m J_m \exp 2\pi i \ell m \\ &= N^2 J_0 + N^2 \sum_m{}' J_m \exp 2\pi i \ell m, \\ &= N^2 J_0 + 2N^2 \underline{\mathrm{Re}}\Big[\sum_{m=1}^{\infty} J_m \exp 2\pi \ell m \Big], \end{aligned}$$

where the primed summation sign excludes the origin term, i.e. $m \neq 0$, and the relationship

$$J_{-m} = J_m^*,$$

was used. This can be proved by deriving J_m for $m \leq 0$. Alternatively it can be seen by expressing J_m as the sum $\sum F_j F_{j+m}^*$ for a given and sufficiently large number, n, of pseudo-unit-cells, which is constant.[46b]

$$J_m = (1/n) \sum_{\substack{j \\ n\text{-unit-cells}}} F_j F_{j+m}^*.$$

Then substituting J_m with Equation (4.14), we have

$$I = N^2 J_0 + N^2\bar{F}^2 \sum_m{}' \exp 2\pi i \ell m + 4\underline{\mathrm{Re}}\Big[(J_f - 2J_t) \sum_{m=1}^{\infty} (-1/2)^{|m|} \exp 2\pi i \ell m\Big],$$

since

$$2\sum_{m=1}^{\infty}\exp 2\pi i\ell m = 2\sum_{m=1}^{\infty}\cos 2\pi\ell m$$
$$=\sum_{m}{}'\varepsilon\chi\rho^{2}\pi i\ell m.$$

By adding and subtracting $N^2\overline{F}^2$ the orgin can be recovered for the first summation:

$$I=N^2J_0+N^2\overline{F}^2\sum_{m}\exp 2\pi i\ell m-N^2\overline{F}^2+\sum_{m=1}^{\infty}(J_f-2J_t)(-1/2)^m\exp[-2\pi i\ell m]\,].$$

J_0, by definition, is the average of the squares of all the structure factors:

$$J_0=\overline{F^2}.$$

Defining

$$[CR]\equiv N^2\overline{F}^2\sum_{m}\exp 2\pi\ell m,$$

since this term corresponds to the usual expression for a crystal reflection with a structure factor $\overline{F}$, we have

$$I=[CR]+N^2(\overline{F^2}-\overline{F}^2)+4\underline{\mathrm{Re}}\,[(J_f-2J_t)\sum_{m=1}^{\infty}(-1/2)^m\exp 2\pi i\ell m\,].$$

Noting that

$$\sum_{m=1}^{\infty}(-1/2)^m\exp 2\pi i\ell m=\{(1+2\cos 2\pi\ell)+i2\sin 2\pi\ell\}/(5+4\cos 2\pi\ell),$$

we have

$$I=[CR]+N^2\overline{F^2}-P^2R^2(A^2+B^2)-8R^2\{(1-\cos\alpha)/(5+4\cos 2\pi\ell)\}\cdot$$
$$\{(A^2-4AB+B^2)(2+\cos\alpha)(1+2\cos 2\pi\ell)+6(A^2-B^2)\sin\alpha\sin 2\pi\ell\} \qquad (4.15)$$

4.2.5 Cases of H and K on the conditions of R, P, and (1-cosα)

In general three conditions can be considered, i.e., whether R, P, and/or (1-cosα) are zero or non-zero. The corresponding conditions on H and K, when they are zero, are

R=0 (I) not applicable (R≡1)

(II) H+5K=(1, 2, 3, 4, 5, or 6) + 7n

(III) H+K=(1, 2, 3, 4, 5, or 6) + 7n,

$P=0$ (I) $H-K=\pm 1+3n$

(II) $H+5K=\pm 7+21n$

(III) $H+K=\pm 7+21n$,

$1-\cos\alpha=0$ (I) $H-K=3n$

(II) $H+5K=21n$

(III) $H+K=21n$.

Of the possible combinations of the three conditions, four cases lead to different intensity expressions:

(i) $1-\cos\alpha=0$ for (I), (II), and (III).

Under these conditions all the structure factors become equivalent and the intensity is simply given by

$$I=[CR].$$

(ii) $R\neq 0$ and $P=0$ for (I), (II), and (III).

Under these conditions $\overline{F}$ is zero, and, therefore, [CR] is zero. Intensity is given by

$$I=N^2\overline{F^2}-8R^2\{(1-\cos\alpha)/(5+4\cos 2\pi\ell)\}$$
$$\cdot\{(2+\cos\alpha)(1+2\cos 2\pi\ell)(A^2-4AB+B^2)+6\sin\alpha(A^2-B^2)\sin 2\pi\ell\}.$$

(iii) $R=0$ for (II) and (III).

Although three sub-cases could be made, i.e. $P=0$, $(1-\cos\alpha)=0$, or $P(1-\cos\alpha)\neq 0$, they all lead to the same intensity expression:

$$I=N^2\overline{F^2}. \qquad (4.16)$$

[CR] is again zero, since $\overline{F}$ is zero.

(iv) $RP(1-\cos\alpha)\neq 0$ for (III)

This formally leads to the full intensity expression given by Equation (4.15). Although there are possible (HK) under this condition for model (III), no non-zero intensity occurs. All the structure factors

are zero.

4.2.6 Conversion of intensities from "in reciprocal space" to "in Debye circle"[47,48]

In powder diffraction patterns, the power, $P(\theta)d\theta$, associated with unit length of a Debye circle is measured. In terms of the intensity distribution $I(H_0K_0\ell)d\ell$ of the reciprocal lattice, we have

$$P_{H_0K_0\ell}(\theta) \propto I(H_0K_0\ell)\{(1+\cos^2 2\theta)/(\sin^2\theta\cos\theta)\}d\ell/d\theta$$

where H and K are assigned constant values of H_0 and K_0, and the quotient $(1+\cos^2 2\theta)/(\sin^2\theta\cos\theta)$ is the Lorenz-polarization factor applicable for the Debye-Scherrer method. If θ_0 is the glancing angle corresponding to $\ell=0$ for a given set of H ($=H_0$) and K ($=K_0$), the relationship between ℓ and θ becomes

$$\ell=(2c/3\lambda)(\sin^2\theta-\sin^2\theta_0)^{1/2}$$

Accordingly we have

$$P_{H_0K_0\ell}(\theta) \propto I(H_0K_0\ell)(1+\cos^2 2\theta)/\{\sin^2\theta(\sin^2\theta-\sin^2\theta_0)^{1/2}\}. \qquad (4.17)$$

This equation is not realisic, since $P(\theta)$ is infinite when $\theta=\theta_0$. Modifications[49] were not made.

4.3 Three Dimensional Disorder Model (Disorder Both Along the c-Axis and Within the ab-Plane)

Although halo (B) in Figure 3.1 was partially explained by models (HKℓ)-(II) and -(III), they fail to explain the fact that halo (B) extends to lower angle than that of [100] for model (II), or {210} for model (III). It can not be reasonably accounted for by the "line width" of [10ℓ] or {21ℓ} reflections. Furthermore another halo (A) in Figure 3.1 at the lower angle cannot be explained by these models.

Models (II) and (III) have dealt with the disorder along the c-axis. They, however, assumed that each layer has a perfectly ordered

AsF_6^- arrangement. Model (I) assumed that the anions are nestled but are totally randomly distributed. The actual samples "C_xAsF_6" are likely to have an arrangement of the anions somewhere between these two extremes for the following reasons. Even if the comfortable nestling of AsF_6^- can persist when $x=14$, x is seldom exactly 14 in actual samples. Perhaps more importantly, as recognized in model (III), there must be R and S arrangements within each gallery (see Figure 4.1). But it is highly unlikely that a gallery would be wholely R or wholely S. It is probable that nestling of AsF_6^- begins at many places within a gallery and that domains of R and S character develop in each gallery. The diffraction characteristics of such a domain structure were explored.

Based on the above considerations a model with a short-range order of AsF_6^- anion arrangement was proposed. This model will be called (hkℓ) model. Now h, k, and ℓ are all continuous variables signifying three dimensional disorder. In order to incorporate the R- and S-structures it is best to assume that domains have a hexagonal lattice constant $a_0=7Ma_g$, where M is an integer. This implicitly assumes the domain has a lattice constant of at least $7a_g$ (see Discussion). The following discussion will be made for the smallest domain, i.e. $M=1$, and the modification will be made later to incorporate the cases with $M>2$.

The model has assumed that all possible sites for AsF_6^- nestling (an arsenic atom between eclipsed carbon atoms) can be occupied by AsF_6^- with an equal probability (same as model (HKℓ)-(I)), and each AsF_6^- anion has an equal probability of being at the center of the domain. There can be four different structures for a given pair of eclipsed carbon atoms. They correspond to Φ_{0101}, $\Phi_{010\bar{1}}$, $\Phi_{0\bar{1}01}$, and $\Phi_{0\bar{1}0\bar{1}}$ of model (HKℓ)-(III). The structure factors are defined between $-1/2 < x,y,z < 1/2$ (except for some

of the fluorine atoms of AsF_6^- anions near the border) with an arsenic atom at the origin (see Equation (4.6)). The disorder in the ab-plane was realized by displacing the origin to one of the 48 other possible sites for AsF_6^- nestling (see Figure 4.1). It is noticed that in models (HKℓ)-(II) and -(III) the "displacement disorder" could be incorporated into the "whole-unit-cell substitution". It was possible because a perfect order was assumed in the ab-plane. In this model, however, displacement must be treated as it is. This statement is equivalent to the requirement $-1/2 \leq x,y,z \leq 1/2$ for Equation (4.6). All domain sizes are assumed to be the same. Carbon layers are assumed to be perfect and do not contribute to the intensities except for the reflections which correspond to usual graphite (HK0) and the corresponding (HKℓ) reflections. The treatment of the stacking disorder was the same as the (HKℓ) models.

Starting with the general equation (Equation (4.5)) for the three dimensional disorder, we have

$$
\begin{aligned}
I &= \sum_{m_1 m_2 m_3} \sum \sum J_{m_1+m_2+m_3} \exp 2\pi i(hm_1+km_2+\ell m_3) \\
&= \sum_{m_1 m_2} \sum J_{m_1+m_2} \exp 2\pi i(hm_1+km_2) \\
&\quad + \sum_{m_1 m_2} \sum \Big(\sum_{m_3}'\Big) J_{m_1+m_2+m_3} \exp 2\pi i(hm_1+km_2+\ell m_3) \\
&= J_0 + \Big(\sum_{m_1 m_2} \sum\Big)' J_{m_1+m_2} \exp 2\pi i(hm_1+km_2) \\
&\quad + \Big(\sum_{m_3}' J_{m_3} \exp 2\pi i \ell m_3\Big) \sum_{m_1 m_2} \sum \exp 2\pi i(hm_1+km_2) \\
&= J_0 - J_{m_1+m_2} + \Big[J_{m_1+m_2} + \sum_{m_3}' \exp 2\pi i \ell m_3\Big] \sum_{m_1 m_2} \sum \exp 2\pi i(hm_1+km_2), \qquad (4.18)
\end{aligned}
$$

where three cases were made for $J_{m_1+m_2+m_3}$:

$$J_{m_1+m_2+m_3} = J_0 \qquad (m_1=m_2=m_3\neq 0)$$

$$J_{m_1+m_2+m_3} = J_{m_1+m_2} \qquad (m_3=0 \text{ and } m_1\cdot m_2\neq 0)$$

$$J_{m_1+m_2+m_3} = J_{m_3} \qquad (m_3\neq 0).$$

Using the same definitons for A, B, and α as in model (HKℓ)-(III), and defining R$'$ as the double summation:

$$R' \equiv \sum_{m=-3}^{3} \sum_{n=-3}^{3} \exp 2\pi i(hm+kn),$$

we have

$$J_0 = \overline{F^2}$$

$$J_{m_1+m_2} = R'^2(A+B)^2/(4\cdot 49)^2$$

$$J_{m_3} = \overline{F^2} + 2(J_f-2J_t)(-1/2)^{|m|}/(4\cdot 49\cdot 3),$$

where

$$J_f-2J_t = 2R'^2(1-\cos\alpha)\{(A^2+B^2-4AB)(2+\cos\alpha)-i3(A^2-B^2)\sin\alpha\}.$$

The last term in equation (4.18) corresponds to the (HKℓ) models, since the double summation $\sum\sum \exp 2\pi i(hm_1+km_2)$ is essentially zero when h and k are non-integers. The equivalency of the last term to the (HKℓ) models is seen by noting that

$$J_{m_1+m_2} + \sum_{m_3}' J_{m_3} \exp 2\pi i\ell_{m_3} = \sum_{m_3} J_{m_1+m_2+m_3} \exp 2\pi i\ell_{m_3}. \qquad (4.19)$$

The similarity of this equation to equation (4.8) is apparent. R$'$ is non-zero only when (h,k)=(7m,7n) where m and n are integers. Although this (hkℓ) model is closely related to model (HKℓ)-(III) in having R$'$ instead of R, because of the disorder in the ab-plane the above equation (Equation (4.19)) is equivalent to model (HKℓ)-(I), and the first two terms in Equation (4.18) will be the cause of the low angle halos (contribution of these two terms to higher angle intensity was found to be very small). Then disregarding the third term for (HKℓ) scattering, we have the intensity expression for the (hkℓ) scattering:

$$I = J_0 - J_{m_1+m_2}$$

$$\propto (4.49)^2 F^2 R'^2 (A+B)^2. \qquad (4.20)$$

When the domain size has a lattice constant $a_0 = 7Ma_g$, the intensity will be given by

$$I \propto \{(4.49M^2)^2 F^2 R'^2 (A+B)^2 [SN]\}[SN], \qquad (4.21)$$

where the factor [SN] is defined as

$$[SN] \equiv \{(\sin[\pi Mh]\sin[\pi Mk]/\sin[\pi h]\sin[\pi k]\}^2.$$

This is because the structure factor G and the intensity GG^* for the larger domain ($a_0 = 7Ma_g$) can be expressed by that of the smaller domain ($a_0 = 7a_g$) according to the equations

$$G = F \sum_{m=0}^{M-1} \sum_{n=0}^{M-1} \exp 2\pi i(hm+kn)$$

$$GG^* = FF^*[SN].$$

M^2 and [SN] in the braces in equation (4.21) were necessary, since the number of the possible sites of AsF_6^- increases by the factor of M^2.

Conversion of intensity from reciprocal space to the Debye-circle was done "digitally" as was the case with the nestled-cell models in Chapter 3, i.e., h, k, and ℓ were assigned values of multiples of 1/20 and the intensities were collected to the corresponding 2θ value with the interval of 1/10 degree. The unit of 1/20 for h, k, and ℓ was small enough to produce a uniform intensity curve. The smaller unit did not enhance the uniformity noticeably.

4.4 Results and Discussion

The calculation of diffraction patterns for the various models involved steps which were sometimes common to two (or all) of the models. Sharp diffraction peaks were anticipated for all models for reflections 00L and for HKL (HK-case (i), see 4.2.5). The calculated pattern for such reflections is shown in Figure 4.4. Models (I) and

(III) each assume an equal mix of R and S AsF_6^- packing arrangements (see Figure 4.1), and as a consequence of this, the (10ℓ) and {70ℓ} (which represent the stacking disorder according to the requirements of Figures 4.2 and 4.3) are identical. The calculated diffraction pattern for such reflections (HK-case (ii)) for models (i) and (III) is shown in Figure 4.5 and should be compared with Figure 4.6, which gives the related data for model (II). Model (II) must be considered as unlikely since it only allows R or S for the entire powder sample. (It is possible that one single crystal could adopt all R or all S packing.) For all other HKℓ reflections (HK-case (iii)) the saw-tooth character represented in Figure 4.7 is calculated for models (II) and (III). They have the same pattern, since the total intensity is the average of the <u>intensities</u> of R and S strustures (see Equation (4.16)). This is because the <u>powder</u> diffraction patterns of the two types of structures are the same. The abrupt low-angle onset of a peak is associated with the leading HK0 reflection of an HKℓ set. As was pointed out in Section 4.2.6, although unrealistic, each on set should be infinite according to Equation (4.17). Figures 4.5, 4.6, and 4.7 are so scaled that the additions of Figures 4.6 to 4.7, and 4.5 to 4.7, respectively, give the total diffuse scattering patterns of models (II) and (III) (HK-cases (ii) and (iii) (see Section 4.2.5)). They are shown in Figures 4.8 and 4.9. They suggest that halo (B) could be caused by the superlattce structure represented in models (II) or (III). But there is a serious failure to cope with the observed halo (A). The final model (referred to as the (hkℓ) model) does simulate that and all other observed features.

In the (hkℓ) model it is assumed that each gallery of the C_xAsF_6 contains domains of R or S arrangements of nestled AsF_6^-. It is

reasonable to assume that these R and S domains occur because of simultaneous development of nestled AsF_6^- close packing at many points within each gallery. Growth about an AsF_6^- nestled at a point R (see Figure 4.1) will not provide for continuity with AsF_6^- at a point S. It is thus easy to visualize how the domain boundaries would arise.

The results corresponding to Equation (4.20) for the (hkℓ) model are shown in Figure 4.10, together with a simulated whole pattern (see below). As was the case with the models in the previous chapter, a gaussian function with a standard deviation of 0.3 degree in 2θ was given to each accumulated intensity with 1/10 degree intervals. Calculations based on Equations (4.20) and (4.21) suggest that the model reproduces the observed pattern well when M=1. Similar calculations for hexagonal domains of multiples of $\sqrt{7}a_g$ indicated that domains of ca. $7a_g$ reproduces the observed pattern best. The intensities calculated from the last term in Equation (4.18) are the same as given in Figures 4.4 and 4.5. The reason for this was explained in the description of the (hkℓ) model (see Section 4.3). The observed pattern was simulated (see Figure 4.10) by combining the new (hkℓ) scattering (curve (a) in Figure 4.10) for this model from Equation (4.20) with the results from the small-cell model shown in Figure 3.11, which would also apply to this case. Figure 3.11 corresponds to a combincation of Figures 4.4 and 4.5. The quartz background scattering (curve (b) in Figure 4.10) was also added. The combination (curve (c)) of curves (a) and (b) and Figure 3.11 contributions to the scattering required some weitghting of one contribution relative to the others to provide a fit to the general form of the observed scattering. The excellent agreement between the observed and calculated scattering shown in Figure 4.11 indicates that the

structural model (hkℓ) is highly satisfactory.

Guinier data with higher resolution and better background would provide more convincing evidence for the structural model (hkℓ), and data from a single crystal are highly desirable. Even with the latter, however, it is probable that R and S domains of small size would occur. This is because, as the close clusterings of AsF_6^- about each AsF_6^- propagate, they develop R or S arms randomly and independently.

Table 4.1. The relationships of the subscripts p, q, r, and s to the carbon-layer types and the AsF_6^- arrangements.

(HKℓ)-(I) model

q \ p	$\bar{1}$	0	1	
$\bar{1}$	B	A	C	-Top carbon layer
	C	B	A	-Bottom carbon layer
1	C	B	A	-Top carbon layer
	B	A	C	-Bottom carbon layer

(HKℓ)-(II) model

r / q p	$\bar{1}$	0	1	r=0, ±1, ±2, and ±3
$\bar{1}$	B	A	C	-Top carbon layer
	R	R	R	-AsF_6^- arrangement
	C	B	A	-Bottom carbon layer
1	C	B	A	-Top carbon layer
	R	R	R	-AsF_6^- arrangement
	B	A	C	-Bottom carbon layer

(HKℓ)-(III) model

r / p	$\bar{1}$		0		1		r=0, ±1, ±2, and ±3
q / s	$\bar{1}$	1	$\bar{1}$	1	$\bar{1}$	1	
$\bar{1}$	C	B	B	A	A	C	-Top carbon layer
	S	R	S	R	S	R	-AsF_6^- arrangement
	B	C	A	B	B	A	-Bottom carbon layer
1	B	C	A	B	B	A	-Top carbon layer
	S	R	S	R	S	R	-AsF_6^- arrangement
	C	B	B	A	A	C	-Bottom carbon layer

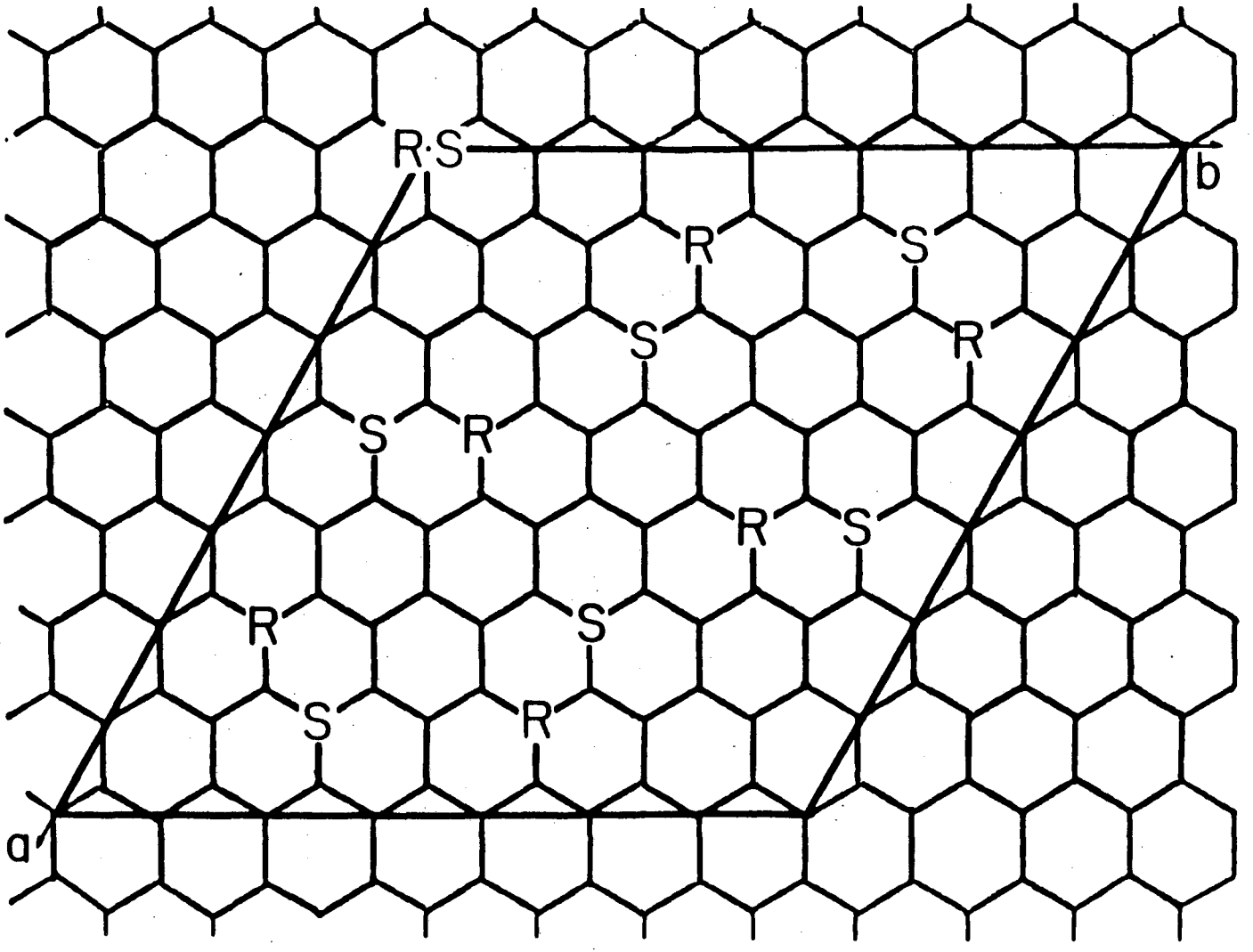

Figure 4.1. Relationship of the R- and S-structures and the commom hexagonal "unit" cell used for the (HKℓ)-(III) model with the lattice constant $a_0 = 7a_g$. XBL 849-3761

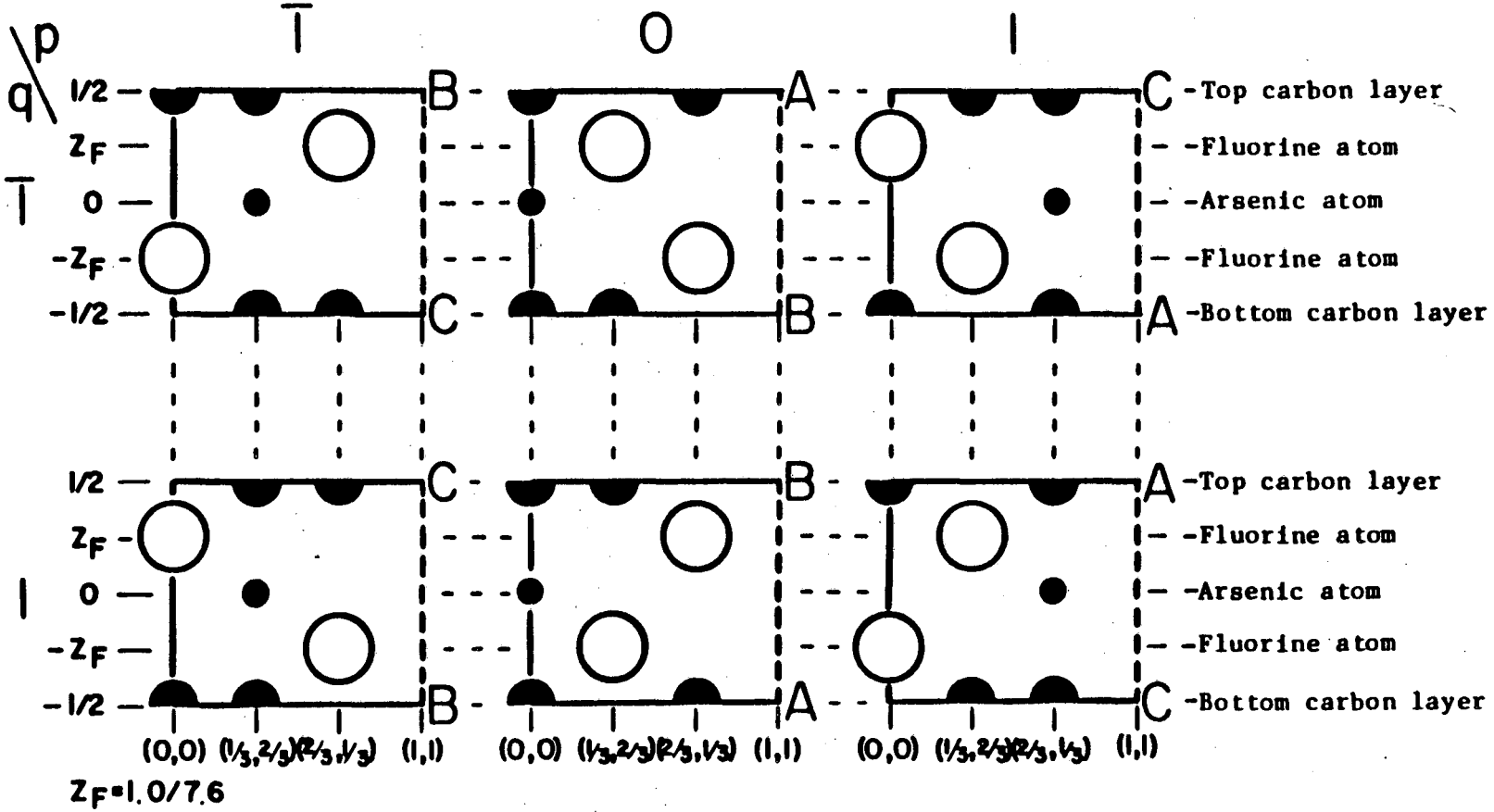

XBL 849-3762

Figure 4.2. Six unit cells, Φ_{pq}, used in the (HKℓ)-(I) model with $a_0 = a_g$ and $c_0 = 7.6$ Å

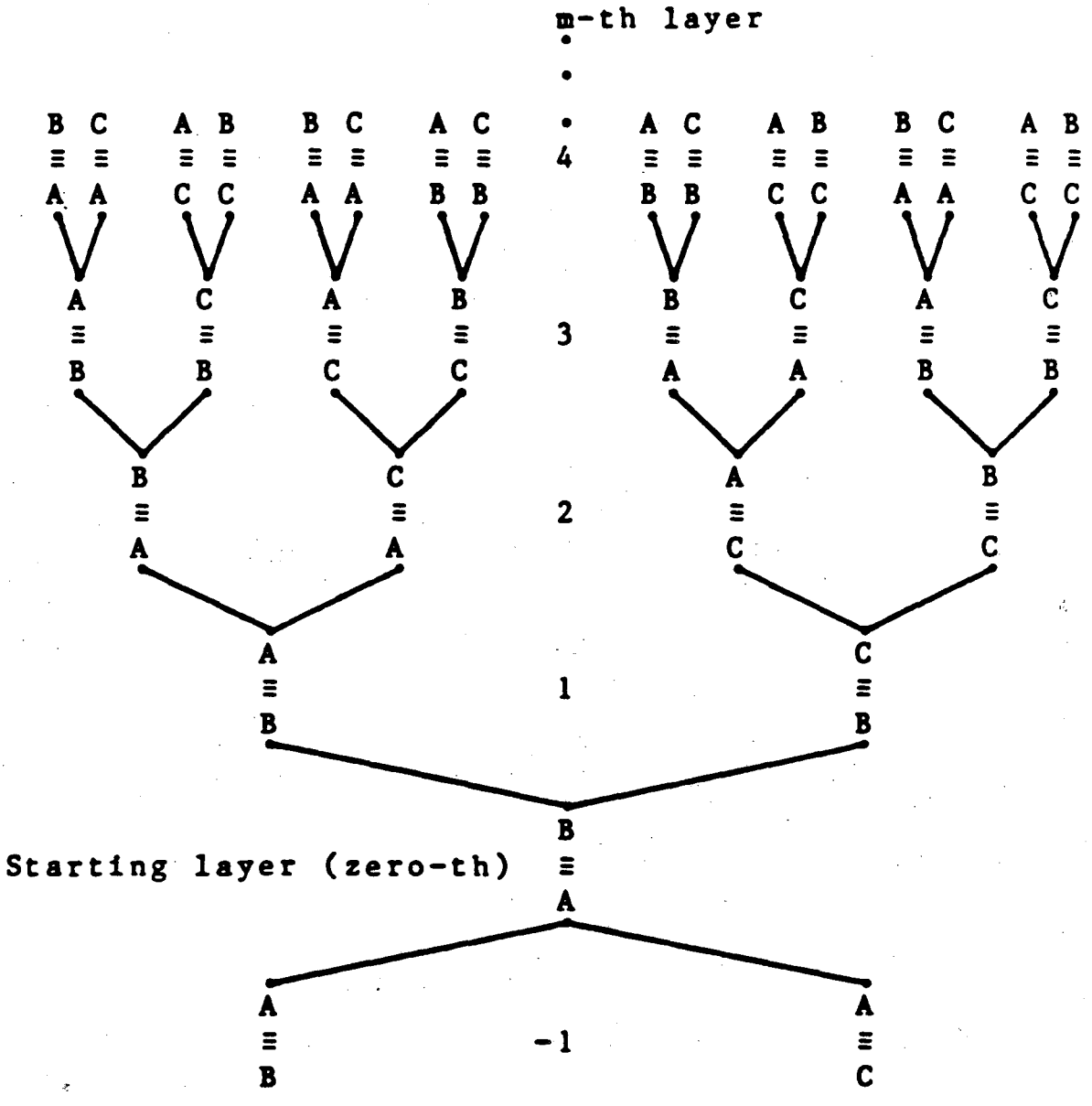

Figure 4.3. Stacking sequences of the unit cells starting with Φ_{01} for model (HKℓ)-(I).

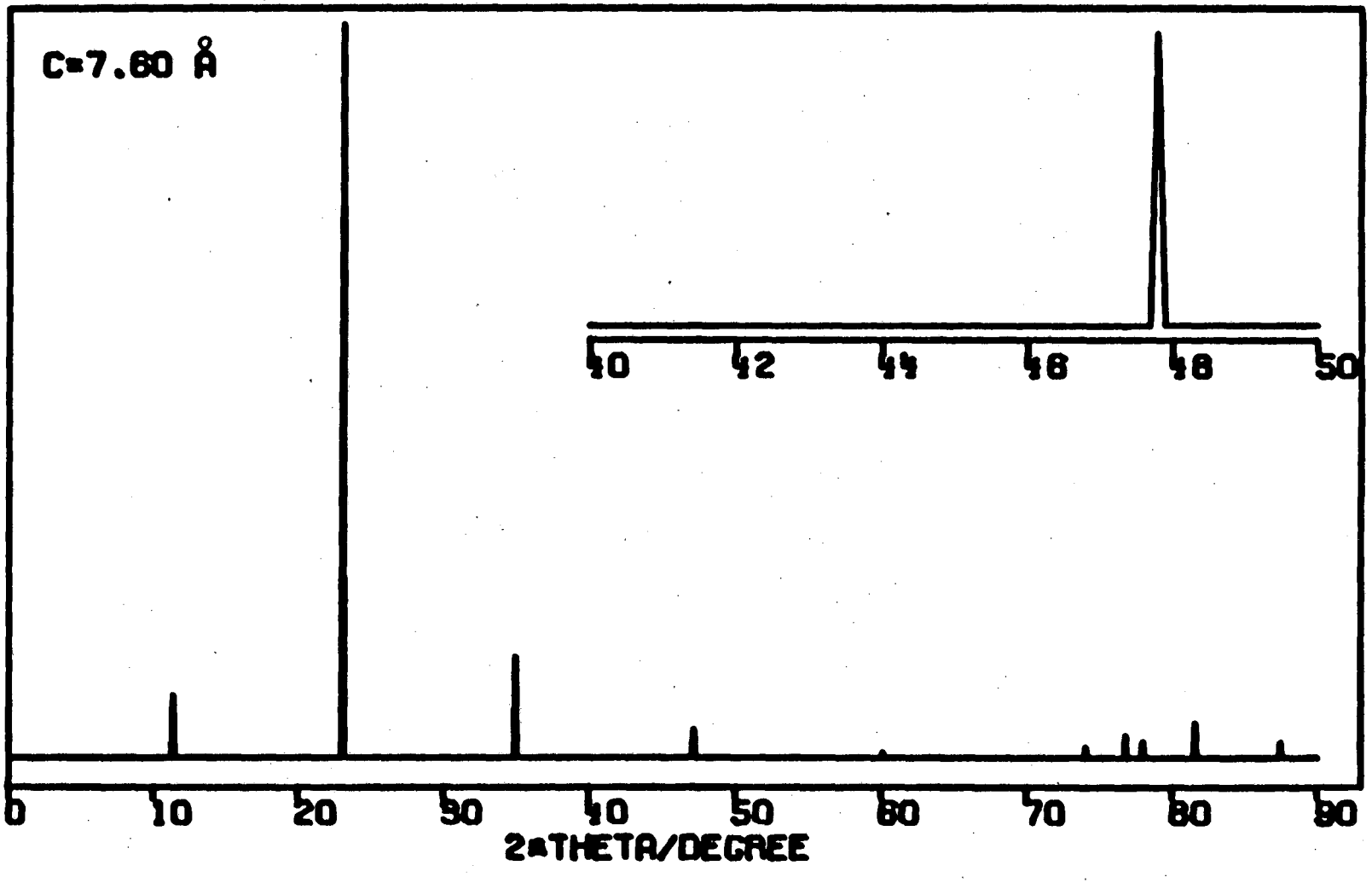

Figure 4.4. Calculated diffraction pattern for models (HKℓ)-(I), -(II), and -(III) with HK-case (i).

XBL 849-3764

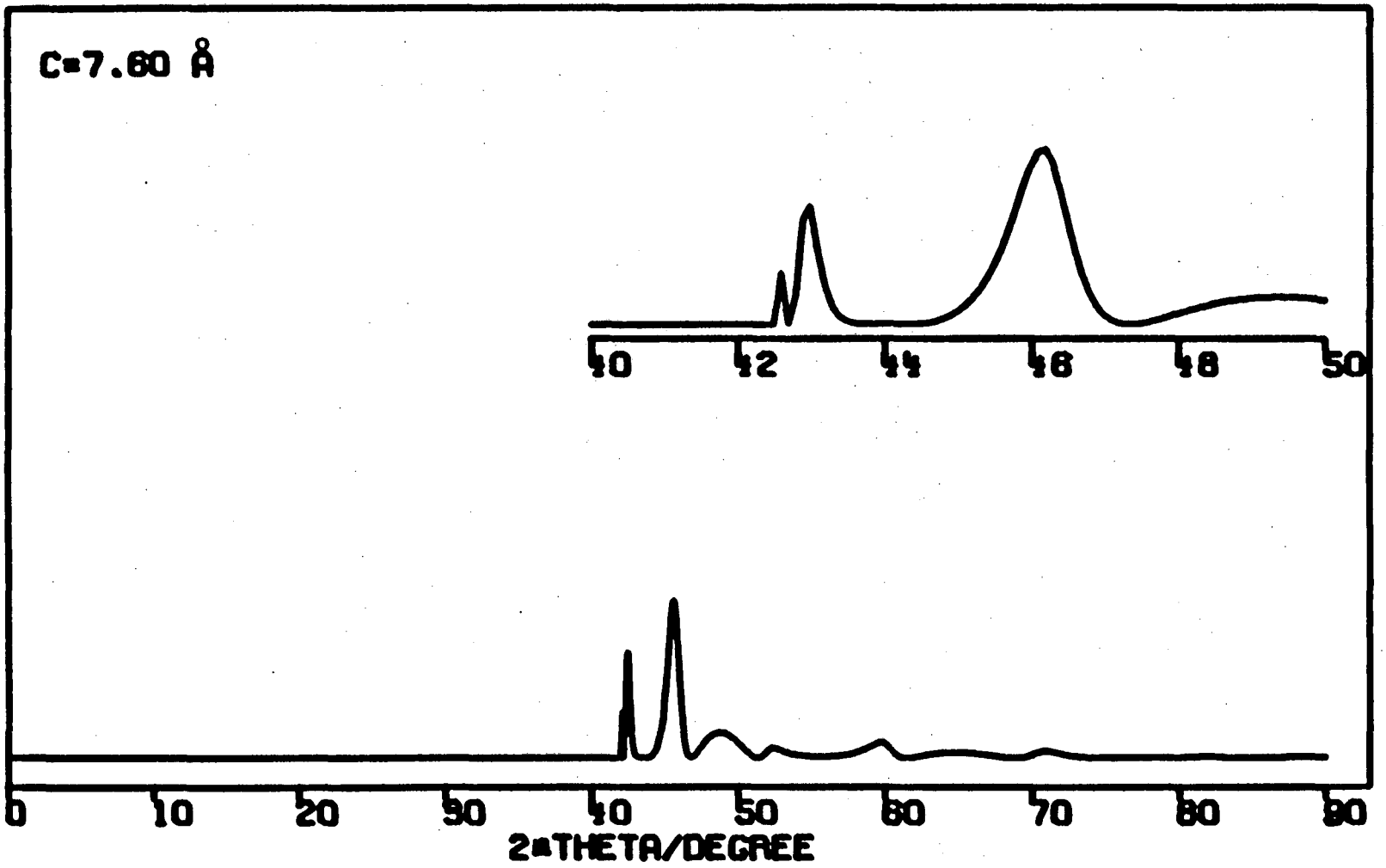

Figure 4.5. Calculated diffuse scattering pattern for models (HKℓ)-(I) and -(III) with HK-case (ii).

XBL 849-3765

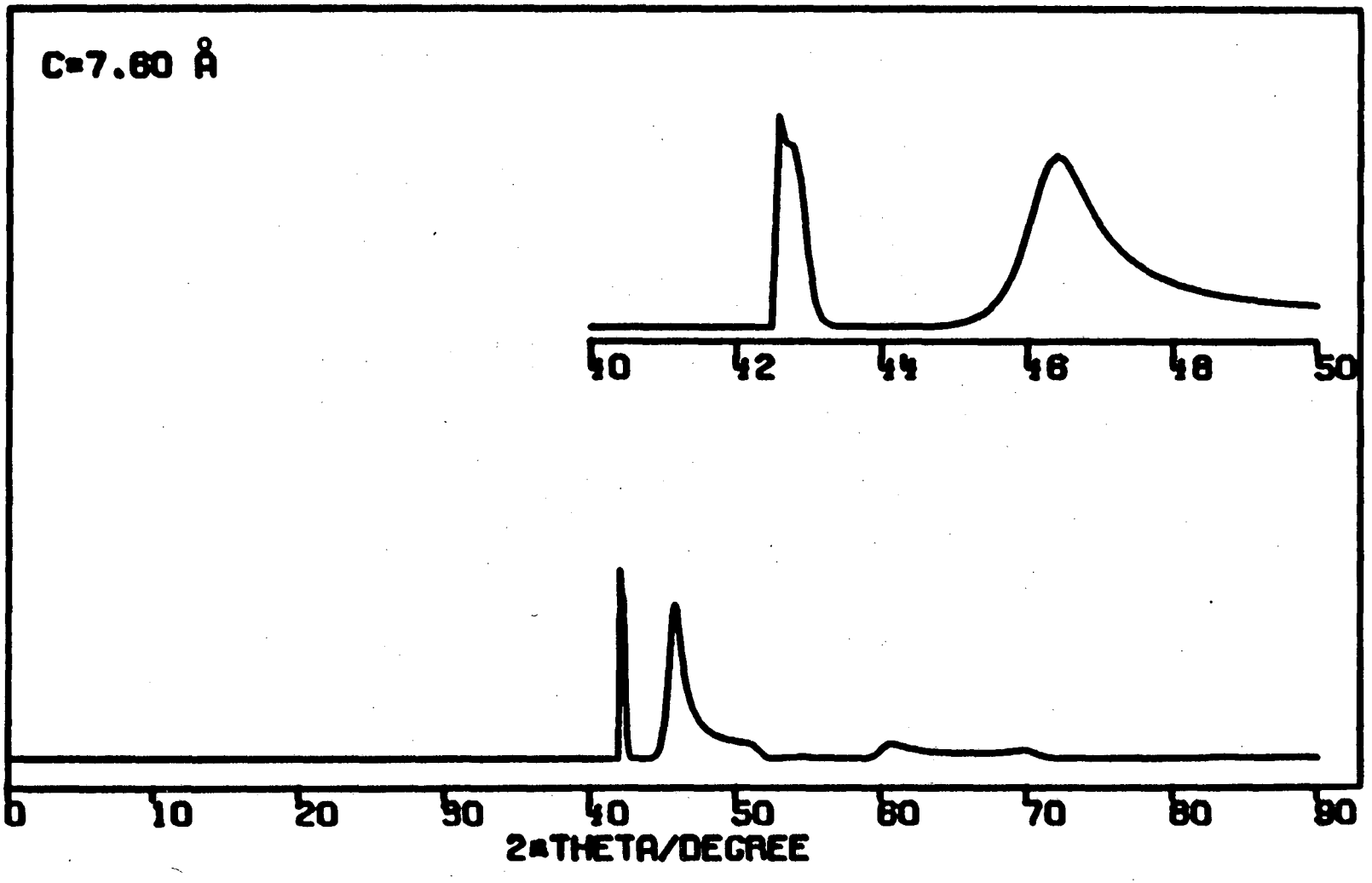

Figure 4.6. Calculated diffuse scattering pattern for model (HKℓ)-(II) with HK-case (ii).

XBL 849-3766

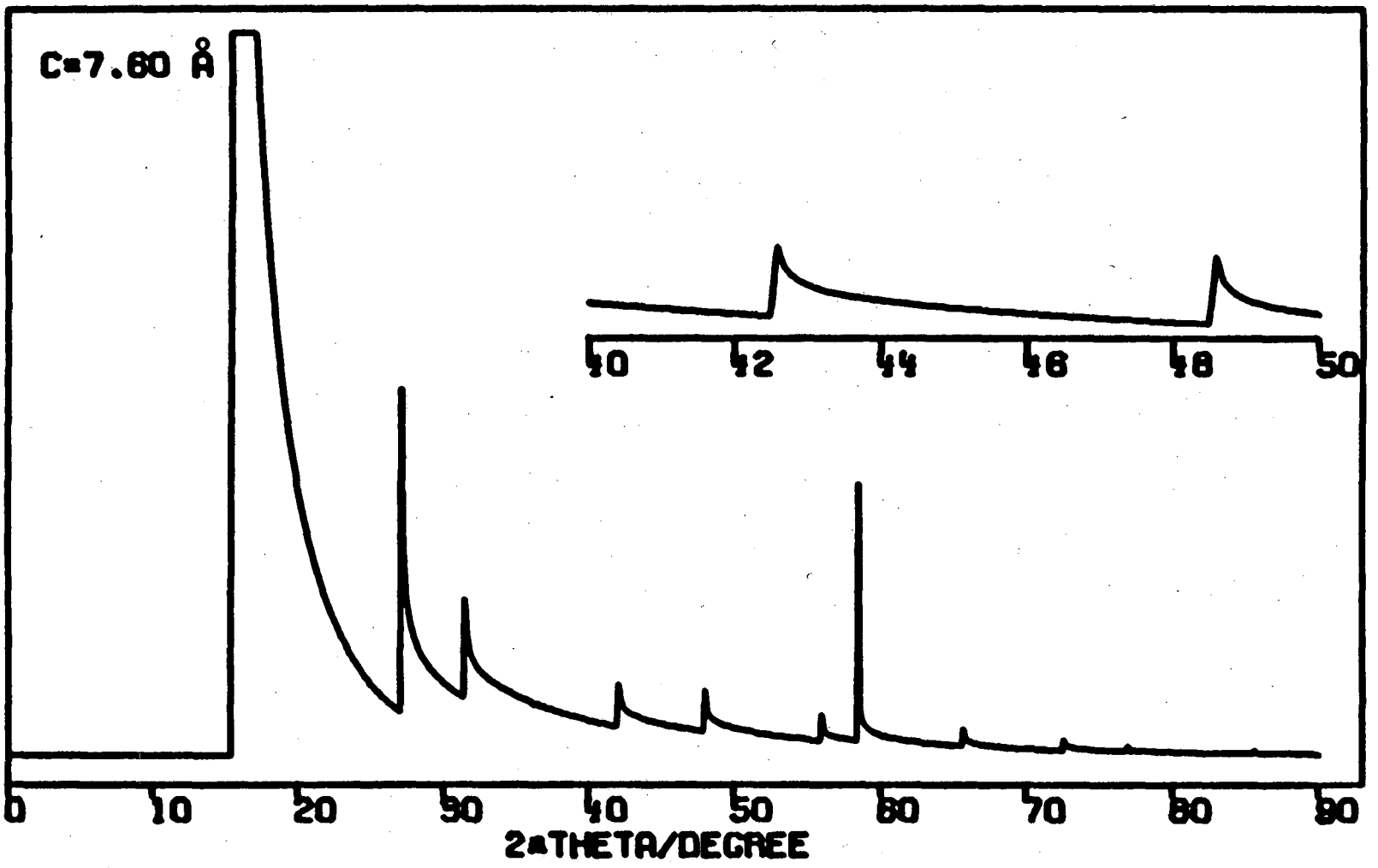

Figure 4.7. Calculated diffuse scattering pattern for models (HKℓ)-(II) and -(III) with HK-case (iii).

XBL 849-3767

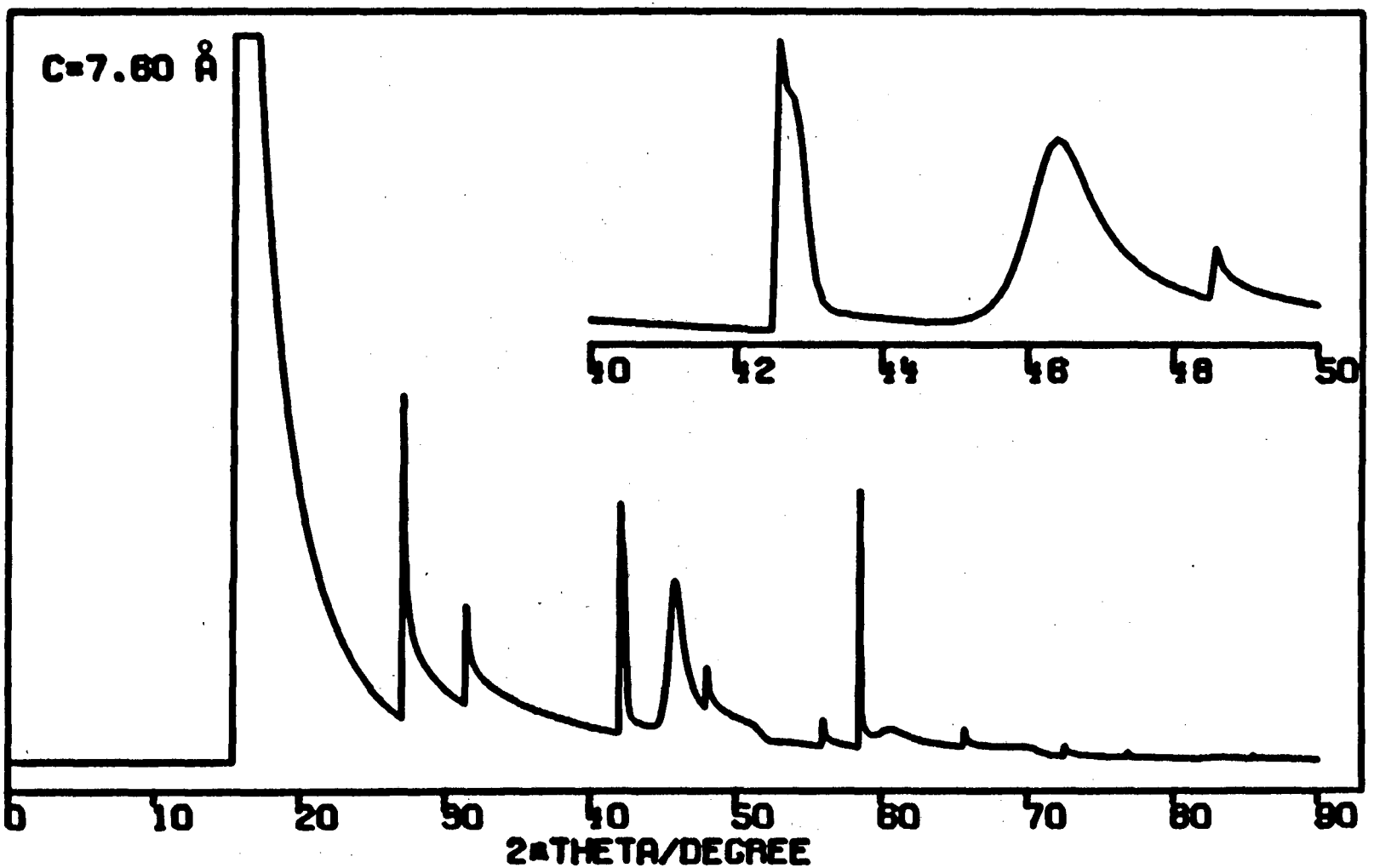

Figure 4.8. Calculated diffuse scattering pattern for model (HKℓ)-(II) (HK-cases (ii) + (iii)).

XBL 849-3768

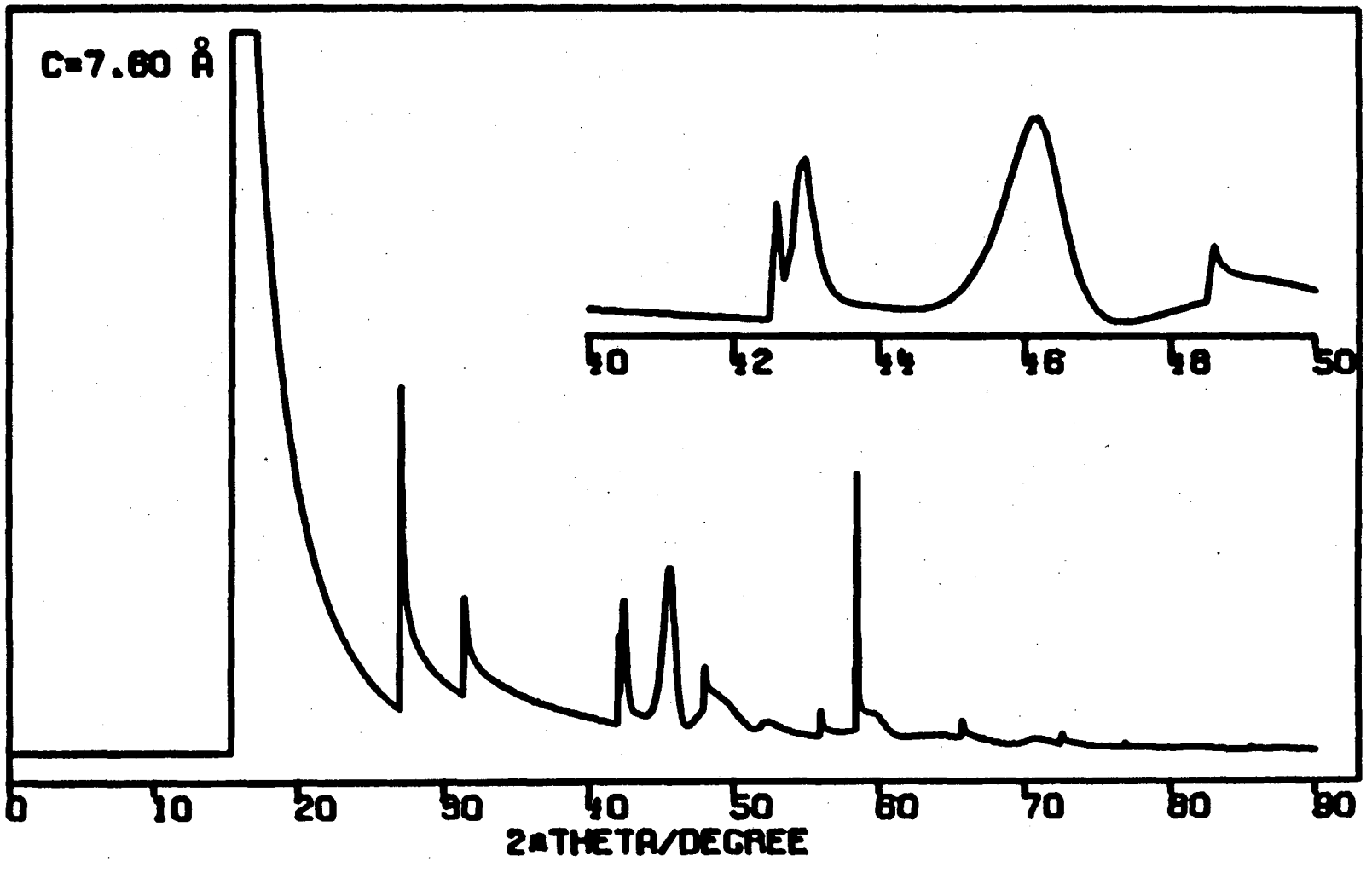

Figure 4.9. Calculated diffuse scattering pattern for model (HKℓ)-(III) (HK-cases (ii) + (iii)).

XBL 849-3769

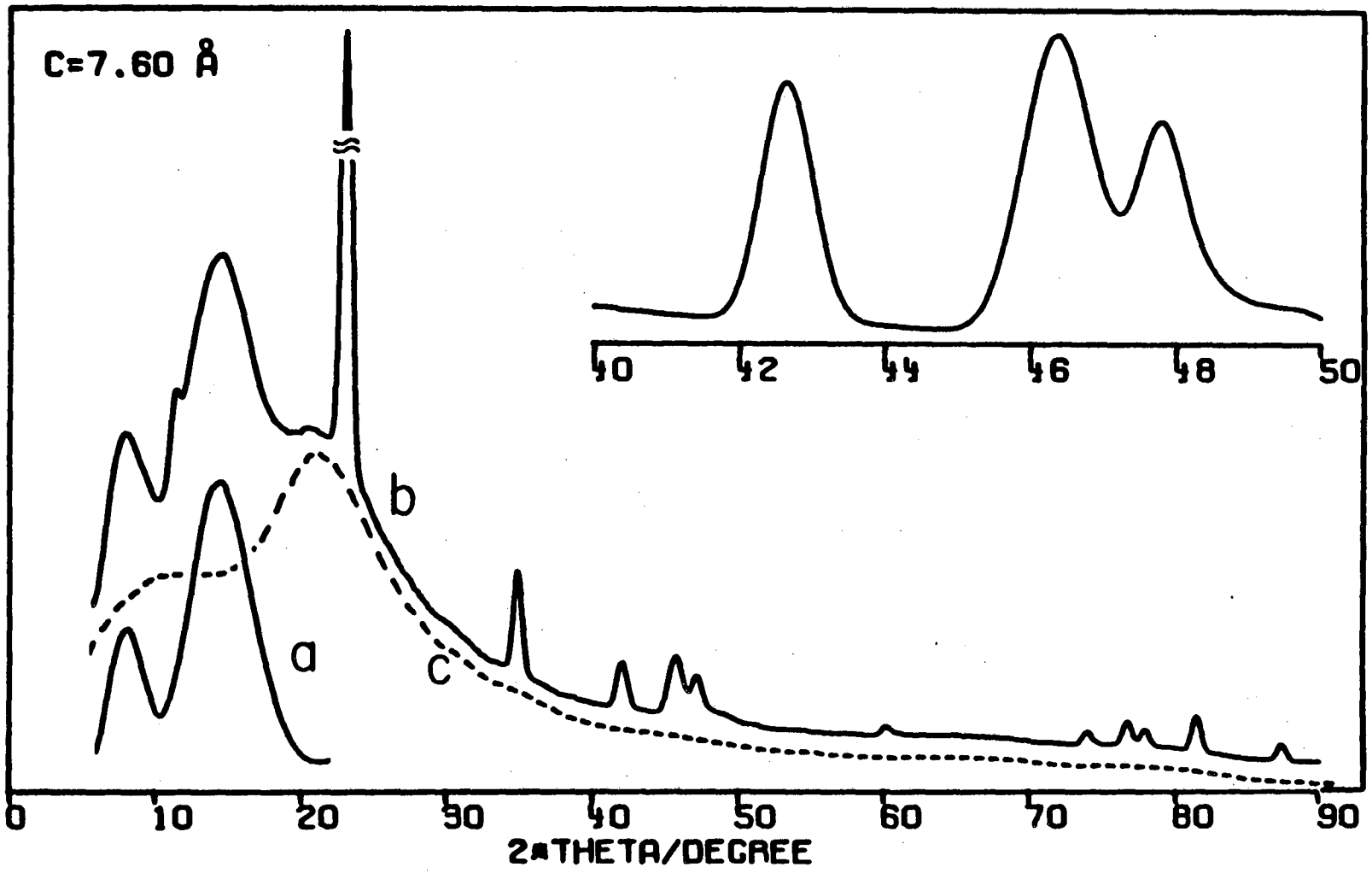

Figure 4.10. Diffraction patterns by the (hkℓ) model in combination with the results by the small-cell model: (a) (hkℓ) scattering by the (hkℓ) model (Equation (4.20)); (b) Combination of (a), (c), and the results of the small-cell model (see Figure 3.11); (c) quartz capillary background.

XBL 849-3770

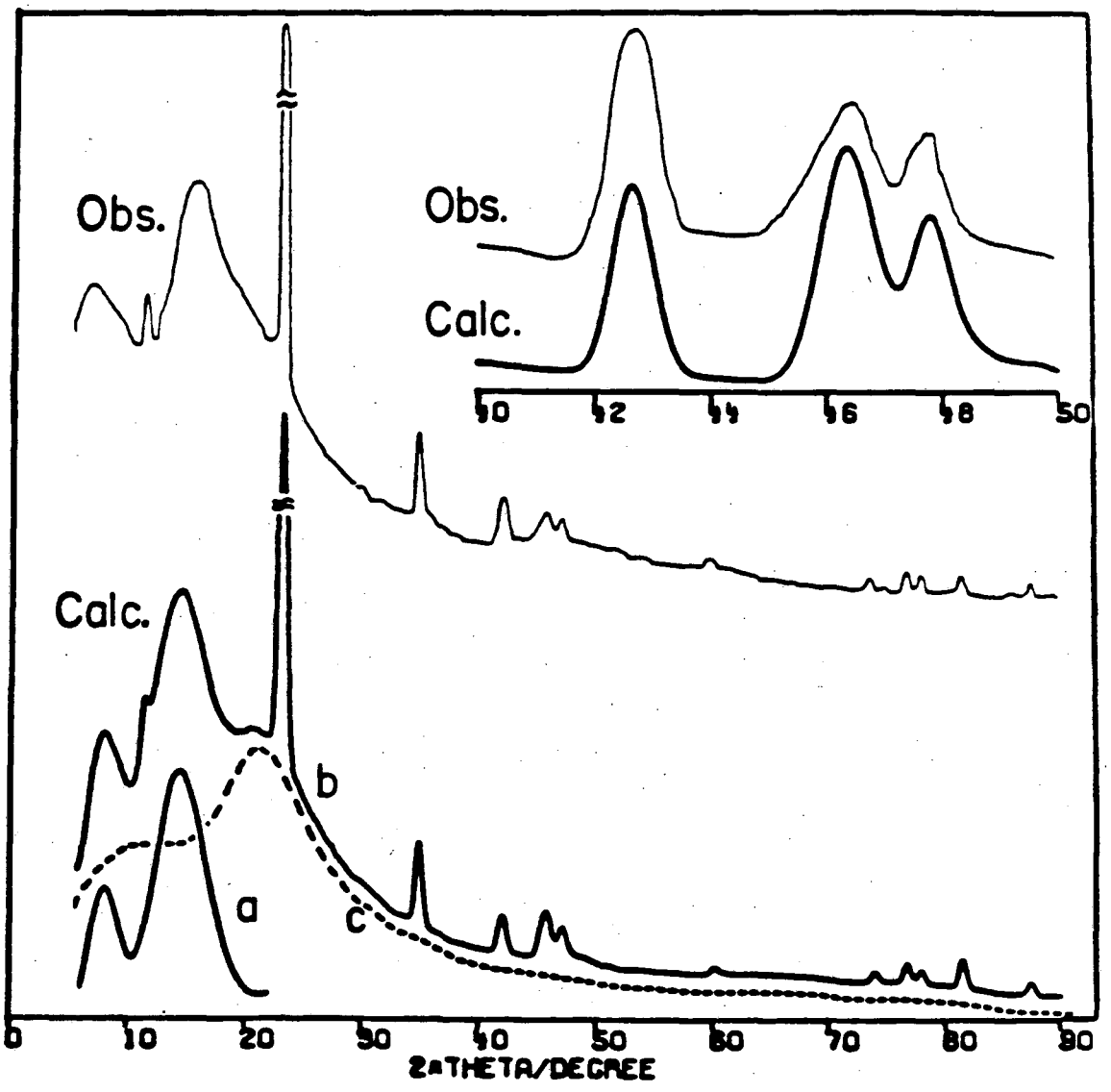

XBL 849-3771

Figure 4.11. Summary of the observed and simulated diffraction patterns. The simulation was made by the (hkℓ) model. See Figures 3.1 and 4.10, respectively, for the observed and calculated patterns.

Chapter 5

REACTIONS OF $C_{14n}AsF_6$ WITH AsF_5, AsF_3, F_2, ETC., AND CONDUCTIVITY MEASUREMENTS

In Chapters 2-4 graphite hexafluoroarsenates and related materials are compositionally and structurally characterized. Since $C_{14n}AsF_6$ materials are vacuum stable and well characterized, they make good starting and/or reference materials. In order to get further insight into the nature of the intercalation compounds, some reactions involving $C_{14n}AsF_6$ are described in this chapter. Data obtained from HOPG chips by in-situ conductivity and X-ray diffraction measurements depend for their interpretation upon the more fully described behaviour of powdered materials. A reproducible procedure for the preparaion of nestled-form powdered $C_{14n}AsF_6$ is described first.

5.1 Preparation of Nestled $C_{14n}AsF_6$

For the majority of experiments materials of composition $C_{14n}AsF_6$ were prepared by treating graphite (SP-1) with AsF_5 and F_2 in the stoichiometry appropriate for

$$14n\ C + AsF_5 + {}^1/_2 F_2 \rightarrow C_{14n}AsF_6$$

The AsF_5 and F_2 were condensed sequentially upon the graphite contained in a stainless steel vessel (5-10 mℓ). The mixture was warmed to room temperature and stirred on a vibrator for two hours or more. All remaining volatiles (always small in amount) were removed under vacuum at room temperature. Constant weight was achieved within three hours, but routinely such samples were submitted to a dynamic vacuum overnight. Each sample was characterized by X-ray powder photography and found to conform to the unit cell dimensions and structure associated with the nestled form, $C_{14n}AsF_6$. The requirements of good vibration-induced

stirring meant that the reaction vessels could only be partially filled. Hence sample weights were usually small (ca. 100 mg). Carbon analyses were made to check gravimetry (see Tables 5.1 and 5.3).

5.2 Reactions of $C_{14n}AsF_6$ with AsF_5, AsF_3, F_2, etc.

5.2.1 $C_{14n}AsF_6$ with addition and removal of AsF_5

AsF_5 (~0.5 mmoles) was condensed on to samples of $C_{14n}AsF_6$ (~0.3 mmoles) at -196 °C in a stainless steel vessels of small volume (~5 mℓ). The closed vessel was warmed to room temperature and the contents were constantly stirred on a vibrator for at least two hours. Volatiles were removed by condensing them at -196 °C for a few minutes in a closed system until the contents of the vessel no longer registered gas pressure (<300-500 μtorr) on a thermocouple pressure gauge. X-ray powder photographs of this AsF_5-rich material always revealed a unit cell with $c_0 \approx 8.0$ Å and the intensity data were indicative of eclipsed carbon layers and un-nestled guest species (see Chapters 3 and 4). The AsF_5 uptake by "$C_{14}AsF_6$" was about half a mole per mole of AsF_6^- (see Table 5.1). When this material was subjected to a dynamic vacuum (~50 hours were taken but less may be necessary), it fell to constant weight close to that of the original $C_{14n}AsF_6$. An X-ray powder photograph of this material was indistinguishable from that of the starting $C_{14n}AsF_6$ material ($I_c \approx 7.6$ Å for nestled AsF_6^- with staggered carbon layers-see Table 3.1 and Figure 3.8).

5.2.2 $C_{14n}AsF_6$ with addition and removal of AsF_3

First-stage $C_{14}AsF_6$ (~0.3 mmoles) prepared as described above was treated with AsF_3 (~1 mmoles) in a stainless steel vessel (~5 mℓ) at room temperature for periods of 1 day to 3 weeks. The contents were constantly agitated by a vibrator. Volatiles were removed by vacuum

distillation to a cold trap (-196°) until there was no detectable gas on a Helicoid gauge (1500 torr full scale). This required several seconds. Infrared spectroscopy of the volatiles revealed the presence of some AsF_5. Carbon analysis of the solid indicated a composition ca. $C_{14}AsF_6 \cdot (0.5)AsF_3$ (see Samples 3 and 4 in Table 5.1). X-ray powder photographs (see Table 5.2 for representative data) indicated a grossly expanded I_c-spacing (≈ 8.15 Å). But the X-ray data also indicates some second- stage material (I_c ≈ 11.6 Å) admixed with a stronger first-stage. The data have not been completely indexed, however, and the these first- and second-stage cells are not completely described.

Removal of AsF_3 was carried out for several days in a dynamic vacuum at 20°. Infrared examination of these volatile revealed only AsF_3. X-ray powder data usually showed the reduced solid to be a mixture of first- and second-stage salts of the $C_{14n}AsF_6$ series. Carbon analysis indicated an overall composition $C_{17.8}AsF_6$ (Sample 3 in Table 5.2) which requires a roughly 2:1 admixture of first-stage $C_{14}AsF_6$ with second-stage $C_{28}AsF_6$. The relative line intensities of the two patterns are in harmony with this requirement. The X-ray data were satisfactorily explained by the nestled $C_{14n}AsF_6$ series. This suggests that the un-indexed lines of the AsF_3-rich compound before evacuation (see Table 5.2) were not due to contamination of the sample by impurities or decomposition products.

5.2.3 Reaction of $C_{14}AsF_6$ with SF_6

Reactions were carried out in a manner similar to that employed for reactions with AsF_5 (see Section 5.2.1). The results (Samples 5 and 6 in Table 5.1) indicate the $C_{14n}AsF_6$ does not incorporate SF_6 in significant quantities.

5.2.4 Reaction of $C_{14n}AsF_6$ with F_2

F_2 (~0.5 mmole) was reacted with $C_{14n}AsF_6$ (ca. 0.2-0.4 mmole). The procedures were essentially the same as those described for AsF_5 and AsF_3. Tensimetry, however, was carefully carried out, since gravimetry and CHN analyses are less definitive in determining uptake of F_2 than of AsF_5 or AsF_3 because of the smaller molecular weight of F_2. It is notoriously difficult to analyse for fluorine in the presence of arsenic because of the kinetic stability of AsF_6^-. Moreover, pyrolysis also yields some carbon fluorides, e.g. CF_4, which also have great kinetic stability. Tensimetry was done by measuring the initial pressure (actually the pressure difference before and after the condensation of some F_2 gas at -196° in the reaction vessel) in a known volume (~ 40 ml: reaction vessel + vacuum line + helicoid gauge), and the final pressure after the reaction by opening the vessel to the vacuum line plus the Helicoid gauge. Since some F_2 is always consumed by the inside wall-surfaces of the vacuum line and the Helicoid gauge, this method was preferred to monitoring the pressure change in the course of the reaction open to the entire vacuum-line system. Tensimetry, gravimetry, and CHN analyses were found to be in satisfactory agreement. Infrared spectra of volatiles over the products usually revealed a small amount of CF_4. The compositions of the products given in Table 5.3, however, were calculated based on CHN analyses with the assumption that the carbon-% change is solely associated with uptake or loss of F_2.

5.2.5 Reaction of $C_{14}AsF_6$ with SO_2ClF

(Reaction of graphite with O_2AsF_6 in SO_2ClF)

Reactions were carried out with SP-1 powder and HOPG chips. Graphite (~5-10 mmoles) was reacted with excess O_2AsF_6 (~3 mmoles) in

SO_2ClF at -23° (CCl_4 slush bath) for 1-5 days. It was found that the solvent SO_2ClF was taken up by the product (see Table 5.4). IR of the volatiles from the solid product revealed only SO_2ClF. The removal of SO_2ClF from the product was found to be a very slow process. The X-ray diffraction patterns on the powdered material (Sample 1 in Table 5.4) indicated that the loss of SO_2ClF is associated with an I_c-spacing decrease and with a corresponding structural change from un-nestled AsF_x to nestled AsF_6^-. Chemical analyses for C, S and Cl were made on different parts of a sample. This is probably the reason, especially for Sample 2 where HOPG chips were employed, why the compositional change is not totally consistent with the simple loss and uptake of SO_2ClF.

5.3 Conductivity Measurements

In situ conductivity measurements were carried out using an HOPG chip (see Chapter 2) of dimensions, ca. $5\times5\times0.5$ mm^3, in a quartz cell shown in Figure 5.1. X-ray (00ℓ) reflection data were also obtained *in situ* on the same sample. A thin-walled bulb was made to minimize X-ray absorption. The cell was attached to a Debye-Scherrer camera and rocked to obtain (00ℓ) reflections. Mo-K_α radiation was employed. Half an hour exposure was sufficient to obtain the necessary information. The estimated standard deviation for the lattice constants was ca. 0.03 Å. This was satisfactory for the present purposes. Reacting gases were condensed in the cold-finger (see Figure 5.1) by liquid nitrogen.

Conductivity measurements were made by the contactless radio frequency (1 kHz) inductive technique.[51] Calibration of the instrument was made using a copper standard of nearly the same size as the HOPG chips used for the reactions. The findings, however, are usually

expressed for convenience by the ratio of the conductivity of the product to that of the initial graphite; σ/σ_g. The conductivity was derived from the relationship:

$$\Delta V = KA^2 t\sigma$$

where ΔV represents the voltage change (sample in field - sample out); K, a proportionality constant; A, the ab-plane surface area; t, the sample thickness; and σ, the specific conductivity. Since the ab-plane dimensions do not change significantly (<0.1 %), σ/σ_g is calculated according to the equation:

$$\sigma/\sigma_g = n \cdot \Delta V \cdot 3.35/(I_0 \cdot \Delta V_g)$$

where n is the stage of the product and ΔV_g is the voltage change for the initial graphite. When a sample is a mixture of first- and second-stage phases, their molar ratio was estimated by the X-ray (00ℓ) reflection intensities. All the compositions given in Table 5.5 were estimated from the known X-ray diffraction-data dependence on composition for powdered materials.

5.3.1 HOPG sample preparation of $C_{14n}AsF_6$ for conductivity measurements

The production of $C_{14n}AsF_6$ material, using the HOPG chips suitable for conductivity work, required the employment of AsF_5/F_2 mixtures in order to obtain pure first-stage material (see Chapter 2 for stage limitation using AsF_5 alone). Because of the dramatic lowering of the in-plane conductivity brought about by the addition of excess fluorine (see Section 5.2.2), it was necessary to limit the fluorine supply to the reaction. Experience with SP-1 powder had shown that stoichiometric $C_{14n}AsF_6$ material could be made by treatment of graphite with AsF_5/F_2 mixtures in the ratio appropriate to form $C_{14n}AsF_6$. The presence of the reactant gases was always kept below an initial pressure in the reactor

of 2-3 atmospheres. For the small quantities of graphite involved in the conductivity sample preparation, it was usual to use a larger quantity of reactant gases than needed to make $C_{14}AsF_6$, but the AsF_5 to F_2 ratio was kept at 2:1. In these circumstnaces gas pressures were always less than 2 atmospheres at the beginning of the preparation and fell as AsF_5 and F_2 were consumed. It should be noted (as documented in Chapter 2) that even in powder preparations, where a two-fold excess of fluorine was employed (i.e. $AsF_5:F_2$ = 1:1), C, As, and F analyses indicated a composition $C_{14n}AsF_6$. Such preparations involved low gas pressures and minimum contact time between graphite and fluorine.

5.3.2 Comparison of the conductivities of $C_{8n}AsF_5$ and $C_{14n}AsF_6$ and the impact of fluorination.

The results of conductivitiy measurements are summarized in Table 5.5.

The initial experiments documented in Table 5.5 under Sample 1 are typical of graphite intercalated by AsF_5 alone. Thus after exposure of the chip to AsF_5 for 6 days a pure first-stage diffraction pattern was observed with I_c = 8.2 Å. This is indicative of material close to that described by others as "C_8AsF_5".[2] Significantly, removal of AsF_5 (and perhaps some AsF_3) to a cold trap in a static vacuum leaves a mixture of first- and second-stage material with a slightly reduced I_c-spacing (8.1 Å) for the first-stage. This parallels the behavior of SP-1 powder which in like circumstances falls to a mixture of first- and second-stages and a gross composition roughly given by "$C_{10}AsF_5$". The ratio σ/σ_g for both "C_8AsF_5" and "$C_{10}AsF_5$" is approximately 11. As is documented under Sample 1 in Table 5.5, addition of fluorine to "$C_{10}AsF_5$" resulted in a marked decrease in conductivity. This decrease

with time is illustrated in Figure 5.2. It is noted, however, that an initial small increase before the decrease was usually observed in such a sample. X-ray diffraction data showed that the final product of this fluorination was a pure first-stage material with $I_c \simeq 7.9$ Å. This corresponds to the experience with fluorinated powder samples of composition $C_{10}AsF_6 \cdot \delta F$ (see Section 5.2.3).

Sample 2, initially prepared in the same way as sample 1, was evacuated before addition of fluorine. Removal of AsF_3 (and AsF_5) from such a sample, under a dynamic vacuum for 4 days did not result in a significant decrease in conductivity (see Figure 5.3). The results are given in terms of ΔV which do not require an estimation of the first/second-stage ratio necessary to obtain specific conductivity. The X-ray data suggest that the initial abrupt drop was associated with an increase of the second-stage ratio relative to first-stage, while the specific conductivity stayed approximately constant. Addition of fluorine to the evacuated material, however, led to a collapse in conductivity to the graphite level ($\sigma/\sigma_g \simeq 1.5$) (see Figure 5.2).

When care was taken to introduce F_2 with AsF_5 in ratio close to that required for $C_{14n}AsF_6$ salt formation, the findings listed under Sample 3 were obtained. The conductivities ($\sigma/\sigma_g \simeq 10$) are comparable to those of C_xAsF_5 materials. Sample 3 following the removal of volatiles (AsF_3 and AsF_5) showed the diffraction behavior typical of nestled first-stage $C_{14}AsF_6$ salts. The material, however, contained a trace of a second-stage phase. The conductivity did not change siginificantly during the evacuation process (see Figure 5.3). Addition of fluorine again led to a drastic decrease in conductivity (see Figure 5.2).

5.4 Discussion

Since the treatment of graphite with AsF_5 alone always gives a mixture of first- and second-stage salts of composition $C_{14n}AsF_6$, the route to pure first-stage material was used which involves AsF_5 and F_2 mixtures close to these required for the stochiometry 14 C + AsF_5 + $\frac{1}{2}F_2$ (see Chapter 2).

The studies involving uptake of AsF_5 by graphite both in the absence and in the presence of fluorine had indicated (see Chapter 2) that C_xAsF_6 salts were in some cases able to take up and lose AsF_5 rather easily. To investigate this behavior, powdered samples (SP-1) of $C_{14n}AsF_6$ were prepared and exposed to AsF_5. The findings are summarized in Table 5.1. The uptake of AsF_5 by powdered $C_{14n}AsF_6$ was essentially complete within two hours at room temperature, and the end composition was ca. $C_{14n}AsF_6 \cdot (0.5)AsF_5$. This material has a much larger carbon-sheet separation (~8.0 Å) than the nestled $C_{14}AsF_6$ and the pattern of line intensities is similar to that described for the eclipsed carbon-sheet structure with highly disordered As and F atom placement. It appears, therefore, that the introduction of AsF_5 destroys the nestled arrangement and introduces greater guest disorder. The process is reversible, however, and removal of AsF_5 volatiles restores the original composition and structure. In contrast to the introduction and removal of AsF_3 (see below) that of AsF_5 is fast. This is probably a consequence of the formation of μ-fluorobridged species such as $As_2F_{11}^-$ $(F_5As\text{-}F\text{-}AsF_5)^-$. Such species, dissociating to AsF_6^- and AsF_5, provide a mechanism for the transportation of AsF_5 into and within the graphite galleries. No such mechanism is readily available to AsF_3 because of its very weak fluoro-acidity. Naturally the existence of $As_2F_{11}^-$, AsF_6^-,

and probably AsF_5 monomer would cause disruption of the nestled $C_{14n}AsF_6$ structure and contribute to the high disorder typical of the eclipsed carbon-sheet structure. The volume required for the a_0=2.46 Å and c_0=7.97 Å unit cell of $C_{15.1}AsF_6 \cdot (0.6)AsF_5$ is 314 Å^3. This is close to that required for close packing of all species, since the required volume for (15.1)C is 132 Å^3, for AsF_6^- ~105 Å^3, and for AsF_5 ~88 Å^3 ($\sum$ = 325 Å^3). Of course we must assume that the loss of coulomb attraction energy (associated with the nestled I_c = 7.6 Å structure passing to the un-nestled eclipsed carbon sheet arrangement with I_c = 8 Å) is compensated for by the screening effect of AsF_5 diminishing the anion-anion repulsion.

Although the uptake of AsF_3 by $C_{14n}AsF_6$ is much slower than for AsF_5 (for the reasons discussed above), the limiting composition (in time) is akin to that for the AsF_5 system (see Table 2). Compositions $C_{13.2}AsF_6 \cdot (0.6)AsF_3$ and $C_{14.3}AsF_6 \cdot (0.4)AsF_3$ are not far from the $C_xAsF_6 \cdot (0.5)AsF_3$ composition identical with $C_{2x/3}AsF_5$. It is unlikely that the AsF_3 forms bridged species to AsF_6^-, although the small amount of AsF_5 formed in the reduction:

$$AsF_3 + 2\ AsF_6^- \rightarrow 3\ AsF_5 + 2\ e^-$$

probably does so. For the most part, however, we expects AsF_3 to be spaced symmetrically between AsF_6^- in a close packed arrangement with six of the latter about the former and three AsF_3 about each AsF_6^-. That there is appreciable order in the guest arrangement is hinted at by the X-ray powder data (see Table 5.2). The data for the AsF_3 containing materials has more lines than the data from the AsF_5 containing materials and is indicative of a well defined arsenic superlattice. So far, however, the unit cell is unknown.

Unlike the complete reversibility observed in the $C_{14n}AsF_6$ + AsF_5 system, the introduction of AsF_3 leads to the formation of some AsF_5. This was expected from the studies described in Chapter 2. As may be seen from Sample 3 in Table 5.1, a material of composition $C_{13.2}AsF_6$ is reduced by AsF_3 to $C_{17.8}AsF_6$ and that material is a mixture of first- and second-stages. This is consistent with the inability of AsF_5 to form a pure first-stage material, even with six or more applications of AsF_5 (see Chapter 2). It is also noticed that the product of AsF_3 addition, $C_{13.2}AsF_6 \cdot (0.6)AsF_3$, before evacuation contained a second-stage phase, even though the starting material was a pure first-stage salt. This is consistent with the staging formula for the C/AsF_5 series being $C_{8n}AsF_5$ whereas that for the nestled AsF_6^- salts is $C_{14n}AsF_6$, where n is the stage. $C_{13.2}AsF_6 \cdot (0.6)AsF_3$ would thus correspond to $C_{8.25}AsF_{4.9}$.

It is curious that, although $C_{14}AsF_6$ incorporates each of AsF_5 or AsF_3 to approximately the same molar extent (~0.5 mole for each), I_c-spacing for the smaller molecule (AsF_3) is greater than for the larger (AsF_5). Thus I_c-spacing for $C_{14}AsF_6 \cdot (0.5)AsF_3$ is 8.15 Å like that for the "$C_{10}AsF_5$" material. This hints at the close relationship of $C_{2p}AsF_5$ to $C_{3p}AsF_6 \cdot (0.5)AsF_3$. Certainly we expect the inorporation of AsF_5 to lead to $As_2F_{11}^-$ formation, whereas AsF_3 will stand separatley from AsF_6^-. With AsF_3, however, we do have the interaction:

$$AsF_3 + 2\ AsF_6^- \rightarrow 3\ AsF_5 + 2\ e^-$$

and this diminishes both the AsF_6^- and AsF_3 concentrations. The AsF_5 formed can in turn make $As_2F_{11}^-$. The charge borne by the carbon sheets (and the guest species) would thereby be reduced. This could account for the greater I_c-spacing for the AsF_3 incorporated material.

In Sections 5.2.1 and 5.2.2 incorporation of AsF_5 and AsF_3 by $C_{14n}AsF_6$ was demonstrated. A part of the reason for their incorporation must be their role as neutral dielectric spacers, but the formation of $As_2F_{11}^-$, and the redox reactions involving AsF_3 and AsF_5 must also play a role. It was found that non-interacting SO_2ClF used as a solvent[25,26,35,37] in the reaction of graphite with O_2AsF_6 is incorporated into the product. It is removed slowly upon evacuation. The process is accompanied by decrease in I_c-spacing (8.0 Å to 7.6 Å), and structural change from un-nestled AsF_6^- to nestled AsF_6^-. The process is reversible. In this case the dielectric spacer effect and the dipole moment are the probable basis for the SO_2ClF incorporation. Despite good dielectric properties of SF_6 it was not readily incorporated. Although SF_6 is larger than SO_2ClF, it is not likely that this is the main reason for the failure of SF_6 to act like SO_2ClF. After all $C_{14}AsF_6$ does incorporate more AsF_6^- to give $C_{10}AsF_6$ (see Figure 2.4). It is more likely that the failure of $C_{14}AsF_6$ to incorporate SF_6 has to do with the lower polarizability of SF_6 compare with SO_2ClF. Moreover SO_2ClF is a dipolar speceis.

Fluorine uptake by C_xAsF_5 has been a controversial issue.[11,12,18,30,34-36] Because of the low molecular weight of fluorine (relative to AsF_x species), gravimetry and CHN analyses usually do not give definitive results. Fluorine analysis could be dubious because of the formation of CF_4 in the analytical processes. Tensimetry is also inexact because of the consumption of F_2 by the inside wall-surfaces of the measuring system. For the study of fluorine uptake beyond that required for AsF_6^- salt formation, the starting materials, as far as possible have been AsF_6^- salts. In the studies involving powdered

graphite there was no difficulty in starting with such materials. In the experiments detailed in Table 5.3, the starting materials were characterized salts of type $C_{14n}AsF_6$. In each case exposure of the salt to F_2 gas resulted in fluorine uptake and it was usual (at least initially) for this uptake to be accompanied by a small contraction in the I_c dimension. The fluorine uptake was assessed by fluorine consumption (tensimetry), gravimetry, and carbon analysis. Although the findings indicate that as much as (2.2)F, in excess of that required to make AsF_6^-, can be incorporated into a first-stage salt of composition $C_{15.6}AsF_6$, there is considerable uncertainty in that value, because of the experimental difficulties already alluded to. There is, however, no difficulty in fitting two fluorine atoms into the nestled $C_{14}AsF_6$ structure. There is sufficient space, even if allowance is made for directed C-F bonding.

First-stage materials prepared with AsF_5 alone and with AsF_5/F_2 (Samples 2 and 3, respectively, in Table 5.5) before evacuation have comparable conductivities ca. 10 times that of graphite. Since the ionization of the host carbon-layer is higher for the latter, it could be argued that the combined factor of the charge (hole) density and the mobility is about the same for the two kinds of materials. Their specific conductivities did not change significantly after 4 days of evacuation (see Figure 5.3). The sample prepared with AsF_5 alone, at the end of evacuation, was roughly a 1:1 mixture of first- and second-stages, whereas that with AsF_5/F_2 was mainly first- with a trace of a second-stage phase. Because of the limited length of evacuation time and the uncertainty in the extent of the removal of the volatiles from the HOPG samples, the evacuated products have to be formulated as

$C_yAsF_{6-\delta}$. In such formulae y and δ are larger for the former sample (Sample 2) than the latter (Sample 3). From the conductivity change during evacuation depicted in Figure 5.3, it is evident that there is unlikely to be further change in conductivities with extended evacuation. Therefore it is surmised that the conductivity of C_yAsF_6 (mainly first-stage) materials is ca. 10 times that of graphite (see below). Addition of fluorine to $C_yAsF_{6-\delta}$ materials drastically reduced the conductivites down to the graphite level (see Figure 5.2). The initial increase in conductivity in Sample 1 is interpreted as due to an increase in the AsF_6^- guest concentration. The maximum conductivity for that sample would then be identical with composition $C_{14}AsF_6$. Consequently, the drastic decrease in conductiviy is ascribed to extra fluorine uptake to form $C_yAsF_6 \cdot \delta F$. The last formulation was demonstrated with SP-1 powder samples (see Table 5.3) on which the HOPG formulations are based by X-ray diffraction data. Sample 1 in Table 5.5 suggests that, even when the guest species density is high ($C_{10}AsF_{5-6}$), fluorine uptake is sufficient enough to bring about a drastic decrease in conductivity (see Figure 5.2).

The combination of powder compositional studies and HOPG conductivity measurements indicate that $C_{14}AsF_6$ salts have conductivities which are an order of magnitude higher than graphite. In this they are qualitatively indistinguishable from the "C_xAsF_5" materials. Undoubtedly fluorination of any of these materials eventually produces poorer coductor (comparable with graphte). This is associated with incorporation for more fluorine than required to form AsF_6^- alone.

Table 5.1. Data relating to interactions of $C_{14n}AsF_6$ with AsF_5, AsF_3, and SF_6.

Sample	Treatment	Duration	%C	Composition[a)]	I_c(Å)-first/second
1[b)]			48.92	$C_{15.1}AsF_6$	7.61
	+ AsF_5	15 hours	38.21	$C_{15.1}AsF_6 \cdot (0.6)AsF_5$	7.97
	Pump	60 hours	48.72	$C_{15.1}AsF_6 \cdot (0.01)AsF_5$	7.65
2[b)]			48.92	$C_{15.1}AsF_6$	7.61
	+ AsF_5	14 hours	38.43	$C_{15.1}AsF_6 \cdot (0.6)AsF_5$	7.98
	Pump	52 hours	47.72	$C_{15.1}AsF_6 \cdot (0.05)AsF_5$	7.66
3[c)]			45.55	$C_{13.2}AsF_6$	7.71
	+ AsF_3	4 days	37.24	$C_{13.2}AsF_6 \cdot (0.6)AsF_3$	8.15/11.68
	Pump[e)]	8 days	53.05	$C_{17.8}AsF_{6-\delta}$	7.65/10.92
4[d)]			47.53	$C_{14.3}AsF_6$	7.71
	+ AsF_3	2 days	41.73	$C_{14.3}AsF_6 \cdot (0.4)AsF_3$	8.12
	Pump[e)]	2 days	49.74	$C_{15.6}AsF_{6-\delta}$	7.63
5[d)]			48.09	$C_{14.6}AsF_6$	7.63
	+ SF_6	2 days	48.71	$C_{14.6}AsF_6$	7.62
6[d)]			47.54	$C_{14.3}AsF_6$	7.63
	+ SF_6	2 days	47.62	$C_{14.3}AsF_6$	7.65

a). Compositions were determined based on %C (CHN analyses). They were given by assuming that the amount of AsF_6^- in each sample remained unchanged during the reaction processes, except for Samples 3 and 4 after the evacuation. These compositions were consistent with the gravimetry, but this was not as precise as %C in fixing the composition.

b). Samples 1 and 2 were obtained in the same preparation from $C/AsF_5/F_2$ system.

c). Obtained by the reaction of $C/AsF_5/F_2$.

d). Obtained by the reaction of C/O_2AsF_6 described in Chapter 2. No SO_2ClF was used.

e). IR of the volatiles indicated the presence of some AsF_5 in the initial voltiles removed.

Table 5.2. X-ray powder diffraction data of the typical ca. $C_{14}AsF_6 \cdot (0.5)AsF_3$ sample.

Intensity	d (obs)	$1/d^2$ (obs)	First Stage $1/d^2$ (HKL) (calc)	Second Stage $1/d^2$ (HKL) (calc)
VS	8.24	.0147	.0150 (001)	
W	6.66	.0225		
M Broad	5.13	.0379		
VS	4.08	.0599	.0601 (002)	
W	3.98	.0630		
S	3.87	.0666		.0660 (003)
S	3.73	.0717		
S Broad	3.48	.0825		
S	3.33	.0900		
VW	3.17	.0993		
VW	3.11	.1036		
W	2.92	.1171		.1173 (004)
M	2.81	.1262		
S	2.71	.1361	.1354 (003)	
W	2.53	.1562		
W	2.46	.1657		
VW	2.36	.1799		
VW	2.29	.1905		
W	2.21	.2056		
S	2.12	.2224	.2221 (100)	.2217 (100)
M	2.04	.2407	.2371 (101)	
M Broad	1.92	.2699		
W	1.86	.2876		.2877 (103)
W	1.84	.2951		
W	1.80	.3088		
VW Broad	1.74	.3295		
VW	1.66	.3619		
VW Broad	1.51	.4394		
W	1.43	.4886		
W	1.39	.5141		
M	1.36	.5415	.5417 (006)	
W	1.24	.6492		
M	1.23	.6652	.6664 (110)	.6653 (110)

Table 5.3. Data relating to interaction of $C_{14n}AsF_6$ with F_2.

Sample	Treatment	Duration	%C	Composition[a)]	I_c(Å)-first/second	
1			46.72	$C_{13.8}AsF_6$	7.85	
	+ F_2	5 days	43.62	$C_{13.8}AsF_6 \cdot (1.3)F$	7.79	
	Pump	5 days	44.09	$C_{13.8}AsF_6 \cdot (1.1)F$	7.78	
2			49.74	$C_{15.6}AsF_6$	7.63	
	+ F_2	3 days				
	Pump	1 days	47.28	$C_{15.6}AsF_6 \cdot (1.0)F$	7.60	
	+ F_2	3 days				
	and Pump	1 day	46.29	$C_{15.6}AsF_6 \cdot (1.5)F$	7.62	
	+ F_2	5 days				
	and Pump	2 days	44.70	$C_{15.6}AsF_6 \cdot (2.2)F$	7.64	
3			65.41	$C_{29.8}AsF_6$		10.94
	+ F_2	5 days				
	and Pump	2 hours	61.60	$C_{29.8}AsF_6 \cdot (1.8)F$		10.92

a). Compositions were determined by CHN analyses (%-carbon). They were given by assuming that the amount of AsF_6^- in each sample remained unchanged during the reaction processes. These compositions were consistent with the gravimetry and tensimetry, but they were not as precise as %C in fixing composition.

Table 5.4. Data relating to interaction of $C_{14}AsF_6$ with SO_2ClF.
(Reaction of graphite with O_2AsF_6 in SO_2ClF)

Sample	Treatment	Duration		C%*	S%*	Cl%*	Composition*	I_c(Å) First/Second*
1	6 C + O_2AsF_6	1 day	Found	42.04	2.55	3.48		7.83
			Required	42	2.9	3.2	for $C_{14}AsF_6 \cdot (0.36)SO_2ClF$	
	Pump	5 days	Found	46.16	0.42	1.58		7.59
			Required	46	0.9	1.0	for $C_{14}AsF_6 \cdot (0.10)SO_2ClF$	
2	4 C + O_2AsF_6	5 days	Found	44.15	1.61	2.82		7.94/11.18
			Required	44	1.8	2.0	for $C_{14}AsF_6 \cdot (0.22)SO_2ClF$	
	Pump	4 days	Found	48.90	0.31	0.74		7.55/10.78
			Required	46	0.5	0.6	for $C_{14}AsF_6 \cdot (0.06)SO_2ClF$	
	+ SO_2ClF	1 day	Found	40.91	1.49	2.44		7.87
			Required	43	2.1	2.4	for $C_{14}AsF_6 \cdot (0.26)SO_2ClF$	

* Carbon, sulfur, and chlorine analyses are done on different parts of each sample after each treatment. Because of the higher inhomogeneity of HOPG-chip sample than of SP-1 powder, the analyses could be less reliable. The inhomogeneity of the sample could explain the observation of a second-stage phase for Sample 2.

Table 5.5. Data relating to conductivity measurements[a] of $C_{14n}AsF_6$ and related materials.

Sample	Treatment	Duration	σ/σ_g	I_c(Å)-first/second	Composition[b]
1	C + AsF_5	6 days	11	8.2	C_8AsF_5
	- AsF_5 (no pumping)		11	8.1/11.3	$C_{10}AsF_{5+\delta}$
	+ F_2	10 days	1	8.0	$C10^{AsF}{}_6 \cdot yF$
	+ F_2	34 days	0.8	7.9	$C_{10}AsF_6 \cdot y+\delta F$
2	C + AsF_5	3 days	10	8.2	C_8AsF_5
	Pump	4 days	11	7.7/10.8	$C_{21}AsF_{6-\delta}$
	+ F_2	4 days	1.5	7.7/10.8	$C_{21}AsF_6 \cdot yF$
3	C + AsF_5 + F_2	2 day	10	8.0	$C_{10}AsF_{5-6}$
	Pump	4 days	9	7.7/10.8	$C_{14}AsF_{6-\delta}$
	+ F_2	4 days	0.2	7.7	$C_{14}AsF_6 \cdot yF$

a). In all cases the conductivity measurements were made on HOPG chips by the contactless method described in the text.

b). Compositions were estimated from the known X-ray diffraction -data dependence on compositon for powdered materials.

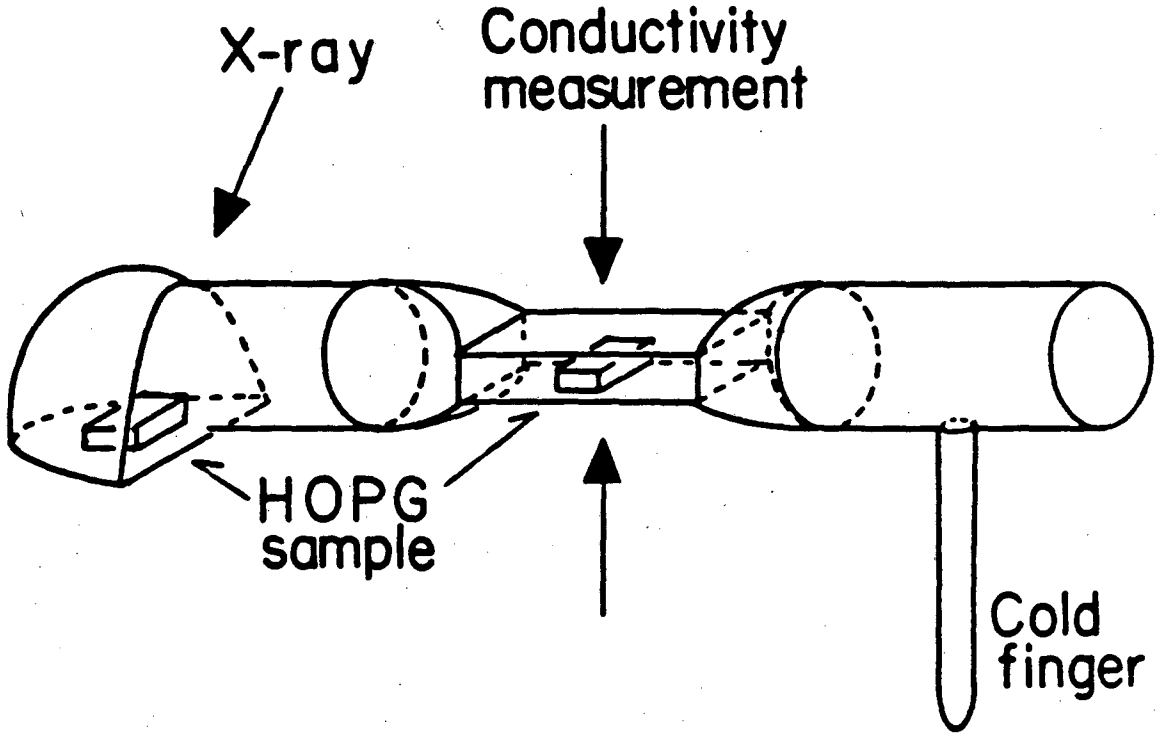

Figure 5.1. Quartz cell for <u>in situ</u> measurements of conductivity and X-ray diffraction.

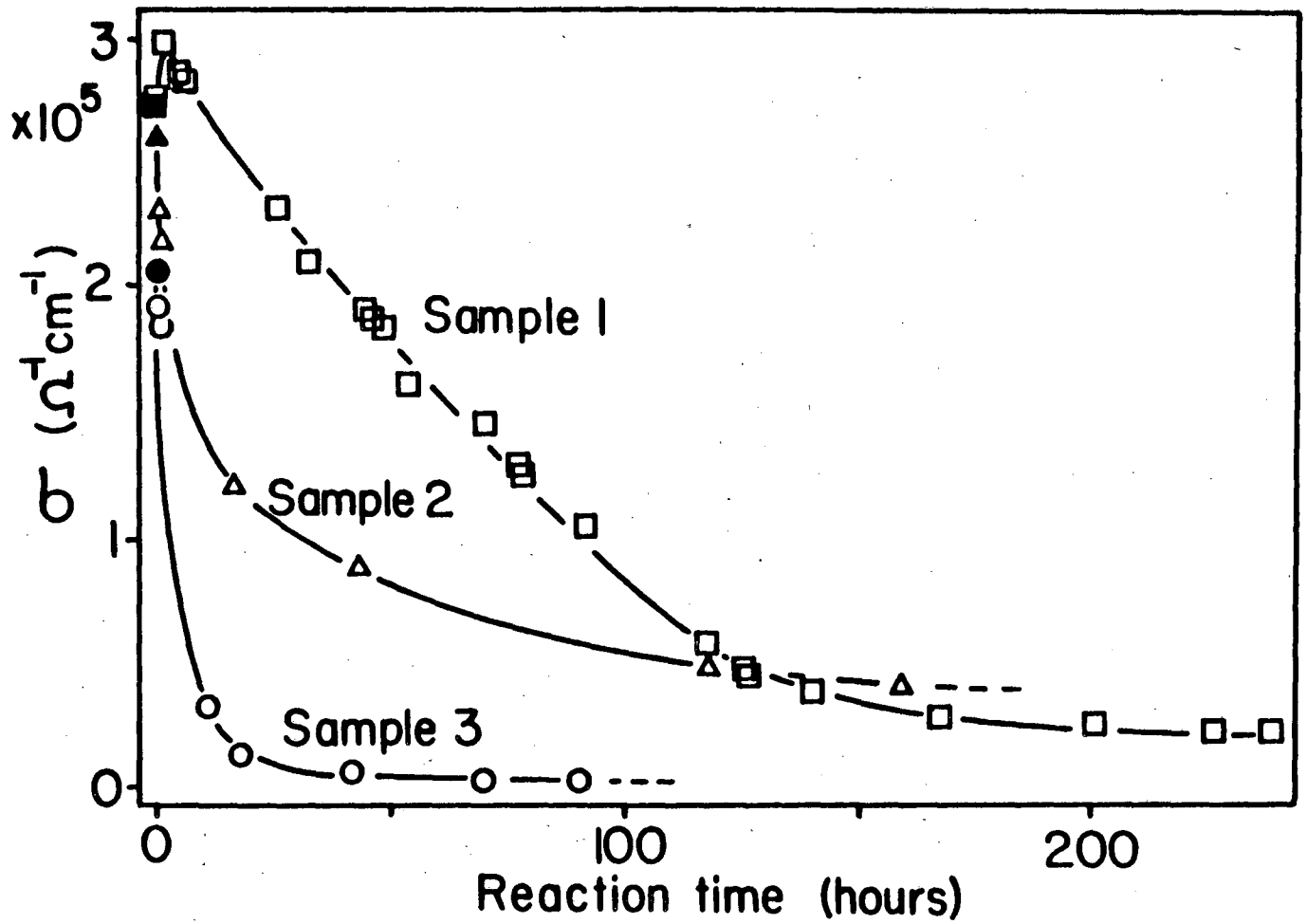

XBL 849-3773

Figure 5.2. Change in specific conductivity as a function of reaction time with F_2. Filled square, triangle, and circle indicate the initial conductivities. See Table 5.5 for the description of Samples 1-3.

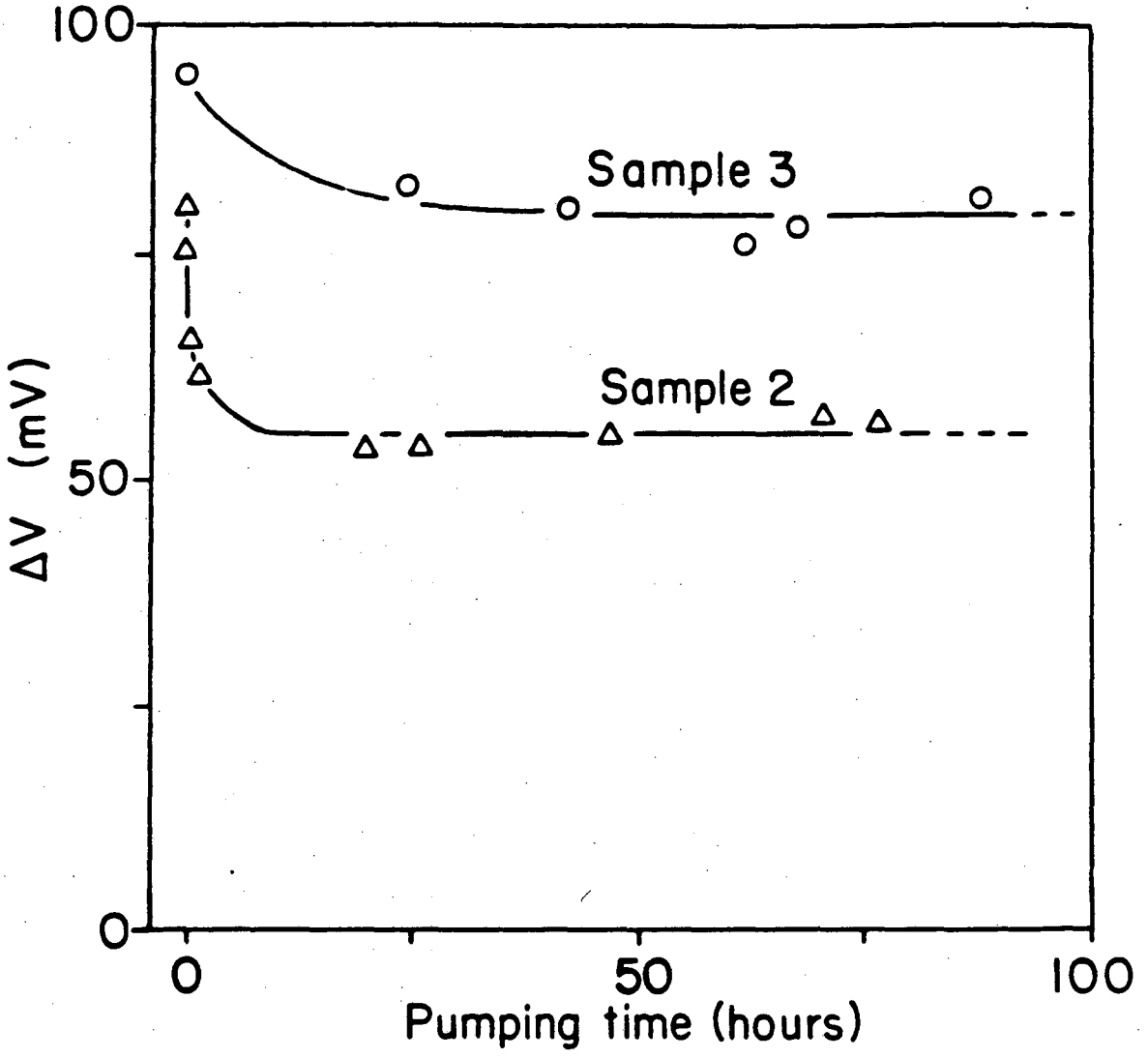

Figure 5.3. Change in conductivity, expressed by ΔV, as a function of pumping time.

REFERENCES

1. L. Chun-Hsu, H. Selig, M. Rabinovitz, I. Agranat, and S. Sarig, Inorg. Nucl. Chem. Lett., 11, 601 (1975).

2. E. R. Falardeau, G. M. T. Foley, C. Zeller, and F. L. Vogel, J. Chem. Soc. Chem. Commun., 389 (1977).

3. G. M. T. Foley, C. Zeller, E. R. Falardeau, and F. L. Vogel, Solid State Commun., 24, 371 (1977).

4. L. B. Ebert, and H. Selig, Mater. Sci. Eng., 31, 177 (1977).

5. L. B. Ebert, Louis Matty, D. R. Mills, and J. C. Scanlon, Mat. Res. Bull., 15, 251 (1980).

6. B. R. Weinberger, J. Kaufer, A. J. Heeger, E. R. Falardeau, and J. E. Fischer, Solid State Commun., 27, 163 (1978).

7. L. B. Ebert, D. R. Mills and J. C. Scanlon, Mat. Res. Bull., 14, 1369 (1979).

8. S. K. Khanna, E. R. Falardeau, A. J. Heeger, and J. E. Fischer, Solid State Commun., 25, 1059 (1978).

9. R. L. Kleinberg, and L. B. Ebert, Synth. Met., 2, 245 (1980).

10. L. V. Interrante, R. S. Markiewicz, and D. W. McKee, Synth. Met., 1, 287 (1979/80).

11. T. E. Thompson, E. M. McCarron, and N. Bartlett, Synth. Met., 3, 255 (1981).

12. N. Bartlett, E. M. MaCarron, and B. W. McQuillan, Synth. Met., 1, 221 (1979/80).

13. C. Zeller, L. A. Pendrys, and F. L. Vogel, J. Mat. Sci., 14, 2241 (1979).

14. M. J. Moran, J. W. Milliken, C. Zeller, R. A. Grayeski and J. E. Fischer, Synth. Met., 3, 269 (1981).

15. S. C. Singhal and A. Kernick, Synth. Met., 3, 247 (1981).

16. B. R. Weinberger, J. Kaufer, A. J. Heeger, J. E. Fischer, M. Moran, and N. A. W. Holzwarth, Phys. Rev. Lett., 41, 1417 (1978).

17. M. J. Moran, J. E . Fischer, and W. R. Slaneck, J. Chem. Phys., 73, 629 (1980).

18. J. W. Milliken, and J. E. Fischer, J. Chem. Phys., 78, 5800 (1983).

19. R. S. Markiewicz, H. R. Hart, Jr., L.V. Interrante, and J. S. Kasper, Solid State Commun., 35, 513 (1980).

20. R. S. Markiewicz, H. R. Hart, Jr., L. V. Interrante, and J. S. Kasper, Synth. Met., 2, 331 (1980).

21. L. R. Hanlon, E. R. Falardeau and J. E. Fischer, Solid State Commun., 24, 377 (1977).

22. L. R. Hanlon, E. R. Falardeau, D. Guerard, and J. E. Fischer, Mater. Sci. Eng., 31, 161 (1977).

23. G. R. Miller, H. A Resing, P. Brant, M. J. Moran, F. L. Vogel, T. C. Wu. P. Billaud, and A. Pron, Synth. Met., 2, 237 (1980).

24. H. A. Resing, M. J. Moran, and G. R. Miller, J. Chem Phys., 76, 1706 (1982).

25. N. Bartlett, R. N. Biagioni, B. W. McQuillan, A. S. Robertson, and A. C. Thompson, J. Chem. Soc. Chem. Commun., 200 (1978).

26. N. Bartlett, R. N. Biagioni, G. McCarron, B. McQuillan, and F. Tanzella, Molecular Metals, 293 (1979).

27. E. R. Falardeau, L. R. Hanlon, and T. E. Thompson, Inorg. Chem, 17, 301 (1978).

28. R. S. Markiewicz, J. S. Kasper. and L. V. Interrante, Synth. Met., 2, 363 (1980).

29. J. E. Fischer, J. Chem. Soc. Chem. Commun., 544 (1978).

30. R. Pentenrieder, and H. P. Boehm, Revue de Chimie minerale, 19, 371 (1982).

31. J. Shamir, and J. Binenboym, Inorg. Chim. Acta., 2, 37 (1968).

32. A. Taylor, J. Scientific Instruments, 28, 200 (1951).

33. R. N. Biagioni, Ph. D. Thesis, University of California, Berkeley (1980).

34. V. Munch and H. Selig, Synth. Met., 1, 407 (1979/80).

35. N. Bartlett, B. McQuillan, and A. S. Robertson. Mat. Res. Bull., 13, 1259 (1978).

36. E. M. McCarron, and N. Bartlett, J. Chem. Soc. Chem. Commun., 404 (1980).

37. E. M. McCarron, Ph. D. Thesis, University of California, Berkeley (1980).

38. H. Selig, M. J. Vasile, F. A. Stevie, and W. A. Sunder, J. Fluorine. Chem., 10, 299 (1977).

39. P. A. W. Dean, R. J. Gillespie, and R. Hulme, J. Chem. Soc. Chem. Commun., 990 (1969).

40. M. L. Dzurus, and G. R. Hennig, J. Am. Chem. Soc., 79, 1051 (1957).

41. T. Mallouk, Ph. D. Thesis, University of California, Berkeley (1983).

42. A. A. Woolf, J. Fluorine Chem., 15, 533 (1980).

43. The indices of the unit cells with a_0 = 2.46 Å and c_0 = 7.6n Å will be given by $\langle hk\ell \rangle$, $\{hk\ell\}$, and $[hk\ell]$, respectively, for n = 2, 3, and 600, and those of the smallest unit cell with a ≈ 2.46 Å and c ≈ 7.6-8.0 Å will be given by $(hk\ell)$. The indices of the larger unit cells with $a_0 = \sqrt{7}$ and $7 \times a_g$, respectiveley, are given in $[hk\ell]$ and $\{hk\ell\}$.

44. R. Chen, P. Trucano, and R. F. Stewart, Acta. Cryst., A33, 823 (1977).

45. M. S. Paterson, J. Appl. Phys. 23, 805 (1952).

46a. A. Guinier, X-Ray diffraction, W. H. Freeman and Company, San Francisco and London, 1963.

46b. A. Guinier, X-Ray diffraction, W. H. Freeman and Company, San Francisco and London, 1963, p. 155.

47. L. V. Azaroff, Elements of X-Ray Crystallography, McGraw-Hill, New York, 1968, pp. 256-281.

48. W. H. Zachariasen, Phys. Rev. 71. 715 (1947)

49. B. E. Warren, Phys. Rev., 59, 693 (1941)

50. For the rest of Chapter 4 summation variables run through negative to positive infinities unless specified otherwise.

51. C. Zeller, A. Denestein and G. M. T. Foley, Rev. Sci. Instrum., 50, 602 (1979)

APPENDIX

The following computer programs, written in VAX-11 BASIC, were used to calulate intensities for the nestled-large-cell model, the (HKℓ)-(III) model, and the (hkℓ) model.

Nestled-large-cell model

```
100 INPUT "TITLE":TITLE$
110 MAP (DATA.FILE) IT2THC.DATA%
120 INPUT " NAME OF DATA AND TERMINAL FORMAT FILES /NAME999999(.DAT & .TFF)/" &
   :FILE$
130 OPEN FILE$+".DAT" FOR OUTPUT AS FILE #3%,SEQUENTIAL,MAP DATA.FILE
140 OPEN FILE$+".TFF" FOR OUTPUT AS FILE #6%,RECORDSIZE 132%
150 DIM PX(21%),PY(21%),PLOT$(5%)
160 A1C=2.31   \B1C=20.8439\A2C=1.02  \B2C=10.2075\A3C=1.5886\B3C=.5687 &
   \A4C=.865   \B4C=51.6512\CC=.2156
170 A1A=16.6723\B1A=2.6345 \A2A=6.0701\B2A=.2647  \A3A=3.4313\B3A=12.9479 &
   \A4A=4.2779 \B4A=47.7972\CA=2.531
180 A1F=3.5392 \B1F=10.2825\A2F=2.6412\B2F=4.2944 \A3F=1.517 \B3F=.2615 &
   \A4F=1.0243 \B4F=26.1476\CF=.2776
190 WL=1.5418\WL_2=.7709\PI=3.1800=3800/PI
200 INPUT "# OF LAYERS":NL%\NA%=21%*NL%
210 DIM CL$(NL%),PA%(NL%),X(NA%),Y(NA%),Z(NA%)
220 NL.14%=NL%*14%\NL.14_1%=NL%*14%+1%\NL.15%=NL%*15%\NL.15_1%=NL%*15%+1%
230 PRINT "INPUT UHH AND UII FOR C, AS AAC F  (UHH=UHH:UHK=UHH/2:UHK=UII=0)" &
   \INPUT "FOR C":UHHC,ULLC\INPUT "FOR AS":UHHA,ULLA\INPUT "FOR F":UHHF,ULLF
240 A=2.456*SQR(7)\C=7.6*NL%\FI2=2*PI\PI5=-PI^2/50\A2=4/A^2/3\C2=1/C^2
250 D2HM=4/WL^2\PRINT "ENTER UPPER LIMIT FOR 1/D^2--MA)INPUT =":D2HM\INPUT D2M
260 D2M=D2MM IF D2M>D2MM\DM=1/SQR(D2M)
270 SN=WL/DM/2\TH2DM%=INT(3600*ATN(SN/SQR(-SN^2+1))/PI)
280 DIM IT2THC(TH2DM%)
290 HM%=INT(SQR(3)*A/2/DM)\LM%=INT(C/DM)
300 PX( 1)= 0   \PX( 2)= 1/21\PX( 3)= 5/21\PX( 4)= 9/21\PX( 5)=13/21
310 PX( 6)=17/21\PX( 7)= 2/21\PX( 8)= 6/21\PX( 9)=10/21\PX(10)=14/21
320 PX(11)=18/21\PX(12)= 3/21\PX(13)= 7/21\PX(14)=11/21\PX(15)=15/21
330 PX(16)=19/21\PX(17)= 4/21\PX(18)= 8/21\PX(19)=12/21\PX(20)=16/21
340 PX(21)=20/21
350 PY( 1)= 0   \PY( 2)= 5/21\PY( 3)= 4/21\PY( 4)= 3/21\PY( 5)= 2/21
360 PY( 6)= 1/21\PY( 7)=10/21\PY( 8)= 9/21\PY( 9)= 8/21\PY(10)= 7/21
370 PY(11)= 6/21\PY(12)=15/21\PY(13)=14/21\PY(14)=13/21\PY(15)=12/21
380 PY(16)=11/21\PY(17)=20/21\PY(18)=19/21\PY(19)=18/21\PY(20)=17/21
390 PY(21)=16/21
400 CL$(1)="A"\PRINT "INPUT POSITION OF AS (1 TO 14)"
410 FOR I%=1% TO NL%-1%\PRINT I%;CL$(I%);\INPUT PA%(I%)
420 GOTO 440 IF CL$(I%)="B"\GOTO 450 IF CL$(I%)="C"
430 IF 2%*INT(PA%(I%)/2)-PA%(I%)<0% THEN CL$(I%+1%)="B"\GOTO 460 &
   ELSE                                  CL$(I%+1%)="C"\GOTO 460
440 IF 2%*INT(PA%(I%)/2)-PA%(I%)<0% THEN CL$(I%+1%)="C"\GOTO 460 &
   ELSE                                  CL$(I%+1%)="A"\GOTO 460
450 IF 2%*INT(PA%(I%)/2)-PA%(I%)<0% THEN CL$(I%+1%)="A"\GOTO 460 &
   ELSE                                  CL$(I%+1%)="B"\GOTO 460
460 IF CL$(NL%)="A" THEN I%=NL%-2%\PRINT "INPUT AGAIN"\GOTO 470 &
   ELSE GOSUB 950
470 NEXT I%
480 IF CL$(NL%)="B" THEN PRINT NL%;CL$(NL%);\INPUT " INPUT EVEN #":PA%(NL%) &
   ELSE                  PRINT NL%;CL$(NL%);\INPUT " INPUT ODD  #":PA%(NL%)
490 I%=NL%\GOSUB 950\ITM=1\FI%=0%\NR%=0%
500 PRINT #6,TITLE$
510 PRINT #6,"H  K  L  1/D^2  2*THETA  INTENSITY*PAXIMUM=1000000  (*ABS.INT)"
520 FOR H1%=0% TO HM%\FOR K1%=0% TO H1%\FOR L2%=0% TO LM%
530 GOTO 730 IF H1%+K1%+L2%=0%
```

```
540 GOTO 730 IF H1%+K1%=0% AND NL%*INT(L2%/NL%)-L2%<0%
550 D2=A2*(H1%^2+H1%*K1%+K1%^2)+C2*L2%^2\GOTO 730 IF D2>D2P
560 NP%=NR%+1%\IT=0\SN=WL_2*SQR(D2)\TH=ATN(SN/SQR(-SN^2+1)) &
   \TH2=TH*2\SS=-D2/4\LP=(1+COS(TH2)^2)/SIN(TH)^2/COS(TH)
570 H2%= H1%     \K2%=      K1%\GOSUB 760\GOTO 690 IF H1%+K1%=0 &
   \                                GOTO 590 IF H1%=K1%
580 H2%=      K1%\K2%= H1%     \GOSUB 760
590 H2%=-H1%     \K2%=     -K1%\GOSUB 760\GOTO 610 IF H1%=K1%

600 H2%=     -K1%\K2%=-H1%     \GOSUB 760
610 H2%=-H1%     \K2%= H1%+K1%\GOSUB 760
620 H2%= H1%+K1%\K2%=-H1%     \GOSUB 760\GOTO 650 IF H1%=K1% &
   \                                GOTO 690 IF K1%=0%
630 H2%= H1%+K1%\K2%=     -K1%\GOSUB 760
640 H2%=     -K1%\K2%= H1%+K1%\GOSUB 760
650 H2%= H1%     \K2%=-H1%-K1%\GOSUB 760
660 H2%=-H1%-K1%\K2%= H1%     \GOSUB 760\GOTO 690 IF H1%=K1%
670 H2%=-H1%-K1%\K2%=      K1%\GOSUB 760
680 H2%=      K1%\K2%=-H1%-K1%\GOSUB 760
690 IF L2%>0 THEN IT=2*LP*IT\GOTO 700 ELSE IT=IT*LP
700 D2TT%=INT(D2*10000)\TH2D%=INT(TH2*PI.1800)
710 IT2THD(TH2D%)=IT2THD(TH2D%)+IT
720 IF IT>ITM THEN ITM=IT\PRINT      H1%;K1%;L2%;D2TT%;TH2D%;"1000000*";IT &
   \PI%=0                    \PRINT #6%,H1%;K1%;L2%;D2TT%;TH2D%;"1000000*";IT &
   ELSE ITN%=INT(1000000*IT/ITP) &
   \                          PRINT      H1%;K1%;L2%;D2TT%;TH2D%;ITN% &
   \                          PRINT #6%,H1%;K1%;L2%;D2TT%;TH2D%;ITN%;"/"; &
   \PI%=PI%+1%\IF PI%-4%*INT(PI%/4%)=0% THEN PRINT #6%\PI%=0% ELSE GOTO 730
730 NEXT L2%\NEXT K1%\NEXT H1%
740 GOSUB 1620
750 CLOSE #3\CLOSE #6\GOTO 1890
760 REM *****  STRUCTURE FACTOR AND INTENSITY  *****
770 FCR=0\FCI=0\FAR=0\FAI=0\FFR=0\FFI=0\FR=0\FI=0
780 FOR J%=1% TO NL.14%
790 T=PI2*(H2%*X(J%)+K2%*Y(J%)+L2%*Z(J%))\FCR=FCR+COS(T)\FCI=FCI+SIN(T)
800 NEXT J%
810 ST=(A1C*EXP(B1C*SS)+A2C*EXP(B2C*SS)+A3C*EXP(B3C*SS)+A4C*EXP(B4C*SS)+CC) &
    *EXP(PI5*(UHHC*(H2%^2+H2%*K2%+K2%^2)*A2+ULLC*L2%^2*C2))
820 FR=FR+FCR*ST\FI=FI+FCI*ST
830 FOR J%=NL.14_1% TO NL.15%
840 T=PI2*(H2%*X(J%)+K2%*Y(J%)+L2%*Z(J%))\FAR=FAR+COS(T)\FAI=FAI+SIN(T)
850 NEXT J%
860 ST=(A1A*EXP(B1A*SS)+A2A*EXP(B2A*SS)+A3A*EXP(B3A*SS)+A4A*EXP(B4A*SS)+CA) &
    *EXP(PI5*(UHHA*(H2%^2+H2%*K2%+K2%^2)*A2+ULLA*L2%^2*C2))
870 FR=FR+FAR*ST\FI=FI+FAI*ST
880 FOR J%=NL.15_1% TO NA%
890 T=PI2*(H2%*X(J%)+K2%*Y(J%)+L2%*Z(J%))\FFR=FFR+COS(T)\FFI=FFI+SIN(T)
900 NEXT J%
910 ST=(A1F*EXP(B1F*SS)+A2F*EXP(B2F*SS)+A3F*EXP(B3F*SS)+A4F*EXP(B4F*SS)+CF) &
    *EXP(PI5*(UHHF*(H2%^2+H2%*K2%+K2%^2)*A2+ULLF*L2%^2*C2))
920 FR=FR+FFR*ST\FI=FI+FFI*ST
930 IT=IT+FR^2+FI^2
940 RETURN
950 REM ***** ASSIGN X, Y AND Z ******
960 I14%=I%*14%\GOTO 990 IF CL$(I%)="B"\GOTO 1010 IF CL$(I%)="C"
970 X(I14%-13%)=PX( 1)\X(I14%-12%)=PX( 3)\X(I14%-11%)=PX( 4) &
    \X(I14%-10%)=PX( 6)\X(I14%- 9%)=PX( 7)\X(I14%- 8%)=PX( 8) &
    \X(I14%- 7%)=PX(10)\X(I14%- 6%)=PX(11)\X(I14%- 5%)=PX(12) &
    \X(I14%- 4%)=PX(14)\X(I14%- 3%)=PX(15)\X(I14%- 2%)=PX(18) &
    \X(I14%- 1%)=PX(19)\X(I14%    )=PX(21)
980 Y(I14%-13%)=PY( 1)\Y(I14%-12%)=PY( 3)\Y(I14%-11%)=PY( 4) &
    \Y(I14%-10%)=PY( 6)\Y(I14%- 9%)=PY( 7)\Y(I14%- 8%)=PY( 8) &
    \Y(I14%- 7%)=PY(10)\Y(I14%- 6%)=PY(11)\Y(I14%- 5%)=PY(12) &
    \Y(I14%- 4%)=PY(14)\Y(I14%- 3%)=PY(15)\Y(I14%- 2%)=PY(18) &
    \Y(I14%- 1%)=PY(19)\Y(I14%    )=PY(21)\GOTO 1030
```

```
990 X(I14%-13%)=PX( 1)\X(I14%-12%)=PX( 2)\X(I14%-11%)=PX( 4) &
    \X(I14%-10%)=PX( 5)\X(I14%- 9%)=PX( 8)\X(I14%- 8%)=PX( 9) &
    \X(I14%- 7%)=PX(11)\X(I14%- 6%)=PX(12)\X(I14%- 5%)=PX(13) &
    \X(I14%- 4%)=PX(15)\X(I14%- 3%)=PX(16)\X(I14%- 2%)=PX(17) &
    \X(I14%- 1%)=PX(19)\X(I14%    )=PX(20)
1000 Y(I14%-13%)=PY( 1)\Y(I14%-12%)=PY( 2)\Y(I14%-11%)=PY( 4) &

    \Y(I14%-10%)=PY( 5)\Y(I14%- 9%)=PY( 8)\Y(I14%- 8%)=PY( 9) &
    \Y(I14%- 7%)=PY(11)\Y(I14%- 6%)=PY(12)\Y(I14%- 5%)=PY(13) &
    \Y(I14%- 4%)=PY(15)\Y(I14%- 3%)=PY(16)\Y(I14%- 2%)=PY(17) &
    \Y(I14%- 1%)=PY(19)\Y(I14%    )=PY(20)\GOTO 1030
1010 X(I14%-13%)=PX( 2)\X(I14%-12%)=PX( 3)\X(I14%-11%)=PX( 5) &
    \X(I14%-10%)=PX( 6)\X(I14%- 9%)=PX( 7)\X(I14%- 8%)=PX( 9) &
    \X(I14%- 7%)=PX(10)\X(I14%- 6%)=PX(13)\X(I14%- 5%)=PX(14) &
    \X(I14%- 4%)=PX(16)\X(I14%- 3%)=PX(17)\X(I14%- 2%)=PX(18) &
    \X(I14%- 1%)=PX(20)\X(I14%    )=PX(21)
1020 Y(I14%-13%)=PY( 2)\Y(I14%-12%)=PY( 3)\Y(I14%-11%)=PY( 5) &
    \Y(I14%-10%)=PY( 6)\Y(I14%- 9%)=PY( 7)\Y(I14%- 8%)=PY( 9) &
    \Y(I14%- 7%)=PY(10)\Y(I14%- 6%)=PY(13)\Y(I14%- 5%)=PY(14) &
    \Y(I14%- 4%)=PY(16)\Y(I14%- 3%)=PY(17)\Y(I14%- 2%)=PY(18) &
    \Y(I14%- 1%)=PY(20)\Y(I14%    )=PY(21)
1030 REM *****   ARSENIC X,Y  ******
1040 TI%=NL%*14%+I%\GOTO 1200 IF CL$(I%)="B"\GOTO 1350 IF CL$(I%)="C"
1050 ON PA%(I%) GOTO 1060,1070,1080,1090,1100,1110,1120 &
                    ,1130,1140,1150,1160,1170,1180,1190
1060 X(TI%)=P)( 1)\Y(TI%)=PY( 1)\GOTO 1500
1070 X(TI%)=P)(18)\Y(TI%)=PY(18)\GOTO 1500
1080 X(TI%)=P)(19)\Y(TI%)=PY(19)\GOTO 1500
1090 X(TI%)=P)( 3)\Y(TI%)=PY( 3)\GOTO 1500
1100 X(TI%)=P)( 4)\Y(TI%)=PY( 4)\GOTO 1500
1110 X(TI%)=P)( 6)\Y(TI%)=PY( 6)\GOTO 1500
1120 X(TI%)=P)(11)\Y(TI%)=PY(11)\GOTO 1500
1130 X(TI%)=P)( 7)\Y(TI%)=PY( 7)\GOTO 1500
1140 X(TI%)=P)( 8)\Y(TI%)=PY( 8)\GOTO 1500
1150 X(TI%)=P)(10)\Y(TI%)=PY(10)\GOTO 1500
1160 X(TI%)=P)(12)\Y(TI%)=PY(12)\GOTO 1500
1170 X(TI%)=P)(14)\Y(TI%)=PY(14)\GOTO 1500
1180 X(TI%)=P)(15)\Y(TI%)=PY(15)\GOTO 1500
1190 X(TI%)=P)(21)\Y(TI%)=PY(21)\GOTO 1500
1200 ON PA%(I%) GOTO 1210,1220,1230,1240,1250,1260,1270 &
                    ,1280,1290,1300,1310,1320,1330,1340
1210 X(TI%)=P)(17)\Y(TI%)=PY(17)\GOTO 1500
1220 X(TI%)=P)(19)\Y(TI%)=PY(19)\GOTO 1500
1230 X(TI%)=P)(20)\Y(TI%)=PY(20)\GOTO 1500
1240 X(TI%)=P)( 1)\Y(TI%)=PY( 1)\GOTO 1500
1250 X(TI%)=P)( 2)\Y(TI%)=PY( 2)\GOTO 1500
1260 X(TI%)=P)( 4)\Y(TI%)=PY( 4)\GOTO 1500
1270 X(TI%)=P)( 5)\Y(TI%)=PY( 5)\GOTO 1500
1280 X(TI%)=P)( 8)\Y(TI%)=PY( 8)\GOTO 1500
1290 X(TI%)=P)( 9)\Y(TI%)=PY( 9)\GOTO 1500
1300 X(TI%)=P)(11)\Y(TI%)=PY(11)\GOTO 1500
1310 X(TI%)=P)(16)\Y(TI%)=PY(16)\GOTO 1500
1320 X(TI%)=P)(12)\Y(TI%)=PY(12)\GOTO 1500
1330 X(TI%)=P)(13)\Y(TI%)=PY(13)\GOTO 1500
1340 X(TI%)=P)(15)\Y(TI%)=PY(15)\GOTO 1500
1350 ON PA%(I%) GOTO 1360,1370,1380,1390,1400,1410,1420 &
                    ,1430,1440,1450,1460,1470,1480,1490
1360 X(TI%)=P)( 6)\Y(TI%)=PY( 6)\GOTO 1500
1370 X(TI%)=P)(17)\Y(TI%)=PY(17)\GOTO 1500
1380 X(TI%)=P)(18)\Y(TI%)=PY(18)\GOTO 1500
1390 X(TI%)=P)(20)\Y(TI%)=PY(20)\GOTO 1500
1400 X(TI%)=P)(21)\Y(TI%)=PY(21)\GOTO 1500
1410 X(TI%)=P)( 2)\Y(TI%)=PY( 2)\GOTO 1500
1420 X(TI%)=P)( 3)\Y(TI%)=PY( 3)\GOTO 1500
1430 X(TI%)=P)( 5)\Y(TI%)=PY( 5)\GOTO 1500
1440 X(TI%)=P)( 7)\Y(TI%)=PY( 7)\GOTO 1500
1450 X(TI%)=P)( 9)\Y(TI%)=PY( 9)\GOTO 1500
1460 X(TI%)=P)(10)\Y(TI%)=PY(10)\GOTO 1500
1470 X(TI%)=P)(13)\Y(TI%)=PY(13)\GOTO 1500
```

```
1480 X(TI%)=PX(14)\Y(TI%)=PY(14)\GOTO 1500
1490 X(TI%)=PX(16)\Y(TI%)=PY(16)
1500 REM  *****  FLUORINE X,Y  *****
1510 NI%=NL%*18%+I%*6%
1520 GOTO 1540 IF 2%*INT(PA%(I%)/2)-PA%(I%)<0%
1530 T=X(TI%)-4/21\X(NI%-5%)=T-INT(T)\T=Y(TI%)+1/21\Y(NI%-5%)=T-INT(T) &
    \T=X(TI%)-1/21\X(NI%-4%)=T-INT(T)\T=Y(TI%)-5/21\Y(NI%-4%)=T-INT(T) &
    \T=X(TI%)+5/21\X(NI%-3%)=T-INT(T)\T=Y(TI%)+4/21\Y(NI%-3%)=T-INT(T) &
    \T=X(TI%)-5/21\X(NI%-2%)=T-INT(T)\T=Y(TI%)-4/21\Y(NI%-2%)=T-INT(T) &
    \T=X(TI%)+4/21\X(NI%-1%)=T-INT(T)\T=Y(TI%)-1/21\Y(NI%-1%)=T-INT(T) &
    \T=X(TI%)+1/21\X(NI%   )=T-INT(T)\T=Y(TI%)+5/21\Y(NI%   )=T-INT(T)\GOTO 1550
1540 T=X(TI%)-5/21\X(NI%-5%)=T-INT(T)\T=Y(TI%)-4/21\Y(NI%-5%)=T-INT(T) &
    \T=X(TI%)+4/21\X(NI%-4%)=T-INT(T)\T=Y(TI%)-1/21\Y(NI%-4%)=T-INT(T) &
    \T=X(TI%)+1/21\X(NI%-3%)=T-INT(T)\T=Y(TI%)+5/21\Y(NI%-3%)=T-INT(T) &
    \T=X(TI%)-4/21\X(NI%-2%)=T-INT(T)\T=Y(TI%)+1/21\Y(NI%-2%)=T-INT(T) &
    \T=X(TI%)-1/21\X(NI%-1%)=T-INT(T)\T=Y(TI%)-5/21\Y(NI%-1%)=T-INT(T) &
    \T=X(TI%)+5/21\X(NI%   )=T-INT(T)\T=Y(TI%)+4/21\Y(NI%   )=T-INT(T)
1550 REM  *******  ZZZZZZZZ  *********
1560 I7.6_1=7.6*(I%-1%)
1570 FOR J%=NI%-5 TO NI%-3\Z(J%)=(I7.6_1+2.8)/C\NEXT J%
1580 Z(TI%)=(I7.6_1+3.8)/C
1590 FOR J%=NI%-2% TO NI%\Z(J%)=(I7.6_1+4.8)/C\NEXT J%
1600 FOR J%=I14%-13% TO I14%\Z(J%)=I7.6_1/C\NEXT J%
1610 RETURN

1620 REM ****  PRINTOUT  *****
1630 PRINT #6\PRINT #6,TITLE$
1640 PRINT #6,"A =";A,"C =";C,"WAVELENGTH =";WL,"# OF LAYERS =";NL%, &
          "# OF ATOMS =";NA%
1650 PRINT #6,"UHH AND U11"\PRINT #6,"  FOR  C= ";UHHC;ULLC &
    \                      PRINT #6,"  FOR As= ";UHHA;ULLA &
    \                      PRINT #6,"  FOR  F= ";UHHF;ULLF
1660 PRINT #6,"# OF CALCULATED REFLECTIONS =";NR%; &
          "No (000) reflections except when I=(# of layers)*n"
1670 PRINT #6,"MAXIMUM 1/D^2 =";D2M;
1680 PRINT #6,"NAME OF TERMINAL FORMAT, & DATA FILE =";FILE$;"(.TEF, & .DAT)"
1690 PRINT #6,"CARBON AND ARSENIC SEQUENCE ="\FOR I%=1% TO NL% &
    \          PRINT #6,"(";STR$(I%);")";CL$(I%);PA%(I%); &
    \          PRINT #6 IF 10%*INT(I%/10%)-I%=0%\NEXT I%\PRINT #6
1700 FOR I%=0% TO TH2DM%\IT2THC%=IT2THC(I%) IF IT2THC(I%)>IT2THC%\NEXT I%
1710 RESTORE #3
1720 FOR I%=0% TO TH2DM%\IT2THC(I%)=IT2THC(I%)*9999/IT2THCM
1730 IT2THC.DATA%=INT(IT2THC(I%))\PUT #3%\NEXT I%
1740 FOR I%=0% TO 7%\PLOT$(4%)=PLOT$(4%)+"0123456789"\NEXT I%
1750 FOR J%=0% TO INT(TH2DM%/80)
1760 PLOT$(5%)=""\FOR I%=0% TO 3%\PLOT$(I%)=""\NEXT I%
1770 FOR K%=80%*J% TO 80%*(J%+1%)-1%\FOR L%=0% TO 3%
1780 GOTO 1820 IF K%>TH2DM%
1790 TI%=INT(IT2THC(K%)/(10^(3%-L%)))
1800 IF TI%=0% THEN PLOT$(L%)=PLOT$(L%)+" " &
    ELSE PLOT$(L%)=PLOT$(L%)+RIGHT$(STR$(TI%),LEN(STR$(TI%)))
1810 NEXT L%\NEXT K%
1820 FOR I%=0% TO 7%\TI%=8%*J%+I%
1830 IF TI%>=10  THEN PLOT$(5%)=PLOT$(5%)+""+STR$(TI%)+"        "\GOTO 1850
    ELSE GOTO 1840
1840 IF TI%>=1 THEN PLOT$(5%)=PLOT$(5%)+""+STR$(TI%)+"         "\GOTO 1850
     ELSE PLOT$(5%)=PLOT$(5%)+"0         "
1850 NEXT I%
1860 FOR L%=0% TO 5%\PRINT #6,PLOT$(L%)\NEXT L%
1870 NEXT J%
1880 RETURN
1890 END
```

(HKℓ)-(III) model

```
100 INPUT "TITLE";TITLE$
110 INPUT "NAME OF TERMINAL FORMAT FILE /NAME999999(.TFF)/";FILE$
120 OPEN FILE$+".TFF" FOR OUTPUT AS FILE #6%,RECORDSIZE 132%
130 DIM PLOT$(6%)
140 A1C=2.31    \B1C=20.843\A2C=1.02  \B2C=10.2075\A3C=1.5886\B3C=.5687 &
   \A4C=.865    \B4C=51.6512\CC=.2156
150 A1A=16.6723\B1A=2.6345 \A2A=6.3701\B2A=.2647  \A3A=3.4313\B3A=12.9479 &
   \A4A=4.2779 \B4A=47.7972\CA=2.531
160 A1F=3.5392 \B1F=10.2625\A2F=2.6412\B2F=4.2944 \A3F=1.517 \B3F=.2615 &
   \A4F=1.0243 \B4F=26.1476\CF=.2776
170 WL=1.5418\WL_2=.7709\WL2=WL^2
180 PI5=-PI^2/90\PI.1800=1800/PI\PI2=2*PI\PI21=PI2/21
190 PRINT "INPUT UHH AND U11 FOR C, AS AND F  (UHK=UHF:UPK=UPF/2:UHK=UP1=0)" &
   \INPUT "FOR C";UHHC,ULLC\INPUT "FOR As";UHHA,ULLA\INPUT "FOR F";UHHF,ULLF
200 A=2.456*7\C=7.6\A2=4/A^2/3\C2=1/C^2\Z=1.0/C\NC2%=84%^2%
210 D2HH=4/WL^2\PRINT "ENTER UPPER LIMIT FOR 1/D^2--MAX)IMUM =";D2HM\INPUT D2M
220 D2P=D2PP IF D2P>D2PP\DP=1/SQR(D2M)
230 SN=WL/DP/2\TH2DM%=INT(2*ATN(SN/SQR(-SN^2+1))*PI.1800)
240 DIM IT2THC(4%,TH2DP%),IT2THCF(6%,TH2DM%)
250 HM%=INT(SQR(3)*A/2/DP)\LM%=INT(C/DP)
270 ITM=1\PRINT #6,TITLE$
280 PRINT #6,"H  K  L  1/D^2  2*THETA  INTENSITY:MAXIMUM=100000  (*ABS.INT)"
285 PRINT #6,"/ H1 K1 AFI *  S R F CAP"
290 FOR H1%=0% TO HM%\FOR K1%=0% TO H1%
291 PRINT "/";H1%;K1%;\PRINT #6,"/";H1%;K1%;
295 HK2%=H1%^2%+H1%*K1%+K1%^2%
296 AFI=COS(PI2*HK2%/7%)\PRINT AFI;\PRINT #6,AFI;
297 GOTO 460 IF COS(PI2*HK2%/7%)<0.9999
298 PRINT "*";\PRINT #6,"*";
300 AHK2=A2*HK2%\GOTO 460 IF AHK2>D2M
310 D2HK=AHK2\SNHK=WL_2*SQR(D2HK)\SNHK2=SNHK^2
320 TH2DHK%=2*ATN(SNHK/SQR(-SNHK2+1))*PI.1800+1
330 GOTO 460 IF TH2DHK%>=TH2DP%
340 H2%= H1%    \K2%=     K1%\IF H1%+K1%=0% THEN MP%=1% ELSE MP%=2%
341                          GOSUB 480\GOTO 460 IF H1%+K1%=0%
345                                GOTO 390 IF H1%=K1%
350 H2%=     K1%\K2%= H1%    \GOSUB 480
390 H2%= H1%+K1%\K2%=-H1%    \GOSUB 480\GOTO 460 IF K1%=0%
400 H2%=-H1%    \K2%= H1%+K1%\GOSUB 480\GOTO 460 IF H1%=K1%
410 H2%=    -K1%\K2%= H1%+K1%\GOSUB 480
420 H2%= H1%+K1%\K2%=    -K1%\GOSUB 480
460 NEXT K1%\NEXT H1%
470 GOSUB 1050\CLOSE #6\GOTO 1420
480 REM  ***** LLLLL *****
490 BT=PI21*3*(H2%+K2%)\AP=PI21*(2*H2%+K2%)\CAF=COS(AF)
500 R=1+2*(COS(BT)+COS(2*BT)+COS(3*BT))
510 P=1+2*CAP
515 PRINT "S";R;P;CAF;\PRINT #6,"S";R;P;CAP;
520 IF ABS(R)<0.0001 THEN PL%=3%\GOTO 540 ELSE 522
522 IF ABS(P)<0.0001 THEN PL%=2%\GOTO 540 ELSE 524
524 IF CAF>0.9999 THEN PL%=1%\GOTO 620 ELSE 535
535 PRINT "IGNORE_C";\PRINT #6,"IGNORED";\GOTO 750
540 FOR TH2D%=TH2DP% TO TH2DM%
```

```
550 TH=TH2D%*PI/3600\TH2=TH*2\SN=SIN(TH)\SN2=SN^2\SRCS2=SQR(SN2-SNMK2)
560 L=C*SRCSN2/WL_2\LPTH=(1+CCS(TH2)^2)/SN/SRDSN2
570 SS=-SN2/WL2\CL2=C2*L^2\GOSUB 760\GOSUB 810
580 IT=IT*LPTH\IT2THC(PL%,TH2D%)=IT2THC(PL%,TH2D%)+IT*PP%
590 IT2THC(4%,TH2D%)=IT2THC(4%,TH2D%)+IT*MP%
600 NEXT TH2D%
610 GOTO 750
620 PRINT\PRINT #6\FOR L2%=0% TO LM%\L=L2%
630 GOTO 740 IF H1%+K1%+L2%=0%



640 CL2=C2*L^2
650 D2=AMK2+CL2\GOTO 740 IF D2>C2P
660 SN=WL_2*SQR(D2)\TH=ATN(SN/SQR(-SN^2+1)) &
   \TH2=TH*2\SS=-D2/4\LP=(1+CCS(TH2)^2)/SIN(TH)^2/CCS(TH)
670 GOSUB 760
680 H3%=H2%\K3%=K2%\L3=L2%\GOSUB 950\IT=AB^2
700 IT=IT*LP\IF L2%>0% THEN LPF%=2% ELSE LMF%=1%
710 D2TT%=INT(C2*10000)\TH2D%=INT(TH2*PI.1000)
720 IT2THC(1%,TH2D%)=IT2THC(1%,TH2D%)+IT*MP%*LMP%
730 IF IT>ITM THEN ITM=IT\PRINT     H2%;K2%;L2%;D2TT%;TH2D%;"100CC00*";IT &
   \PI%=0                    \PRINT #6,H2%;K2%;L2%;D2TT%;TH2D%;"100CC00*";IT &
   ELSE ITN%=INT(1000000*IT/ITM) &
   \                          PRINT     H2%;K2%;L2%;D2TT%;TH2D%;ITN% &
   \                          PRINT #6,H2%;K2%;L2%;D2TT%;TH2D%;ITN%;"/"; &
   \PI%=PI%+1%\IF PI%-4%*INT(PI%/4%)=0% THEN PRINT #6%\PI%=0% ELSE GOTO 740
740 NEXT L2%
745 PRINT\PRINT #6
750 RETURN
760 REM  *****  SCATTERING FACTORS  *****
770 SC=1*(A1C*EXP(B1C*SS)+A2C*EXP(B2C*SS)+A3C*EXP(B3C*SS)+A4C*EXP(B4C*SS)+CC) &
   *EXP(PI5*(LMMC*AMK2+ULLC*CL2))
780 SA=2*(A1A*EXP(B1A*SS)+A2A*EXP(B2A*SS)+A3A*EXP(B3A*SS)+A4A*EXP(B4A*SS)+CA) &
   *EXP(PI5*(LMMA*AMK2+ULLA*CL2))
790 SF=2*(A1F*EXP(B1F*SS)+A2F*EXP(B2F*SS)+A3F*EXP(B3F*SS)+A4F*EXP(B4F*SS)+CF) &
   *EXP(PI5*(LMMF*AMK2+ULLF*CL2))
800 RETURN
810 REM  *****  STRUCTURE FACTORS & INTENSITY  *****
820 H3%=H2%\K3%=K2%\L3=  L\GOSUB 950\AA1=AB
830 H3%=K2%\K3%=H2%\L3=-L\GOSUB 950\AA2=AB\AA=AA1+AA2
840 H3%=H2%\K3%=K2%\L3=-L\GOSUB 950\BB1=AB
850 H3%=K2%\K3%=H2%\L3=  L\GOSUB 950\BB2=AB\BB=BB1+BB2
860 JQ=(AA1^2+AA2^2+BB1^2+BB2^2)/4
870 IT=NC2%*JQ\GOTO 940 IF PL%=3%
900 P2L=PI2*L
910 T=(2+CAF)*(1+2*COS(P2L))*(AA^2-4*AA*BB+BB^2)
920 T=T+6*SIN(AP)*SIN(P2L)*(AA^2-BB^2)
930 IT=IT-8*R^2*(1-CAF)*T/(5+4*COS(P2L))
940 RETURN
950 REM  ***** AB *****
960 PH2K1=P21*(2*H3%+K3%)\PHK=P21*(H3%-K3%)\PH1K2=P21*(H3%+2*K3%)
965 PH3K9=P21*(3*H3%+9*K3%)\PL=PI*L3\P2LZ=PI2*L3*Z
968 TC=0\TF=0\TA=0
969 GOTO 981 IF PL%=3%
970 FOR M%=0% TO 6%\FOR N%=0% TO 6%
975 T=P21*3*(P%*H3%+N%*K3%)-PL
980 TC=TC+COS(T)+COS(T+PH2K1)\NEXT N%\NEXT M%
981 GOTO 1030 IF AFI<0.9999
982 FOR M%=0% TO 6%\MPH3K9=M%*PH3K9\T=PPH3K9-P2LZ
1000 TF=TF+COS(T-PH2K1)+COS(T+PHK)+COS(T+PH1K2)
```

```
1010 TA=TA+COS(MPH3KS)
1020 NEXT MX
1030 AE=2*SC*TC+2*SF*TF+SA*TA
1040 RETURN
1050 REM ****  PRINTOUT  *****
1060 PRINT #6\PRINT #6,TITLE$
1070 PRINT #6,"A =";A,"C =";C,"WAVELENGTH =";WL
1080 PRINT #6,"Umm AND U11"\PRINT #6,"  FOR  C= ";CMMC;ULLC $
     \                      PRINT #6,"  FOR As= ";CMMA;ULLA $
     \                      PRINT #6,"  FOR  F= ";UMMF;ULLF
1090 PRINT #6,"MAXIMUM 1/D^2 =";D2M;
1100 PRINT #6,"   NAME OF TERMINAL FORMAT FILE IS ";FILE$;"(.TFF)"\PRINT #6
1110 FOR IX=0% TO 7%\PLOT$(4%)=PLOT$(4%)+"0123456789"\NEXT IX



1120 FOR MX=1% TO 4%\IT2THDM=0
1125 PRINT "NEGATIVE 2TH"\PRINT #6,"NEGATIVE 2TH"
1126 FOR IX=0% TO TH2DM%\IF IT2THD(MX,IX)<0 THEN IT2THD(MX,IX)=-IT2THD(MX,IX) $
     \PRINT MX;IX;"/";\PRINT #6,IX;"/"; ELSE 1127
1127 NEXT IX\PRINT #6
1130 FOR IX=0% TO TH2DM%\IT2THDM=IT2THD(MX,IX) IF IT2THD(MX,IX)>IT2THDM\NEXT IX
1135 GOTO 1150 IF IT2THDM=0
1140 FOR IX=0% TO TH2DM%\IT2THDF(MX,IX)=IT2THD(MX,IX)*9999/IT2THDM\NEXT IX
1150 NEXT MX
1160 FOR MX=5% TO 6%
1170 FOR IX=0% TO TH2DM%\IT2THDF(MX,IX)=IT2THD(MX-4%,IX)*9999/IT2THDM\NEXT IX
1180 NEXT MX
1190 FOR MX=1% TO 6%
1200 ON MX GOTO 1210,1220,1230,1240,1250,1260
1210 PRINT #6,"#1 F<>0 AND COS(ALPHA)=1  SHARP"\GOTO 1270
1220 PRINT #6,"#2 P<>0 and F=0"\GOTO 1270
1230 PRINT #6,"#3 P=0"\GOTO 1270
1240 PRINT #6,"#4 = #3 + #2  ERCAO"\GOTO 1270
1250 PRINT #6,"#5 = #2  NORMALIZED BY #4"\GOTO 1270
1260 PRINT #6,"#6 = #3  NORMALIZED BY #4"\GOTO 1270
1270 FOR JX=0% TO INT(TH2DM%/80)
1280 PLOT$(5%)=""\FOR IX=0% TO 3%\PLOT$(IX)=""\NEXT IX
1290 FOR KX=80%*JX TO 80%*(JX+1%)-1%\FOR LX=0% TO 3%
1300 GOTO 1340 IF KX>TH2DM%
1310 TIX=INT(IT2THDP(MX,KX)/(10^(3%-LX)))
1320 IF TIX=0% THEN PLOT$(LX)=PLOT$(LX)+" " $
     ELSE PLOT$(LX)=PLOT$(LX)+RIGHT$(STR$(TIX),LEN(STR$(TIX)))
1330 NEXT LX\NEXT KX
1340 FOR IX=0% TO 7%\TIX=8%*JX+IX
1350 IF TIX>=10  THEN PLOT$(5%)=PLOT$(5%)+"*"+STR$(TIX)+"        "\GOTO 1370
     ELSE GOTO 1360
1360 IF TIX>=1 THEN PLOT$(5%)=PLOT$(5%)+"*"+STR$(TIX)+"         "\GOTO 1370
     ELSE PLOT$(5%)=PLOT$(5%)+"*0          "
1370 NEXT IX
1380 FOR LX=0% TO 5%\PRINT #6,PLOT$(LX)\NEXT LX
1390 NEXT JX
1400 NEXT MX
1410 RETURN
1420 END
```

(hkℓ) model

```
100 INPUT "TITLE":TITLE$
110 INPUT "NAME OF TERMINAL FORMAT FILE /NAME$9999(.TFF)/":FILE$
120 OPEN FILE$+".TFF" FOR OUTPUT AS FILE #6%,RECORDSIZE 132%
130 DIM PLOT$(6%),XX(3%),YL(3%),YR(3%)
140 FOR M%=1% TO 3%\XX(M%)=3*M%\NEXT M%
150 YL(1%)=9\YL(2%)=-3\YL(3%)=6
160 YR(1%)=-6\YR(2%)=9\YR(3%)=3
170 A1A=16.6723\B1A=2.6345 \A2A=6.0701\B2A=.2647  \A3A=3.4313\B3A=12.9479 &
   \A4A=4.2779 \B4A=47.7972\CA=2.531
180 A1F=3.5392 \B1F=10.2825\A2F=2.6412\B2F=4.2944 \A3F=1.517 \B3F=.2615 &
   \A4F=1.0243 \B4F=26.1476\CF=.2776
190 WL=1.5418\WL_2=.7709\WL2=WL^2
200 PI$=-PI^2/50\PI.1800=1800/PI\PI2=2*PI\P21=PI2/21\P7=PI2/7
205 INPUT "L11 FOR As and F":LLLA,ULLF
210 INPUT "LMF(=UMM=2UMM) for As and F":LMMA,LMMF
220 INPUT "SIZE OF DOMAIN (MULTIPLE OF 2.456*7)":NA
230 PNA=PI*NA\NN2=(4*49*NA)^2
240 A=2.456*7\A2=4/A^2/3
250 C=7.6\C2=1/C^2\Z=1/7.6
260 INPUT"ENTER LOWER AND UPPER LIMITS FOR 2*THETA":TH2MIN,TH2MAX
270 D2MIN=(2*SIN(PI*TH2MIN/360)/WL)^2\D2MAX=(2*SIN(PI*TH2MAX/360)/WL)^2
280 DMAX=1/SQR(D2MAX)
290 SN=WL/DMAX/2\TH2DM%=INT(2*ATN(SN/SQR(-SN^2+1))*PI.1800)
300 DIM IT2THE(2%,TH2DM%)
310 INPUT "H, K, AND L BY":NN
320 HNMAX%=INT(NN*SQR(3)*A/2/CMAX)
330 LNMAX%=INT(NN*C/CMAX)
340 ITM=1\PRINT #6,TITLE$
350 PRINT #6,"HN%  KN%   1/D^2  2*THETA  INTENSITY:MAXIMUM=1000000(*ABS.INT) /"
360 PRINT #6,"and/or HN% KN% IT (for negative intensity)/"
370 FOR HN%=0% TO HNMAX%\FOR KN%=0% TO HN%
380 GOTO 530 IF HN%+KN%=0%
390 H1=HN%/NN\K1=KN%/NN
410 HK2=H1^2+H1*K1+K1^2
420 AHK2=A2*HK2\GOTO 530 IF AHK2>D2MAX OR AHK2<D2MIN
430 GOTO 530 IF AHK2<D2MIN
440 D2HK=AHK2\SNHK=WL_2*SQR(D2HK)\SNHK2=SNHK^2
450 TH2DHK%=2*ATN(SNHK/SQR(-SNHK2+1))*PI.1800+1
460 GOTO 530 IF TH2DHK%>=TH2DM%
470 H2= H1    \K2=     K1\GOSUB 550
480                      \MP=4\MP=2 IF HN%=KN%
490 H2= H1+K1\K2=-H1     \GOSUB 550
500                      \MP=4\MP=2 IF KN%=0%\GOTO 530 IF HN%=KN% OR KN%=0%
510 H2=    -K1\K2= H1+K1\GOSUB 550
520                      \MP=4
530 NEXT KN%\NEXT HN%
540 GOSUB 1110\HGHT=0.75\GOSUB 1470\CLOSE #6\GOTO 1570
550 REM  *****  INTENSITY  *****
552 T1=0\T2=0\FOR M%=0% TO 3%
554 T1=T1+COS(P7*(H2*M%+K2*N%))\FOR N%=-3% TO 3%\T2=T2+COS(P7*(H2*M%+K2*N%))
556 NEXT N%\NEXT M%\Q=T1+2*T2\G2=G^2
560 FOR LN%=0% TO LNMAX%
570 L2=LN%\CL2=C2*L2^2\D2=AHK2+CL2
580 GOTO 620 IF D2>D2MAX OR D2<D2MIN
620 SN=WL_2*SQR(D2)\TH=ATN(SN/SQR(-SN^2+1)) &
   \TH2=TH*2\SS=-D2/4\LP=(1+COS(TH2)^2)/SIN(TH)^2/COS(TH)
630 GOSUB 840\GOSUB 880
```

```
640 SH=SIN(H2*PI)\SK=SIN(K2*PI)
650 IF ABS(SH)<0.0001 THEN SH=AA ELSE SH=SIN(H2*PHA)/SH
660 IF ABS(SK)<0.0001 THEN SK=AA ELSE SK=SIN(K2*PHA)/SK
665 SN2=(SH*SK)^2
670 IT=(HH2*AE-Q2*AA88^2*SN2)*SN2*LP*MP



680 GOTO 710
690 PRINT HH%;KN%;IT;"/": IF IT<-0.1
700 PRINT #E,HH%;KN%;IT;"/": IF IT<-0.1
710 D2TT%=INT(C2*10000)\TH2C%=INT(TH2*PI.1800)
720 IF LN%>.5 THEN LMP=2 ELSE LMP=1
730 IT2THC(I%,TH2C%)=IT2THC(I%,TH2D%)+IT*LMP
740 GOTO 830
750 IF IT>ITM THEN ITM=IT ELSE 790
760 PRINT      HN%;KN%;D2TT%;TH2D%;"1000000";IT
770 PRINT #E%,HN%;KN%;D2TT%;TH2D%;"1000000";IT
780 GOTO 820
790 ITN%=INT(1000000*IT/ITM)
800 PRINT      HN%;KN%;D2TT%;TH2D%;ITN%;"/";
810 PRINT #E%,HN%;KN%;D2TT%;TH2D%;ITN%;"/";
820 NEXT LN%
830 RETURN
840 REM  ***** SCATTERING FACTORS *****
850 SA=(A1A*E)P(B1A*SS)+A2A*E)P(B2A*SS)+A3A*EXP(B3A*SS)+A4A*EXP(B4A*SS)+CA) &
    *EXP(PI5*(LMHA*AHK2+ULLA*CL2))
860 SF=(A1F*E)P(B1F*SS)+A2F*EXP(B2F*SS)+A3F*EXP(B3F*SS)+A4F*EXP(B4F*SS)+CF) &
    *EXP(PI5*(LMHF*AHK2+ULLF*CL2))
870 RETURN
880  REM  **** INTENSITY *****
890 L3=L2\GOSUB 930\AA1=FL\BB2=FR
900 L3=-L2\GOSUB 930\AA2=FR\BB1=FL
910 AB=(AA1^2+AA2^2+BB1^2+BB2^2)/4\AABB=AA1+AA2+BB1+BB2
920 RETURN
930 REM  ***** F *****
940 PH2K1=P21*(2*H2+K2)\PHK=P21*(H2-K2)\PH1K2=P21*(H2+2*K2)
950 P2LZ=PI2*L3*Z
960 TFL=0\TFR=0\TAL=0\TAR=0
970 TFC=COS(-PH2K1-P2LZ)+COS(PHK-P2LZ)+COS(PH1K2-P2LZ)
980 FOR MX=1% TO 3%
990 T=P21*(H2*XX(MX)+K2*YL(MX))
1000 TFL=TFL+COS(T-PH2K1-P2LZ)+COS(T+PHK-P2LZ)+COS(T+PH1K2-P2LZ)
1010 TFL=TFL+COS(T+PH2K1+P2LZ)+COS(T-PHK+P2LZ)+COS(T-PH1K2+P2LZ)
1020 TAL=TAL+COS(T)
1030 T=P21*(H2*XX(MX)+K2*YR(MX))
1040 TFR=TFR+COS(T-PH2K1-P2LZ)+COS(T+PHK-P2LZ)+COS(T+PH1K2-P2LZ)
1050 TFR=TFR+COS(T+PH2K1+P2LZ)+COS(T-PHK+P2LZ)+COS(T-PH1K2+P2LZ)
1060 TAR=TAR+COS(T)
1070 NEXT MX
1080 FL=2*SF*(TFC+TFL)+SA*(1+2*TAL)
1090 FR=2*SF*(TFC+TFR)+SA*(1+2*TAR)
1100 RETURN
```

```
1110 REM ****  PRINTOUT  *****
1120 PRINT #6\PRINT #6,TITLE$
1130 PRINT #6,"SIZE OF DOMAIN  2.456*7**":NA
1140 PRINT #6,"H and K are devided by":NA
1150 PRINT #6,"A =":A,"C =":C,"WAVELENGTH =":WL
1155 PRINT #6,"LLL for As=":LLLA:"and for F=":LLLF
1160 PRINT #6,"UHH for As=":UHHA:"and for F=":UHHF
1170 PRINT #6,"MAXIMUM 1/D^2 =":D2M:
1180 PRINT #6,"LOWER 2*THETA =":TH2MIN:"  UPPER 2*THETA =":TH2MAX
1190 PRINT #6,"   NAME OF TERMINAL FORMAT FILE IS ":FILE$:"(.TFF)"\PRINT #6
1200 FOR I%=0% TO 7%\PLOT$(4%)=PLOT$(4%)+"0123456789"\NEXT I%
1210 FOR I%=0% TO TH2DM%
1220 FOR J%=I%-30% TO I%+30%
1230 GOTO 1250 IF J%<0% OR J%>TH2DM%
1240 IT2THD(2%,J%)=IT2THD(2%,J%)+IT2THD(1%,I%)*EXP(-(J%-I%)^2/18)
1250 NEXT J%\NEXT I%
1260 FOR H%=1% TO 2%\IT2THDM=0

1270 PRINT "negative 2TH"\PRINT #6,"negative 2TH"
1280 FOR I%=0% TO TH2DM%\IF IT2THD(H%,I%)<0 THEN IT2THD(H%,I%)=-IT2THD(H%,I%) &
    \PRINT H%;I%;"/";\PRINT #6,I%;"/"; ELSE  1290
1290 NEXT I%\PRINT #6
1300 FOR I%=0% TO TH2DM%\IT2THDM=IT2THD(H%,I%) IF IT2THD(H%,I%)>IT2THDM\NEXT I%
1310 IF IT2THDM=0 THEN PRINT "IT2THDM=0"\STOP ELSE 1320
1320 FOR I%=0% TO TH2DM%\IT2THD(H%,I%)=IT2THD(H%,I%)*9999/IT2THDM\NEXT I%
1330 FOR J%=0% TO INT(TH2DM%/80)
1340 PLOT$(5%)=""\FOR I%=0% TO 3%\PLOT$(I%)=""\NEXT I%
1350 FOR K%=80%*J% TO 80%*(J%+1%)-1%\FOR L%=0% TO 3%
1360 GOTO 1400 IF K%>TH2DM%
1370 TI%=INT(IT2THD(H%,K%)/(10^(3%-L%)))
1380 IF TI%=0% THEN PLOT$(L%)=PLOT$(L%)+" " &
    ELSE PLOT$(L%)=PLOT$(L%)+RIGHT$(STR$(TI%),LEN(STR$(TI%)))
1390 NEXT L%\NEXT K%
1400 FOR I%=0% TO 7%\TI%=8%*J%+I%
1410 IF TI%>=10  THEN PLOT$(5%)=PLOT$(5%)+""+STR$(TI%)+"        "\GOTO 1430
    ELSE GOTO 1420
1420 IF TI%>=1 THEN PLOT$(5%)=PLOT$(5%)+""+STR$(TI%)+"         "\GOTO 1430
     ELSE PLOT$(5%)=PLOT$(5%)+"0         "
1430 NEXT I%
1440 FOR L%=0% TO 5%\PRINT #6,PLOT$(L%)\NEXT L%
1450 NEXT J%\PRINT #6\NEXT H%
1460 RETURN
1470 REM *****  BAR GRAPH  *****
1480 FOR I%=0% TO TH2DM% STEP 2%
1490 PRINT #6," "; IF I%<100%
1500 PRINT #6," "; IF I%<10%
1510 PRINT #6,I%;
1520 T1%=IT2THD(2%,I%)*HGHT/100
1530 GOTO 1550 IF T1%=0%
1540 FOR J%=1% TO T1%\PRINT #6,"#";\NEXT J%
1550 PRINT #6,\NEXT I%
1560 PRINT #6\RETURN
1570 STOP\END
```

ACKNOWLEDGEMENT

I would like to thank Professor Neil Bartlett for his warm guidance throughout my graduate career. This work would never have been completed without his ability to enthusiastically simplify complex problems and his personal encouragement during my most difficult time.

I would like to thank Tom Mallouk for his warm presence in the lab. His work, especially X-ray intensity calculations, helped my work a great deal; Guy Rosenthal for his help via his experience with related work; Ray Brusasco and Mike Wagner mainly for helping me to use computers; Professors Leo Brewer, Hans-Rudolf Wenk and David Templeton for valuable suggestions; Tom Richardson, Sam Yeh, Dino Kourtakis, Margrett Atkinson and all the other people who, one way or another, helped me to finish this work.

This work was supported by the U.S. Department of Energy under Contract DE-AC03-76SF00098

TECHNICAL INFORMATION DEPARTMENT
LAWRENCE BERKELEY LABORATORY
UNIVERSITY OF CALIFORNIA
BERKELEY, CALIFORNIA 94720